THÈSE EN COTUTELLE PRÉSENTÉE

POUR OBTENIR LE GRADE DE

DOCTEUR DE

L'UNIVERSITÉ DE BORDEAUX

ET DE L'UNIVERSIDADE FEDERAL DE CAMPINA GRANDE

ÉCOLE DOCTORALE DES SCIENCES PHYSIQUES ET DE L'INGÉNIEUR
PROGRAMA DE PÓS-GRADUAÇÃO EM ENGENHARIA ELÉTRICA
SPÉCIALITÉ : ELECTRONIQUE

Par Marlo ANDRADE SANTOS

Wireless system for passive surface acoustic wave sensors

Système d'interrogation à distance de capteurs passifs à ondes acoustiques de surface

Sous la direction de Corinne DEJOUS
et de Raimundo C.S. FREIRE

Soutenue le 19 juillet 2024

Membres du jury :

M.	PRIMEROSE, Antoine	Professeur	ESPACE-DEV - Université de Guyane	Rapporteur
M.	CATUNDA, Sebastian	Professeur	Universidade Federal do Rio Grande do Norte	Rapporteur
Mme.	SÉBÉLOUÉ, Martine	Maîtresse de Conférences	Université de Guyane	Examinatrice
M.	GURJÃO, Edmar	Professeur	Universidade Federal de Campina Grande	Examinateur et Président
Mme.	HALLIL, Hamida	Maîtresse de Conférences	IUT GEII - Université de Bordeaux	Examinatrice
M.	DE LIMA, Robson	Professeur	Universidade Federal da Bahia	Examinateur
Mme.	DEJOUS, Corinne	Professeur des Universités	Bordeaux INP ENSEIRB-MATMECA	Directrice de thèse
M.	FREIRE, Raimundo	Professeur	Universidade Federal de Campina Grande	Directeur de thèse
M.	TAMARIN, Ollivier	Maître de Conférences	ESPACE-DEV - Université de Guyane	Co-encadrant - Invité

Abstract

With the advancement in the development of connected devices and the Internet of Things (IoT), continuous monitoring of physical and chemical parameters has become a current challenge for our society. Additionally, surface acoustic wave (SAW) devices, widely used as filters in telecommunications, now serve the function of sensors. It is within these two contexts that the work of this thesis is situated.

The goal is to develop a wireless reading system using one of these sensors, particularly the Love Wave (LW) sensor with recognized sensitivity in liquid media. Few studies involve this device by performing a remote reading, and exclusively using its acoustic response. In this thesis, we employ a more general approach considering its electromagnetic response and a specific measurement and data acquisition protocol for detecting saline solutions on its surface. Given its passive nature, a wireless reading system is demonstrated, as well as discussion on its key characteristics, advantages, disadvantages, and limitations.

Keywords: passive sensor, Love wave, wireless, system, liquid medium

Résumé

Avec les progrès du développement des appareils connectés et de l'Internet des objets (IoT), la surveillance continue des paramètres physiques et chimiques est devenue un défi actuel pour notre société. De plus, les dispositifs à ondes acoustiques de surface (SAW), largement utilisés comme filtres dans les télécommunications, remplissent désormais la fonction de capteurs. C'est dans ces deux contextes que se situent les travaux de cette thèse.

L'objectif est de développer un système de lecture sans fil utilisant l'un de ces capteurs, notamment le capteur à ondes de Love (Love Wave ou LW) à sensibilité reconnue en milieu liquide. Peu de travaux impliquent ce dispositif en effectuant une lecture à distance, et exclusivement en utilisant sa réponse acoustique. Dans cette thèse, nous employons une approche plus générale considérant sa réponse électromagnétique et un protocole spécifique de mesure et d'acquisition de données pour détecter des solutions salines à sa surface. Compte tenu de sa nature passive, un système de lecture sans fil est présenté, ainsi qu'une discussion sur ses principales caractéristiques, avantages, inconvénients et limites.

Mots clés:: capteur passif, onde de Love, sans fil, système, milieu liquide

Resumo

Com o avanço no desenvolvimento de dispositivos conectados e da Internet das Coisas (IoT), o monitoramento contínuo de parâmetros físicos e químicos tornou-se um desafio atual para a nossa sociedade. Além disso, dispositivos de ondas acústicas de superfície (SAW), amplamente utilizados como filtros em telecomunicações, agora servem como sensores. É nestes dois contextos que se situa o trabalho desta tese.

O objetivo é desenvolver um sistema de leitura sem fio utilizando um desses sensores, particularmente o sensor Love Wave (LW) com sensibilidade reconhecida em meios líquidos. Poucos trabalhos envolvem este dispositivo realizando uma leitura remota e utilizando exclusivamente sua resposta acústica. Nesta tese, empregamos uma abordagem mais geral considerando sua resposta eletromagnética e um protocolo específico de medição e aquisição de dados para detecção de soluções salinas em sua superfície. Dada a sua natureza passiva, é demonstrado um sistema de leitura sem fio, bem como discutidas as suas principais características, vantagens, desvantagens e limitações.

Pavavras-chave: sensor passivo, Love wave, , sem-fio, sistema, meio líquido

Acknowledgments

I would like to begin by expressing my deepest gratitude to my supervisors, Prof. Corinne Dejous and Prof. Raimundo C.S. Freire, for their expertise, guidance, and unwavering encouragement throughout the course of my thesis. Their exceptional patience and continuous support were instrumental in helping me navigate the challenges I encountered during this research.

I am also immensely grateful to my co-supervisors, Assoc. Prof. Hamida Hallil and Prof. Ollivier Tamarin, whose valuable insights and scientific discussions were critical to the development of this work. Additionally, their global perspective provided opportunities for international exchanges that significantly enriched my research experience.

I extend my sincere thanks to Professors Anthony Ghiotto, Alexandre Jean René Serres, Paulo Fernandes da Silva Júnior, and Smail Tedjini for their advice and collaboration. I also wish to acknowledge the support and discussions with engineers Jean-Luc Lachaud and Franck Chebila. Furthermore, I am grateful to David Bédènes and Serge Destor for their assistance with technical aspects. My heartfelt thanks also go to the other members of the MDA IMS Bordeaux research team (Yang Yang, Bernard Bobby Ngoune, Maxence Rube, and Asawari Choudhari) and LIMC UFCG (Stephanie Kamarry, Marcos Bernardo, and Arthur Souza) for their occasional and ongoing contributions throughout this thesis. The numerous technical and scientific discussions were fundamental in understanding the complexities and challenges of my project.

I wish to express my sincere appreciation to the University of Bordeaux and the Federal University of Campina Grande for providing this collaboration. I also thank the Federal Institute of Education, Science, and Technology of Pernambuco for their support, especially campus director Diogo Lopes da Silva and president José Carlos de Sá Júnior.

A personal thank you goes to Emilie Bonin, Nicolas Goiricelaya, Julie Laygues, Amandine Galais, Thaíssa Chaparro, and André Oliveira for their friendship over the years.

I want to express my profound gratitude to my family: Antônio Bento, Maria Gilza, Glédson, and Shirley. Words cannot fully convey my thanks for their unwavering support and love. With immense pride and gratitude, I dedicate this thesis to my father.

Contents

List of Acronyms

LW Love Wave

SAW Surface Acoustic Wave

VNA Vector Network Analyzer

RF Radio Frequency

RFID Radio-Frequency IDentification

IoT Internet of Things

MEMS Microelectromechanical Systems

NFC Near Field Communication

VHF Very-High-Frequency

RCS Radar Cross Section

BAW Bulk Acoustic Wave

DNA Deoxyribonucleic Acid

SH Shear Horizontal

IDT Interdigital Transducers

AF Amorphous Fluoropolymer

ISM Industrial, Scientific and Medical

PMMA polymethylmethacrylate

TDS Time Domain Sampling

FDS Frequency Domain Sampling

S-FSCW Stepped Frequency Continuous Wave

FM Frequency Modulation

FMCW Frequency-Modulated Continuous Wave

CW Continuous Wave

VCO Voltage Controlled Oscillator

PLL Phase Locked Loop

DDS Direct Digital Synthesis

SDR Software Defined Radio

TCF Temperature/Frequency Coefficient

PFA Power-Flow Angle

QUCS Quite Universal Circuit Simulators

UHF Ultra-High-Frequency

CEA Carcinoembryonic Antigen

DMMP dimethylmethylphosphonate

CPW coplanar waveguide

SL Scattering Level

AM Amplitude Modulation

TENG Triboelectric Nanogenerator

AUT Antenna Under Test

ETSI European Telecommunications Standards Institute

List of Figures

List of Tables

1 Introduction

The current society is immersed in a process of operation based on permanent surveillance. Access to information and being connected and informed is a real necessity. In this context, the market for object connectivity has experienced steady growth. In recent decades, wireless communication has become essential for various civilian, industrial, and military applications. It is especially important to access harsh environments that require the monitoring and measurement of physical quantities such as temperature, pressure, and particles in gas and liquid environments. The increased use of these systems is made possible by the high performance of the sensors and the characteristics of the electronic reading devices, which enable wireless measurement. In this context, Surface Acoustic Wave (SAW) sensors have been increasingly occupying space and applicability. Their sensitivity to environmental disturbances allows their use in the measurement of temperature, pressure, and the presence of gases and liquids. Additionally, they are passive devices that can be remotely interrogated [1].

Among these sensors, Love Wave (LW) transducers have demonstrated great sensitivity for biological and chemical detection in gas and liquid media, especially in the environmental and healthcare sectors. So far, most detection applications using LW rely on dedicated reading circuits connected to the sensor. Innovative methods capable of identifying and interrogating passive wireless devices using the principle of Vector Network Analyzer (VNA) and various wireless reading techniques have been studied in the last decade. These systems are designed based on characteristics of the transduction type, such as propagation of electromagnetic and acoustic waves, geometry, materials, recommended sensitivity depending on the application, and frequency range of the transducers to be monitored. In a typical wireless configuration, a sensor sensitive to a

quantity to be measured (such as physical parameters of water) is connected to an antenna, coil, or LC oscillator. In fact, for the remote detection part, the relationship between the emitted and received power by the reader depends on the characteristics of the Radio Frequency (RF) parameters and changes in the impedance response of the sensor due to the properties of the liquid deposited onto its surface. Thus, the resonance frequency or amplitude of the backscattered signal takes into account the parameter of the liquid medium to be monitored [2].

Passive LW sensors have been studied and developed at IMS-Bordeaux (Laboratory for the Integration from Material to System) over the past decades. The sensor has been applied to gases and liquids with wired instrumentation and utilizes electroacoustic transduction with a frequency order of hundreds of MHz [3], [4]. Specifically, LW sensors designed at IMS and the subject of study in this work exhibit significant insertion losses in their acoustic energy, making it difficult to wirelessly read the mechanical parameters of the liquid they affect. However, these same sensors have demonstrated sensitivity in liquid media when considering a more comprehensive analysis of their behavior. Recent studies have also explored their electromagnetic response, obtaining an enriched analysis of energy conversion and flow within the sensor [5]. In this direction, the electromagnetic response is incorporated into its acoustic response. By temporally separating their responses, the LW sensor can be conceived as a multiparametric device [5]. To be interrogated remotely, these sensors require a reader that is compatible with their operational characteristics.

1.1 Objectives

The aim of this thesis is to propose an instrumentation protocol and a data acquisition methodology for wired and wireless interrogation of LW sensors dedicated to liquid quantity measurements, specifically:

- Directly connected to the VNA: signal analysis in reflection and transmission
- Associated with antennas and circuits and wirelessly interrogated from a distance: signal analysis in reflection
- Validation of an instrumentation and data protocol acquisition
- Passive nature, without battery or energy harvesting.

This project is part of a Cooperation Program involving partners in Brazil, with the participation of the Federal University of Campina Grande (UFCG), and in France, with the

participation of the University of Bordeaux and the University of French Guiana. It is focused on the design and development of LW sensor-based systems for applications in liquid and gaseous environments.

1.2 Thesis structure

This thesis is organized into three distinct parts. In the second chapter, the context of the study is presented, including an overview of the field of connected objects. The basic concepts of wireless systems and their connections to SAW devices, which are important for understanding the whole work, are also addressed. The objective is to demonstrate the relevance of wireless measurement in the field of electronics and its development applied to SAW sensors, focusing on the wireless reading of LW sensors, based on the state of the art.

The third chapter is dedicated to wired measurements using the LW sensor. The operating principle and general applications of SAW are presented, along with interest in LW sensors. The focus is on the wired experimental setup enabling the detection and classification of NaCl solutions. The relationship between the sensor's input impedance and the concentrations of the solutions is established, providing an indication of how the sensor can be detected remotely, aligning with the central focus of this thesis.

The last chapter demonstrates the feasibility of wireless reading using LW sensors based on experimental setups, culminating in the remote detection of liquid at different NaCl concentrations. The issues, advantages, and disadvantages of the experimental setups will be addressed. Finally, a comparison between the proposed solutions is presented.

The conclusion summarizes the main results, highlights some limitations of the systems, and new study perspectives are suggested.

1

2

State of Art: wireless interrogation for passive sensors

Contents

2

The objective of this chapter is to establish the utilization of wireless readers in the context of passive sensors, starting with a comprehensive examination of general passive sensors applications The focus will be directed towards electromagnetic and surface acoustic wave sensors, progressing to an exploration of advances in LW sensors and the possibilities of wireless connection and reading based on Radio-Frequency IDentification (RFID) and radar systems In this chapter, the latest work for remote reading of passive sensors and a state-of-the-art synthesis of key information related to implemented systems will be presented. Operational frequency, measurement parameters, distance capabilities, power requirements, architectural typology, and analysis of signals and antennas employed will be detailed. The advantages and limitations inherent in these implementations will be systematized. The purpose is to contextualize current research in the broader domain of sensor investigation, rationalizing its significance based on the specific requirements of sensor technology. Finally, a concise exposition of the proposed test strategy that involves sensors, antennas, and system configurations will be outlined, with detailed elaboration provided in subsequent sections and chapters.

2.1 Wireless sensing systems

Millions of new sensor devices have been deployed in recent years, and the future trend indicates that these devices will be widely used for object connectivity. This signifies a pivotal step towards scaling today's Internet of Things (IoT) into the vast IoT of the future. A typical system comprises a microcontroller, a radio transceiver, sensors, and a power source. However, the limited lifespan of such devices remains a primary constraint for these systems. With recent advancements in ultra-low power signal processing and wireless communications, there is potential for replacing a battery with a solution that enables the device to be powered by its surrounding energy. This facilitates battery-free sensor applications, contributing to a more environmentally friendly approach [6].

Wireless detection systems are widely used in various fields, such as aerospace applications, defense, soil mapping, substance detection, healthcare, transportation, and logistics, among others. The amount of energy reflected by the target depends on the material properties of the object, its geometry, angle of incidence, distance from the transmitter, transmitted energy, and operating frequency. An overview of how these systems are integrated into people's daily lives is illustrated in Fig.2.1. Wireless systems are multidisciplinary and include fields such as electrical engineering, RF, mechanics, chemistry, physics, biology, environmental science, and more. Many of these wireless systems organize and streamline human life. In this context, data can be obtained remotely from a

target (such as a toxic gas leak, for example), and action plans can be devised with precautions to ensure the safety. One of such reading systems can be a radar or RFID system, where the target is a sensor.

Figure 2.1: Schematic illustration of wireless sensors for environmental monitoring, human monitoring, industrial production, and daily life [7].

A change in the state and properties of the sensor can be read and subsequently manipulated to generate a useful result. There are essentially two elements. The transducer element is the focal point, responsible. The instrumentation system is the detection part required to convert the changes in the transducer element's composition during interaction with the substance. It consists typically of electrical connections and electronic systems that interpret the sensor element's output, such as changes in resistance, voltage, current, etc., into a readable quantity. The output is presented as a relation of the variation of the studied property over time (or frequency) [8].

Existing detection techniques have been divided into two categories. One technique focuses on wired-based detection, while the other is a wireless-based technique. Wired-based sensors are already well-established, but wireless-based detection systems are increasingly prevalent in modern applications, as shown in Fig.2.2.

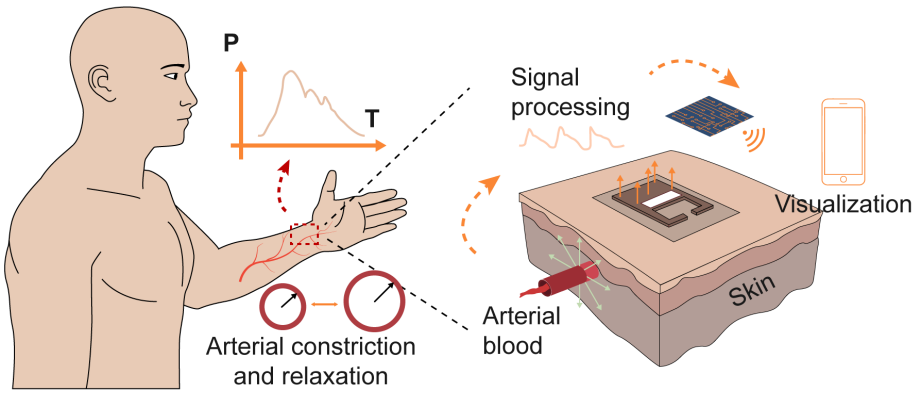

(a)

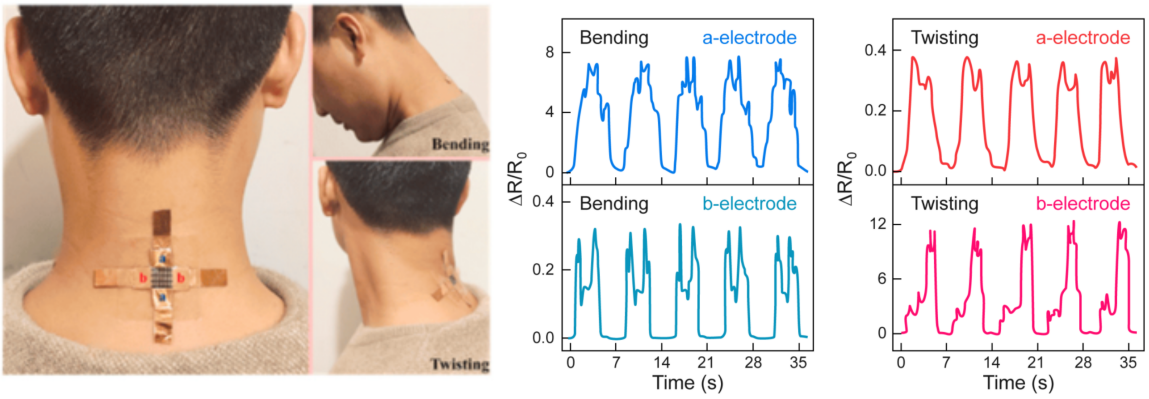

(b)

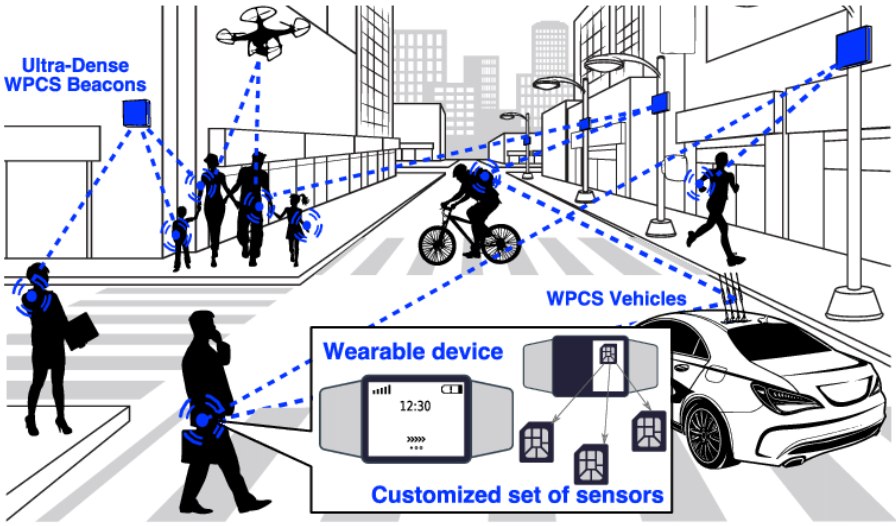

(c)

Figure 2.2: (a) Self-powered and multi-mode flexible sensing film with patterned conductive network for wireless monitoring in healthcare [9]; (b) The beating of the human heart causes the radial artery vasodilatation, resulting in a slight pressure change on the skin surface [10]; (c) Wirelessly powered urban crowd sensing [11].

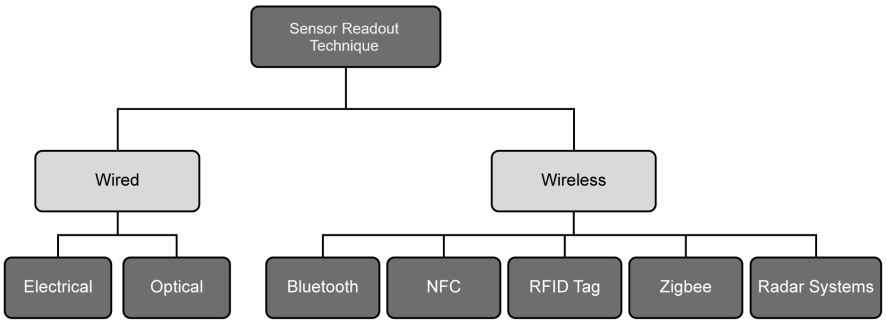

Figure 2.3: Types of sensor readout techniques [12].

Wired detection utilizes physical connections between the components of the instrumentation system involved in the detection process. Such detection system has its advantages and disadvantages. Being easily available, and with limited development in the field of wireless communication in the past, the wired-based detection technique has been implemented in two ways mainly, based on electrical or optical physical connections from the detection system to the power source and the signal output system, as synthesized in Fig.2.3. A variation in current, voltage, frequency or impedance provides the required electrical output signal value, which can be an image of any change in optical wave (light intensity, phase, frequency). Wireless detection also involves the use of electronic instrumentation to transmit and receive RF signals [13], [14]. Due to advancements in Microelectromechanical Systems (MEMS) technology, digital electronics, and wireless communications, significant progress has been made in the field of sensors, particularly considering their size and passive nature [15].

The wireless detection technique has been widely utilized, with numerous advancements in the readers and antennas employed for signal transmission and reception. In this context, notable technologies include Bluetooth, Near Field Communication (NFC), RFID, and Zigbee [16]–[18]. NFC is a battery-free platform and is read by an Ultra-High-Frequency (UHF) RFID reader. It links powered devices using a short-range backscatter communication mechanism. Radio-Frequency Identification (RFID) technology is based on wireless communication. The use of RFID tags spans various sectors such as healthcare, environmental pollution monitoring, food safety, public transportation, logistics, and more. The RFID system consists of two fundamental components: a memory microchip (tag) that stores electronic information and a network of readers connected via antennas for receiving and analyzing signals. In Fig.2.4, a query signal was emitted by the network analyzer at an energy level to activate the sensor tag under the electromagnetic field condition of the reader's antennas. The signal was processed and subsequently redirected back at another

energy level.

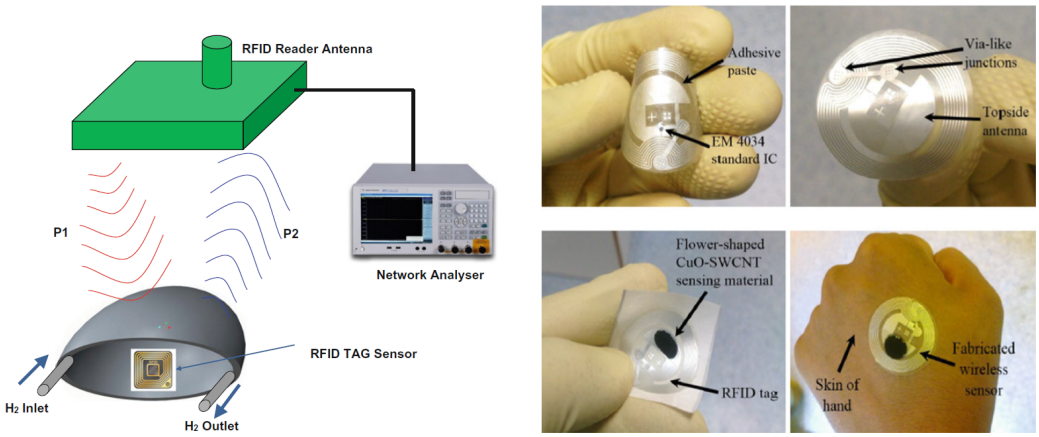

(a) (b)

Figure 2.4: (a) Schematic diagram of hydrogen gas sensing by the UHF-RFID tag sensor system having RFID sensor tag and antenna; (b) RFID tag on the flexible substrate [19]

.

Chipless wireless sensors and various transduction schemes

Wireless sensors can be classified into two categories: active and passive. Active sensors are types of sensors powered by batteries and are typically integrated with other electronic devices, such as batteries, microcontrollers, and energy harvesting circuits. These sensors offer the advantage of being readable at greater distances and they are able to process more data. However, these devices are expensives and with a limited autonomy. Some popular examples of such sensors are the CC3200 based on the Texas Instruments IoT platform and sensor tags from CAO Gadgets LLC [13]. On the other hand, passive sensors do not require a battery, depending on whether they have an integrated active chip. These can be classified into chip-based and chipless sensors. Chip-based sensors obtain the necessary power for chip activation through energy harvesting or through the interrogation signal sent by the reader [20]. Commercial RFID tags, for example, use this principle. The interrogation signal is used both for the radio front-end reception and for transmitting the identification signal through the modulated signal backscattering scheme. On the other hand, chipless radiofrequency sensors offer the benefits of a longer lifespan and a lower cost compared to chip-based sensors [21].

A comprehensive classification of chipless radiofrequency sensors based on their operation is illustrated in Fig.2.5. Here, low-frequency chipless tags are read using time and frequency domain analyses, traditionally in the near field, with LC coupling circuits. For tags at higher frequencies,

principles of radar, backscatter, and delay lines are used as interrogation techniques. In this work, the interest and focus is on passive sensors without chips and at higher frequencies in the Very-High-Frequency (VHF) band.

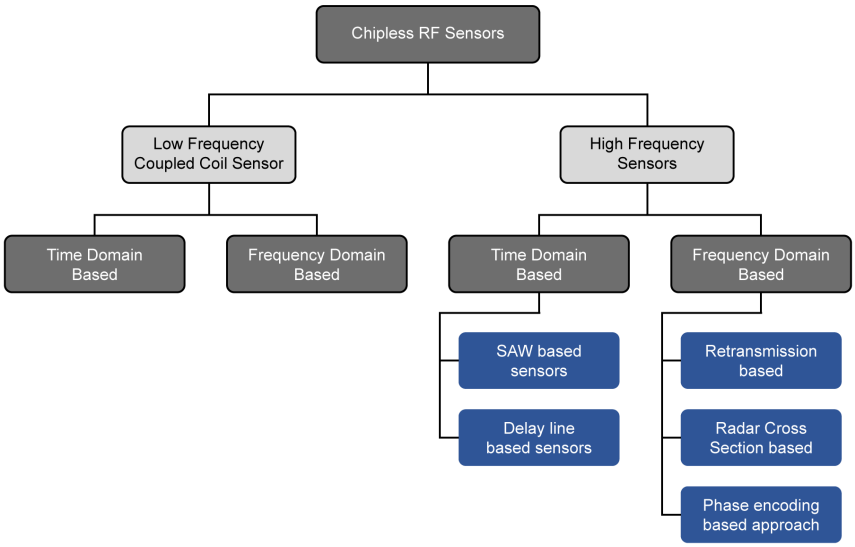

Figure 2.5: Chipless passive RF sensors classification based on their principle of operation and interrogation. [13]

2.1.1 Radar systems

Radar technique is used in many applications such as level measurement, obstacle detection for automobiles, meteorology, military, etc. The small amplitude signals received by the interrogator will therefore have to inform us about physical parameters such as the distance between the radar and the sensor, but it can be also about a pollutant detection value coming from the scanned measurement cell. Extracting such dual information in the case of a chemical sensor, or other multiple parameter depending on the application, is important and involves an exploration of solutions to bring out the interrogator design. By a combination of the waveforms used and the choice of radar technology, the conditions for remote measurements can be satisfied. The backscattering of the radar wave by the sensor is a function of its reflection parameters. If the input reflection parameter varies with the pollutant, the Radar Cross Section (RCS) level also varies and the measurement can be detected by the radar reader. The fundamental components of radar systems consist of a transmitter, receiver, and antennas. The transmitter generates an electromagnetic signal, which is transmitted into space through an antenna. When the transmission signal encounters an object, it is reflected, and the reflected signal can be detected by a receiving antenna in the radar system, as shown in Fig.2.6. The received signal is then processed to extract

information (such as velocity, RCS, distance, etc.) about the target [22].

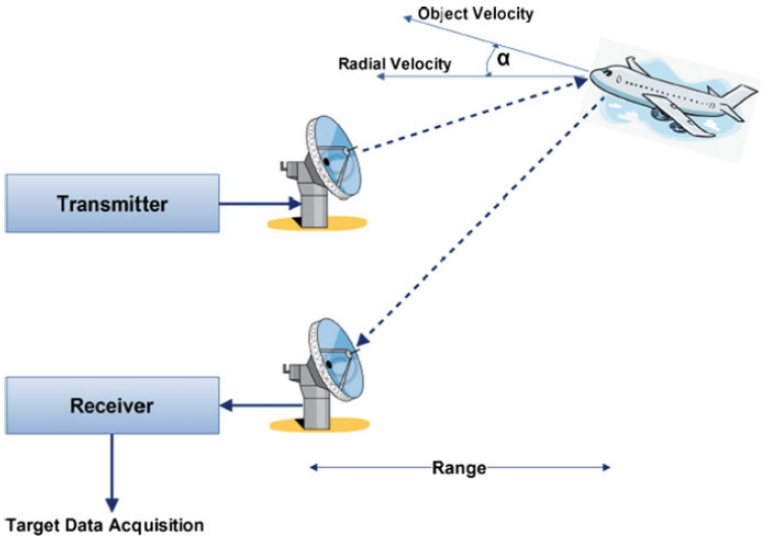

Figure 2.6: Basic radar concept [12].

Radar equation

Radar range is a key point for interrogating sensors. It will depend on several factors inherent to the technical specifications of the radar and its environment. The transmission power levels of the radar to be carried out must be sufficient so that each sensor in the network can be detected and measured at distances of several meters, depending on the techonogy and aplication. These levels will depend on the operating frequencies of the radar system, the RCS of interrogated targets, as well as environmental disturbances around the sensor network. The maximum range R_{max} is identified as the distance at which the radar can detect the minimum power level [23], [24], according to the

$$R_{max} = \sqrt[4]{\frac{\lambda^2 G_t G_r \sigma P_t}{(4\pi)^3 (kTBF)(S/N) L_s L_{atm}}}. \tag{2.1}$$

Here, R_{max} is for the maximum radar range in meters, λ, the wavelength in meters, G_t and G_r, the antenna gain during transmission and reception respectively, σ, the RCS, P_t, the maximum transmitted power, k, the Boltzmann's constant, T, the reference temperature, B, the reception bandwidth, F, the noise factor during reception, (S/N), the signal-to-noise ratio, L_s and L_{atm}, the system and atmospheric losses, respectively.

Radar cross section

The most common RCS measurement technique consists of the relationship between the power transmitted and sent back by the target in the far field using the S parameters acquired with a VNA. The RCS is the ability of a target to radiate electromagnetic energy received from the radar. It is the expression of the ratio of the energy re-emitted to the density of energy received per unit area [25]. The RCS depends on the wave polarization, the radar wavelength, the reflecting surface of the target and its constitutive materials. It is expressed in m^2 or in its logarithmic form in dBsm (decibels referenced to a square meter). The RCS to a given object is expressed by

$$\sigma = \lim_{R \to \infty} 4\pi R^2 \frac{|E_r|^2}{|E_i|^2}. \tag{2.2}$$

Here, σ is the RCS (m^2), E_r, the energy reflected back to source and E_i, the incident energy [22], [26]. The RCS of a target can be viewed as a comparison of the reflected signal from the target to the reflected signal from a perfectly smooth sphere of cross sectional area of 1 m^2. Measurement of an object's RCS is done by inversely using the radar equation, which links the received power to the transmitted one for a distance R and the gain characteristics G of the radar's receiving and emitting power and its wavelength λ, as in this expression:

$$\sigma = \frac{4\pi^3 R^4 P_r}{\lambda^2 G_t G_r P_t}. \tag{2.3}$$

The basic setup of two RCS measurements are represented on Fig.2.7 and 2.8, in monostatic configuration (one single antenna to transmit and receive signals) and in bistatic configuration (one antenna to transmit and another one to receive). For targets with simple shapes, like spheres, cylinders, metal plates and reflectors, the RCS can be expressed analytically as a function of several parameters, such as frequency and observation angle, then calculated. These objects can be useful as a known RCS reference, they provide a way to estimate a RCS of any remotely interrogated object, by calculating the corresponding power ratios [22].

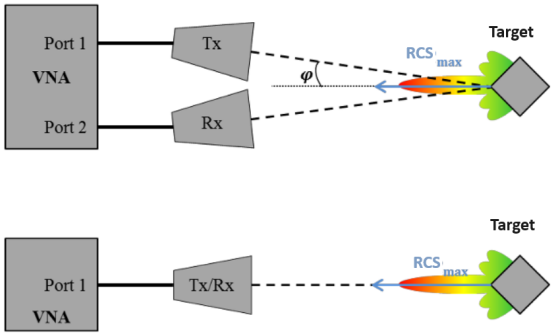

Figure 2.7: Configurations of the two possible measurement benches: one or two antennas for transmitting energy and receiving the reflected one [27].

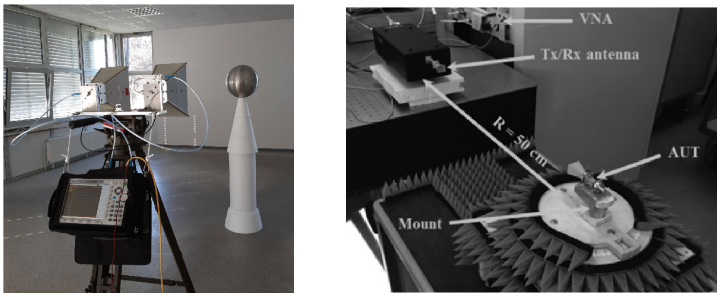

(a) (b)

Figure 2.8: (a) Bistatic RCS measurement unit [28]; (b) Monostatic setup to measure a loaded horn antenna. The T_x/R_x antenna and the AUT put on the support are aligned with a laser beam [27].

2.1.2 Electromagnetic coupling

Passive RFID tag

Passive RFID tags are the most widely adopted and have shown significant growth in terms of units sold in recent years. The frequency range most commonly used is between 860 and 960 MHz. At these frequencies, the preferred mode of operation for RFID systems is the far field. This allows for greater reading ranges to be achieved. A tag typically consists of a dipole-type antenna designed to capture electromagnetic radiation. This antenna is engineered to have an impedance compatible with that of the chip, which is directly connected to its terminals. The overall diagram of the principle of a RFID system is depicted in Fig. 2.9. Passive tags operate without a battery, relying on the electromagnetic field from the base station to power the tag's chip [20].

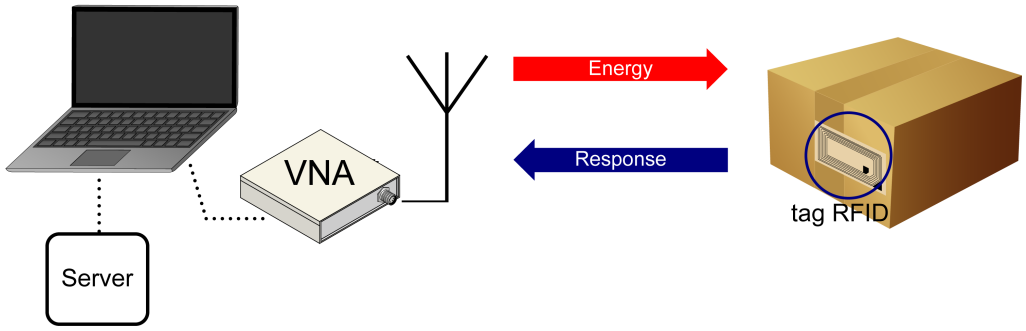

Figure 2.9: Operation principle of a RFID system [29].

The interaction between the tag and the reader is modeled by two voltage sources, as shown in Fig.2.10. At the tag level, the quantity $V_{bs}.K_1$ represents the voltage across the reader antenna radiation resistance (V_{bs}) multiplied by a factor K_1, which includes free-space attenuation, radiation efficiency, polarization efficiency, mismatch losses, and gain of both the reader and tag antennas. When approximating the far-field region, this factor K_1 decreases by 1/R as a function of distance. Similarly, the interaction of the tag with the reader is modeled by a voltage source of magnitude $V_{tag}.K_2$. The term V_{tag} represents the voltage across the tag antenna radiation resistance. This voltage depends on the voltage detected by the tag ($V_{bs}.K_1$) and the impedance state of the chip. The term K_2 is equal to the term K_1 if the reader antenna is used for both transmission and reception (principle of antenna reciprocity). Quantifying these terms is of interest for establishing link budgets and estimating reading ranges [29].

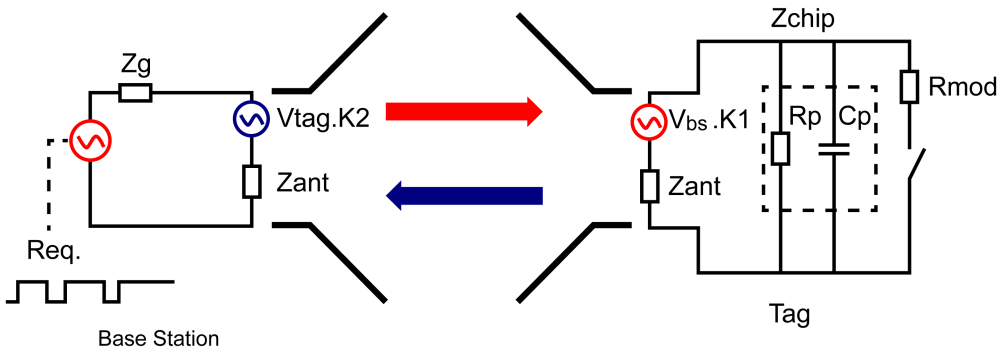

Figure 2.10: Operation principle of a passive tag. [29]

Up to this point, optimal energy transfer to the chip has been considered. Fig.2.11 represents the equivalent electrical diagram that models the energy transfer between the chip and the antenna in the matched (a) and short-circuited (b) cases. To maximize the energy transfer from the tag antenna to the chip (or load), complex conjugate matching must be achieved [30], [31]. In the case

of complex conjugate matching, half of the energy is dissipated in the chip (the real load), and the other half is dissipated in the antenna resistance, which typically consists of two parts: a radiation resistance and another loss resistance modeling losses in the antenna (Joule losses and dielectric losses).

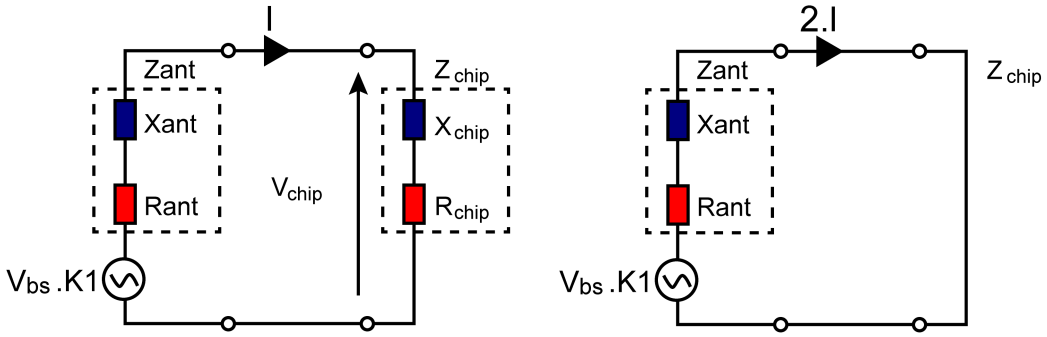

(a) (b)

Figure 2.11: (a) Adaptation of the antenna to the chip in non-modulated mode; (b) Equivalent circuit when the chip is modulated (parallel short-circuit)[29].

.

The principle of generating the tag response to the reader is based on the variation of backscattered power between two very distinct states. The base station detects a signal whose variation is directly dependent on the impedance state variation of the load. The tag antenna is a key element that directly influences its reading range. The design of an antenna must take into account parameters such as efficiency, matching, and radiation pattern. Size constraints and the environment often impose performance limits. The increase in the tag's reading range depends on the antenna gain. There is a trade-off between the antenna size, its operating frequency, and its radiation characteristics [32]. To determine the detection ranges, it may be interesting to use the antenna's RCS, which is a parameter linked to its geometry on the one hand (structural mode) and to its load (antenna mode) on the other. The RCS represents the area that would capture the power density transmitted by a source located in the far field at a distance R and re-emit it into space, all in the far-field approximation [33].

RFID technologies cover different principles. Basically, two key elements are found in an RFID tag, namely an electronic chip connected to an antenna. Chipless RFID is a technological variant that breaks away from the communication scheme used by radio frequency identification systems. With no electronic components, typical communication protocol such as amplitude or phase modulation using clock-based synchronization, used in conventional RFID technologies, is

not possible. The physical principles implemented for chipless RFID tag design are varied and can be classified based on how their electromagnetic signatures are utilized. The approaches used are most often temporal, frequency-based, or based on a radar principle. A chipless RFID tag can be seen as a static radar target with a specific electromagnetic signature. The design of a chipless RFID reader, therefore, resembles an airborne radar that detects the signature of flying machines, scaled to the dimensions and power involved [34].

2.2 Surface acoustic wave sensor (SAW)

Radar systems and electromagnetic coupling have been successfully employed in the field of wireless sensors with purely electromagnetic response. As the aim of this work is to develop a wireless system using Love wave-based SAW sensors, it is necessary to understand the main characteristics of these devices, mainly used in wired configuration, and also how wireless reading has been achieved with them. This will be discussed in the following section.

2.2.1 Wired interrogation

Currently, chemical and biochemical detection has become a significant research theme, and many SAW/Bulk Acoustic Wave (BAW) sensors have been developed and investigated for such applications. The LW sensor, for example, is widely studied due to its high sensitivity in liquid detection [1]. The principle of SAW sensors based on Rayleigh and Love waves (the most representative ones) can be seen in Fig.2.12.

When the acoustic wave is perturbed due to the presence of additional mass or changes in properties such as viscoelasticity and other surrounding physical parameters, it results in the modification of its operating frequency, gain, and phase. Therefore, the detection of different substances is enabled by analyzing these electrical parameters through the S_{ij} parameters. In our case, with a two-port sensor, S_{21} (or S_{12}) and S_{11} (or S_{22}) represent the sensor responses in transmission and reflection, respectively. In 1979, Wohltjen and Dessy first applied and used chemical (gas) sensors based on SAW devices [35]. Since then, various sensors using the same principle have been developed and applied to detect various substances, such as CH_4, NO_2, CO_2, etc [36], [37].

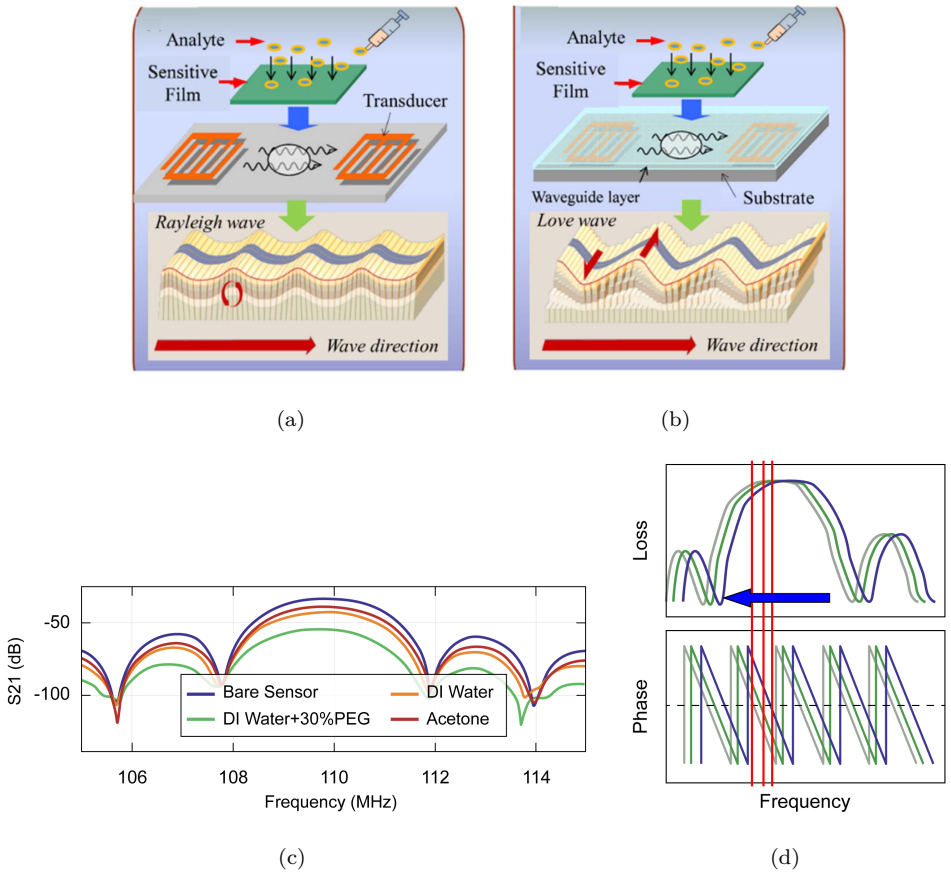

Figure 2.12: SAW sensing: Schematic of (a) Rayleigh wave, having both surface-normal and longitudinal components with respect to propagation direction; (b) Shear-horizontal (SH) LW sensing principle, an added guiding layer confines most of SH vibration close to surface [38]; (c) LW liquid detection based on S_{21} magnitude attenuation and resonance frequency shift [39]; (d) LW detection principle based on S_{21} magnitude resonance frequency shift and S_{21} phase shift [40]

.

In addition to applications in gas environments, SAW sensors are also utilized with liquids. In this case, they predominantly involve waves with horizontal polarization, as vertical components rapidly attenuate in the presence of liquids. In this context, SAW and LW devices have garnered interest among the scientific community. Among the liquid phase applications are those in the field of biosensors for the detection of Deoxyribonucleic Acid (DNA) with the potential for remote interrogation [41]–[44]. They have also been employed for the detection of proteins such as streptavidin, cardiac troponin I, antibodies, and Carcinoembryonic Antigen (CEA) [45]–[47]. More recently, some sensors have been applied for the detection of the COVID virus [48]. Other applications involve microfluidic devices, liquid flow, concentrations of saline solutions, electronic tongue technology, identification of fruit juices, pH measurement, and water quality [49]–[55]. In Fig.2.13 two examples of experimental platforms for liquid applications are represented.

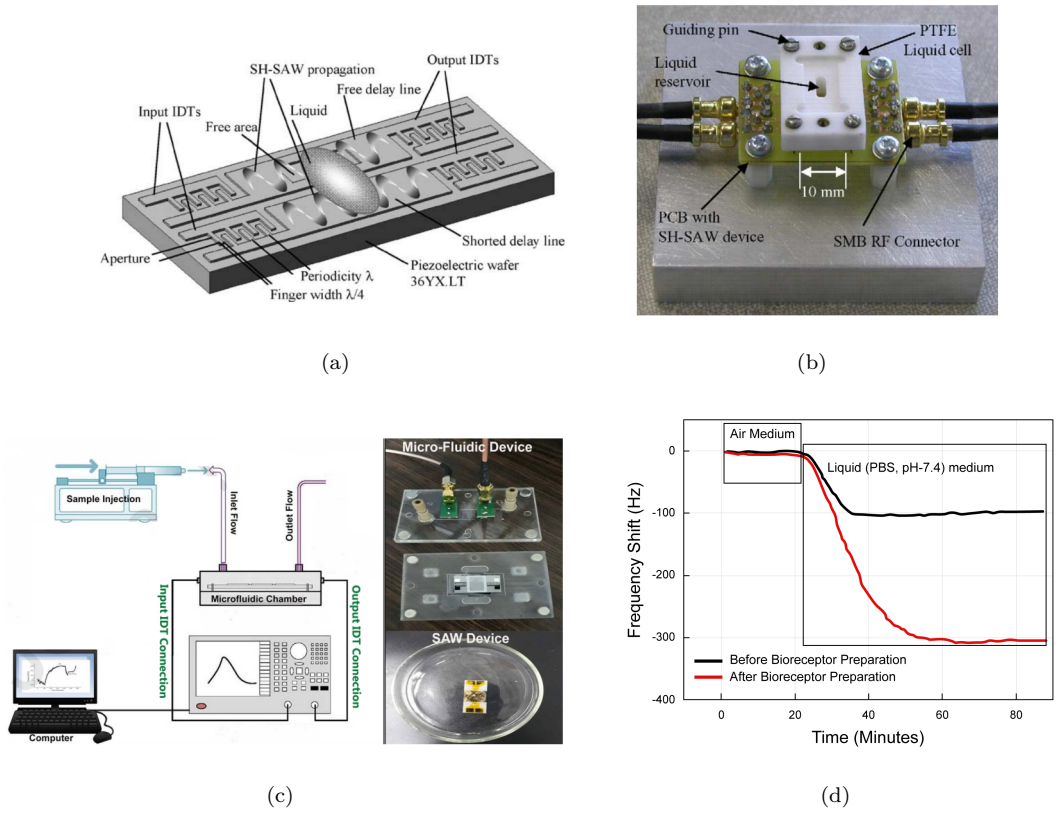

(a) (b)

(c) (d)

Figure 2.13: SAW wired sensing: (a) Schematic of dual-delay line SH-SAW taste sensor; (b) Photograph of miniature total analysis taste system or electronic tongue; (c) Biosensing set-up, microfluidic device and SAW device; (d) Resonance frequency shift of SAW device under air and liquid injection [47], [52].

.

LW sensors have enabled the detection of very low concentrations (metal ions Cd^{2+}, Hg^{2+} were successfully detected in the concentration range from 10^{-10} M to 10^{-4} M) of heavy metals in liquid medium [56]. Numerous studies have been conducted on the measurement of viscosity, turbidity, pollutants, poly(ethylene glycol), and bacteria with good reproducibility and sensitivity [57]–[63].

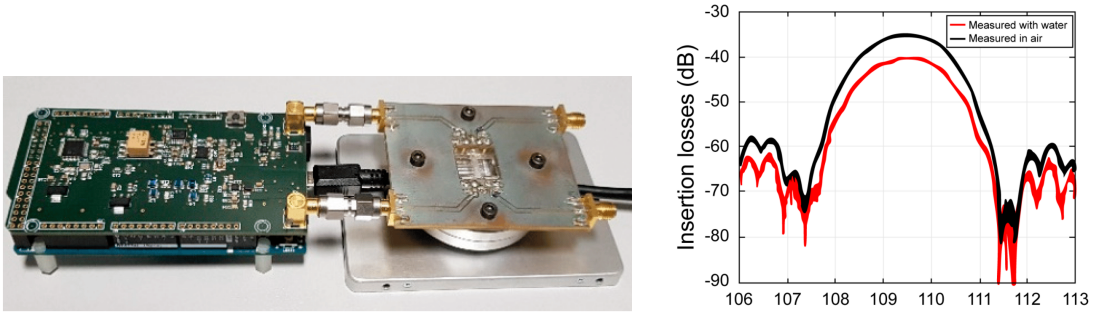

(a) (b)

Figure 2.14: LW wired sensing: (a) Readout electronic circuit operating with a LW sensor; (b) S_{21} frequency domain responses of the LW sensor in air and water media measured with a VNA [59].

Love wave sensor global response

Before delving into the architectures and interrogation techniques for chipless sensors in this chapter, it is proposed to start with the operational principle of the Love wave sensor utilized in this work. Initially, the focus will be on identifying the physical phenomena that constitute the sensor's response during interrogation. These phenomena include energy flows (electromagnetic and acoustic) occurring within the device and are pivotal for comprehending how these devices are perturbed and determining which remote interrogation techniques are more suitable. The detailed description of the sensor itself, as used in this study, can be found in Chapter 3. The flows of electromagnetic and acoustic energy can be examined by viewing the sensor as a multiphysical target that undergoes variations in its energy flow when disturbed.

Initially, the Interdigital Transducers (IDT) can be likened to a planar interdigital capacitor. Consequently, the variation in the electric field and the energy conduction path of this structure is altered when there is an electrical disturbance in the environment. Interdigitated capacitors are widely employed sensors for chemical detection based on the variation in their electrical impedance [64], [65]. The impedance of an IDT is modeled by an equivalent electrical circuit comprising basically a static input capacitance and a radiation impedance related to the generation of the electroacoustic wave. The radiation impedance is associated with the mechanical parameters of the transducer materials, and more specifically the piezoelectric substrate. This acoustic wave propagates along the acoustic path, being attenuated and delayed based on the material and environmental parameters. The induced electromagnetic coupling between the input and output IDTs generates a third energy path. In this context, three energy flows are evidenced: input

capacitive impedance, electromagnetic coupling, and acoustic propagation.

In Fig.2.15, we provide an overview of these energy flows due to the physical mechanisms in the sensor and their influence in terms of the S parameters. As demonstrated in [5], the S_{11} parameter is linked to the input IDT impedance and is sensitive to the electrical and mechanical parameters. A disturbance at the input IDT (port1) causing a modification of the S_{11} parameter, which represents the energy reflection at the input, will also result in a modification of the S_{21} parameter, which represents the energy transmission between the input and output transducers. This applies similarly to port 2 (output IDT), and consequently to the S_{22} and S_{12} parameters. The energy flow paths from the input to the output of the sensor (electromagnetic coupling and acoustic wave) are disrupted by the dielectric and acoustic properties of the medium. The propagation time of the electroacoustic wave between the input and output IDTs is in the order of a few microseconds, while the electromagnetic coupling establishment time is almost instantaneous (far shorter than the acoustic wave, with a velocity 10^5 times faster). Therefore, it is possible to separate these two energies (electromagnetic and acoustic) using time gating to isolate and identify each of them.

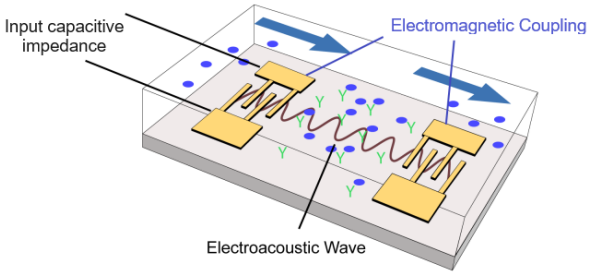

(a)

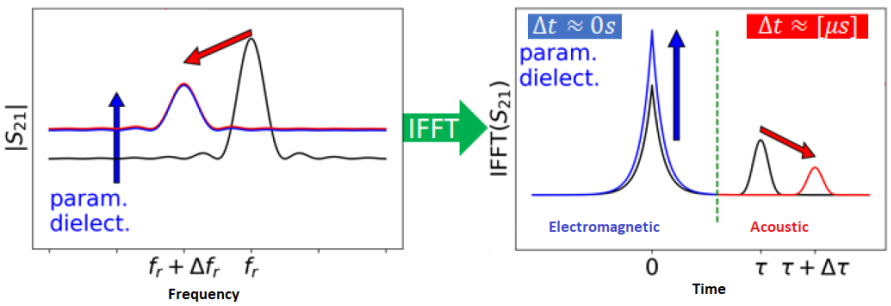

(b)

Figure 2.15: (a) Acoustic and electromagnetic wave propagation and the input capacitive impedance of the LW sensor; (b) Physical parameters of a liquid influencing the LW device transmission response (S_{21}) of the LW sensor. Decomposition of the temporal signature of the delay line configuration [5].

.

This LW sensor is based on a quartz substrate with a low electromechanical coupling constant, and the current device exhibits high transmission losses, making it uneasy to use the S_{21} signal for remote and passive reading. This could be considered based on SAW sensors with low energy losses in signal transmission, such that the energy at the sensor output is detectable by a receiver. In addition, there are issues related to impedance matching that affect the energy flows and that will also play a role in targeted wireless interrogation. As a consequence, the S_{11} signal is also of interest and could even facilitate further wireless interrogation, similar to the reading techniques used in chipless RFID. Not surprisingly, as exhibited in recent research results, such sensor has been promising in utilizing the sensor's electromagnetic energy to detect variations in the sensor's input impedance and its correlation with the substance deposited on its surface [5]. Furthermore, the objective in this work is not to focus solely on the acoustic aspect, which is already well documented in the literature as indicated in the Section 2.2.2, but also to explore variations in the sensor input impedance and the electromagnetic coupling of the LW sensor, especially in a wireless reading. In this context, this work is moving towards utilizing the LW sensor in a passive and wireless interrogation system, not focusing on its traditional acoustic response but rather on the additional electromagnetic one. If a variation in the impedance of the sensor or in the coupling capacitance between the IDTs is observed, it can be treated as a target, allowing interrogation similar to radar or some backscattering technique.

Main applications

SAW sensors exhibit a wide range of applications, extending beyond sensor functionalities to include roles as filters and oscillators. These versatile applications are enabled by employing piezoelectric components as the core of device development. SAW sensors find widespread use in diverse fields such as mechanical, chemical, electrical, physical, and biological applications. In Tab. 2.1, the extensive scope of applications is evident, primarily attributed to their multi-parameter measurement capability. Sensors equipped with SAW technology demonstrate high sensitivity in detecting and classifying various substances.

Table 2.1: Classification of SAW sensing applications and associated detection parameters

Domains	**Mechanical [66], [67]**	**Biological [68]–[71]**	**Chemical [72]–[75]**	**Gas [2], [76]**	**Microfluidics [77]–[79]**
Applications	Structural health monitoring Powder transportation	Cancer cells Antigen-Antibody Biotoxins	Vapors Warfare agents and Explosives	Organic and inorganic vapors	Liquid sensing Contaminants Fluid manipulation
Detection Parameter	Density Conductivity Acoustic modulus Temperature	Mass Viscosity Density Conductivity	Conductivity Viscosity Pressure Temperature Density	Conductivity Pressure Temperature	Viscosity Conductivity Density

One pivotal domain where SAW sensors have made significant contributions is in biosensors. Extensive research has been conducted on the detection of cancer cells, antibodies, antigens, blood materials, and toxins in liquid media. In gas applications, SAW sensors have proven instrumental in detecting vapors in the industrial sector, as well as identifying explosives and toxic gases. Over the past few years, these sensors have garnered attention in the microfluidics sector, particularly in medical applications for the control, administration, and classification of pharmaceutical drugs [76].

2.2.2 Wireless interrogation

The early designs of chipless and time-encoded tags quickly transitioned to the use of piezoelectric substrates such as quartz (SiO_2) or lithium niobate ($LiNbO_3$). SAW filters are commonly used to produce compact and high-order RF filters. In these devices, the piezoelectric effect is utilized to transform an electromagnetic wave into an acoustic wave. To achieve this, a pair of wave-carrying conductors is connected to a transducer consisting of IDT's deposited on the piezoelectric substrate. The propagation velocity of the acoustic wave is in the range of 3000 to 5000 m/s, or 100000 times slower than the speed of electromagnetic wave. This makes it an ideal component for creating a delay line. SAW tags consist of an antenna directly connected to an electroacoustic transducer. A wave in the form of a short electromagnetic pulse is transmitted by the reader and captured by the tag's antenna. The wave energy is converted into acoustic wave that propagates slowly through the substrate. Reflectors are positioned along its path to generate reflections toward the antenna, which are then converted back into electromagnetic waves and re-irradiated towards the reader, as shown in Fig.2.16. The reflectors are typically metallic elements with various geometric configurations, deposited on the piezoelectric substrate [80].

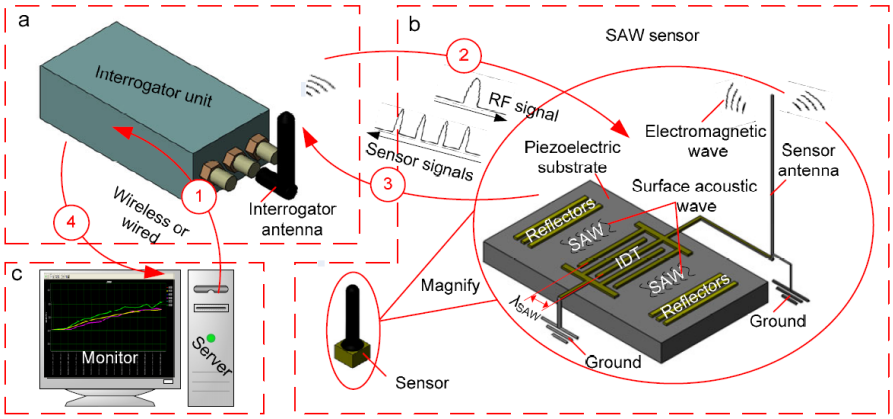

Figure 2.16: Wireless passive surface acoustic wave sensing measurement system[81].

In addition to being small, simple, and robust, SAW devices can operate without a battery when wirelessly interrogated [82]. These devices have been widely used as standard RF communication components, SAW sensors, and their reading units can be cost-effective with several commercially available solutions [83]–[85]. SAW sensors operated wirelessly are especially interesting for applications in harsh environments, being used in backscatter mode and controlled by the RF reader located at a fixed point. Two configurations have been the most commonly employed:

- Reflective delay lines (R-DL): an antenna is connected to the IDT with reflectors on the propagation path surface, as shown in Fig.2.17. The interrogation system sends electromagnetic energy to the sensor. The IDT converts the electromagnetic pulse from the antenna into acoustic energy, which propagates on the sensor's surface and has part of its energy reflected based on the acoustic impedance difference. This reflected energy is transformed back into an electromagnetic wave by the IDT and the antenna, directed towards the interrogator. If environmental parameters are altered, it is possible to observe a variation in time between reflected waves and a variation in magnitude. It is essentially a time domain analysis that, based on reflections, makes it possible to identify various sensors. For wireless R-DL (and considering that the round trip times are quite slow and the objective of this configuration to work with strong acoustic signals) it is crucial to use substrates with high electromechanical coupling coefficient (k^2) and low propagation loss. For example, the quartz substrate has a k^2 on the order of 0.12%, and $LiNbO_3$ has it on the order of 5.0%. Therefore, more electromagnetic energy is converted into acoustic energy for the $LiNbO_3$ substrate and vice versa. From this constant, one can analyze the figure of merit concerning the possibility of wireless reading [86]. The reflections obtained and separated over time create a sort of

geometrically executed barcode on the plate. The challenge for the designer is to create a physical structure with the IDTs and substrates in such a way that the reflection peaks have the same amplitude.

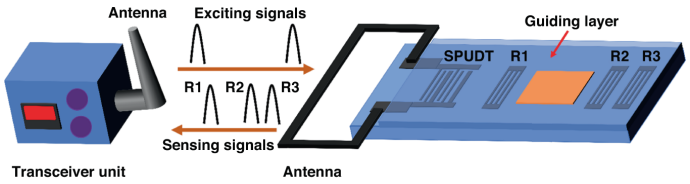

Figure 2.17: Principle of a wireless SAW sensor in reflective delay line configuration.[87]

- Resonators: an IDT is placed between two Bragg acoustic mirrors to form a resonant device, as depicted in Fig.2.18. The sensor is interrogated at a frequency close to its resonance frequency. When the signal is withdrawn, the resonator continues to oscillate freely for a period of time at its natural frequency, which depends on the environmental parameters. In addition to the k^2, this configuration can be optimized based on the sensor's quality factor (Q). With a higher Q, it is possible to achieve a narrower frequency bandwidth. In this sense, the product Q x k^2 allows determining the backscattering efficiency of the sensor. The higher this value, the more acoustic energy is efficiently converted into electromagnetic energy, and the greater the reflected energy, directly influencing its ability to be remotely interrogated.

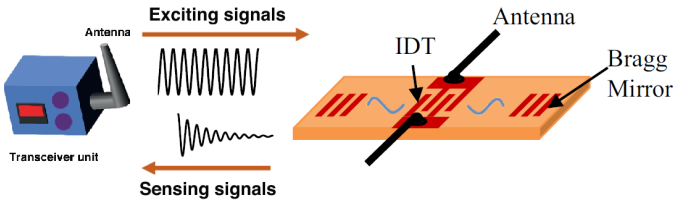

Figure 2.18: Principle of a wireless SAW sensor in resonator configuration[2].

SAW-based wireless setups

Acoustic waves can be generated from the electroacoustic conversion of a RF electromagnetic signal received at an antenna coupled to its terminals, as shown in Fig.2.19. Wen *et al.* utilized a wireless SAW R-DL gas sensor with Teflon Amorphous Fluoropolymer (AF) as the sensitive layer for CO_2 detection [88]. Lim *et al.* developed a remotely controlled SAW R-DL sensor for the detection of both NO_2, CO_2, along with temperature measurement [36]. Xu *et al.* designed a wireless SAW sensor for the detection of organophosphorus compounds, demonstrating linearity and reproducibility [89]. Murphy *et al.*, presented the development of a fully implantable wireless

sensor capable of providing continuous and accurate pressure measurements in real time [90]. Pan *et al.* developed a SAW-based passive gas sensor for the detection of dimethylmethylphosphonate (DMMP) [87]. Jeltiri *et al.* used commercial SAW devices mounted on steel rebar to conduct an initial feasibility study of wirelessly reading the deformation of a concrete beam subjected to bending load [91].

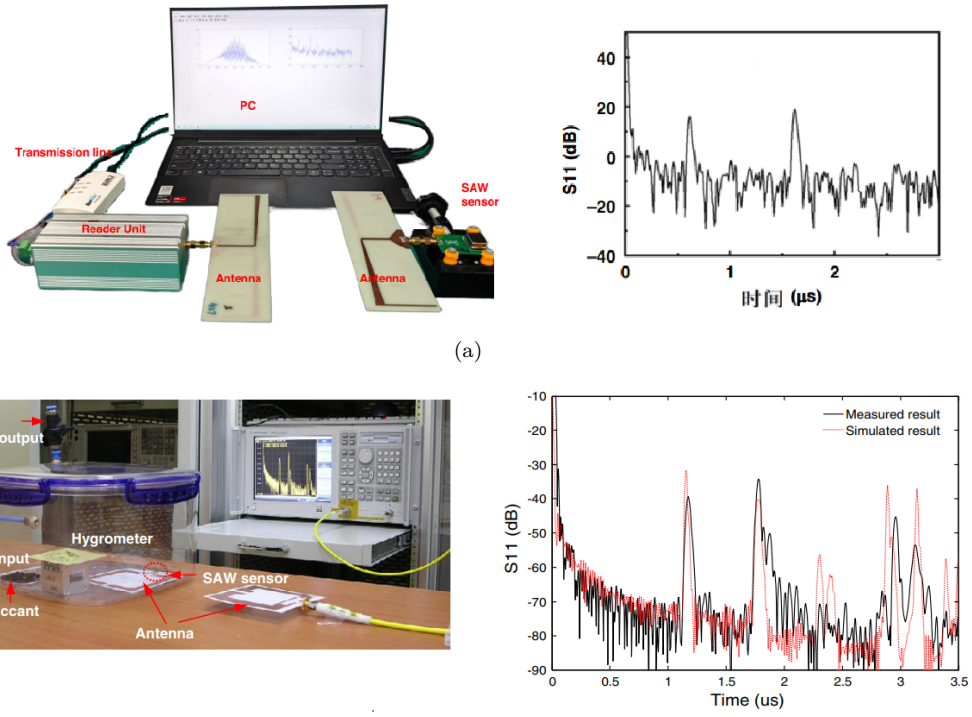

Figure 2.19: SAW wireless sensing: Schematic of (a) Wireless measurement setup of the SAW sensor system; (b) Measured and simulated S_{11} in the time domain of the fabricated sensor in absence of gas infusion[87], [88].

Leonte *et al.* developed a SAW-based system operating in the Industrial, Scientific and Medical (ISM) bands of 433 MHz and 869 MHz that can be remotely interrogated for wireless identification and characterization of bioliquids [92]. Hassani *et al.* proposed a similar system, but at a lower frequency of 262 MHz and they demonstrated the feasibility of detection using SH-SAW sensors [93]. In the works by Oh *et al.* [94] and Song *et al.* [95], wireless interrogation of a LW biosensor was conducted using a polymethylmethacrylate (PMMA) waveguide layer and protein receptor layers on a $LiNbO_3$-based piezoelectric substrate for immunoglobulin detection, as shown in Fig. 2.20. A 440 MHz R-DL, composed of unidirectional transducers and three reflectors, was manufactured as the sensing element. The fabricated devices were wirelessly characterized using a network analyzer as the reading unit. Good linearity, reproducibility, and high sensitivity were observed. Another

advantage is also presented, namely a simple wireless measurement method.

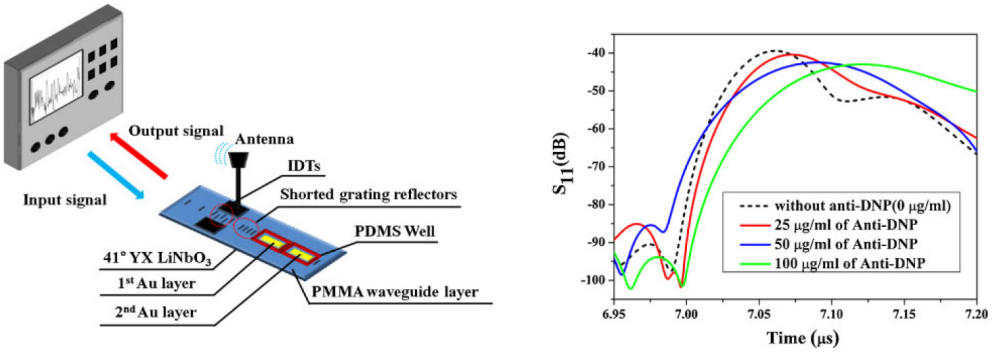

(a)

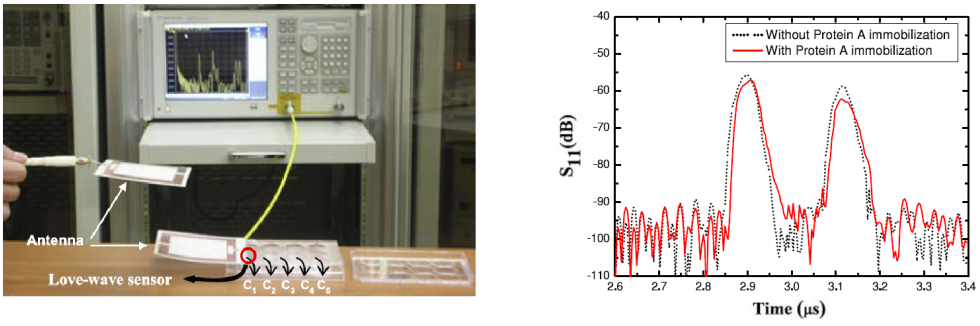

(b)

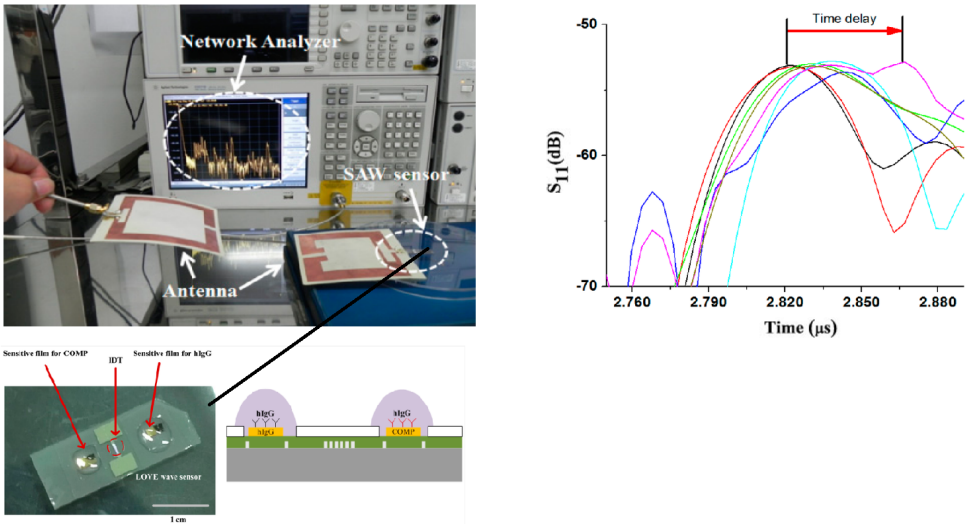

(c)

Figure 2.20: LW wireless sensing: (a), (b) and (c) Schematic of diagram of the wireless LW biosensor system; (a) Measured S_{11} response of the twelfth reflected peak under fixed antibodies anti-deoxyribonucleoprotein (DNP) concentration (6.25 μg/ml) on the first sensitive film and varied concentrations of 25, 50, and 100 μg/ml anti-DNP on the second sensitive film [95]; (b) The measured S_{11} with and without protein A immobilization [94]; (c) Reflection peak was shifted in the time domain; the immunoglobulin G (IgG) concentrations were also varied from 1 to 100 μg/ml [96]

.

The majority of works involving wireless interrogation of SAW sensors are applied in the measurement of physical parameters and gas environments [2]. The performance of experimental reproducibility remains incomplete or not realized in most studies. Despite recent efforts to configure both wired and wireless setups, a detailed comparison between the two setups has not been provided. These studies are still in the research stage and this type of sensor has not yet been commercialized due to the challenges of packaging the sensor in its environment. Furthermore, wireless interrogation of such sensors in a liquid environment is largely unexplored and would require further study. However, it should be noted that wired interrogation in liquid environments is well established.

In this context, there is a challenge in integrating wireless reading of SAW sensors, particularly when focusing on liquid-medium applications, and it remains an area to be explored on various levels. On the sensor side, the focus is on the use of new materials to enhance selectivity and sensitivity to target parameters. On the reader side, the investigation and development of architectures and reliable interrogation techniques enabling remote monitoring with reduced energy consumption (autonomy) are crucial. The operating frequency of the sensors, the test cell and the overall system setup environment are key factors. The VNA has proven to be an excellent alternative for initial testing in wireless systems, given its versatility and accessibility in today's market. As LW sensors are based on the acoustic transduction generated by the piezoelectric phenomenon, both electrical and mechanical parameters can be utilized as sensing data. Through signal processing techniques, it is possible to separate these signals, both in the time and frequency domains, and perform a more comprehensive analysis of the sensor response. In this way, an analysis of the electrical and electroacoustic behavior of the sensor can be performed rather than restricting the measurement interest solely to the mechanical interactions between the sensor and the liquid. This approach is also compelling for remote interrogation of these sensors, as a change in the electrical parameters of a target allows for a remote reading similar to that performed for a passive chipless RFID tag.

Market size

Wireless sensors are devices designed to measure and transmit data without the burden of wired connections. Using technologies such as Wi-Fi, RFID, Bluetooth, and Zigbee, among others, these sensors communicate information to a central system or other interconnected devices. Examples include biosensors and sensors for gas, temperature, pressure, and motion applied in industrial, medical, aerospace, defense, environmental, and agricultural sectors. The primary advantage lies

in their ability to provide real-time data without the limitations imposed by wired systems. In this regard, they facilitate deployment in unconventional, hard-to-reach, and hazardous locations. Additionally, they serve as a fundamental element in the IoT, playing an indispensable role in decision-making processes and increasing connectivity. In 2022, biosensors held the largest market share, accounting for 21% based on sensor type [97]. This category of wireless application involves devices that detect biological/chemical responses and convert them into measurable electrical signals. The trend indicates the emergence of wearable biosensors with the advancement of personalized medicine, enabling continuous health monitoring and faster, decentralized testing. The global market size for wireless sensors reached 18.78 billion of dollars in 2023 and is projected to reach approximately 105.18 billion of dollars by 2032. Fig.2.21 illustrates the global market size in a forecast for 2023 to 2032. In terms of regional markets, North America held the largest share in this revenue, accounting for 38% in 2022, and maintains a substantial stake in the wireless sensor market owing to a robust technological infrastructure, widespread adoption of IoT applications, and a high degree of industrial automation. The Asia-Pacific region is expected to witness the most significant growth and commands a noteworthy share in the wireless sensor market due to rapid industrialization, technological advancements, and the proliferation of IoT applications across various sectors [98].

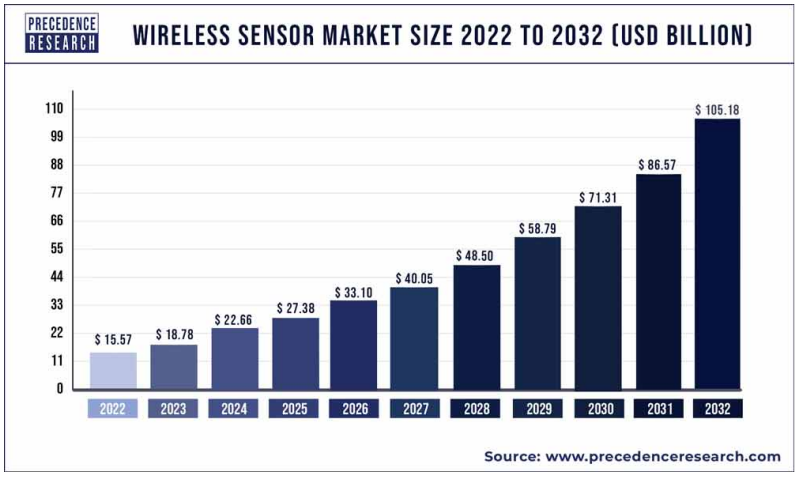

Figure 2.21: Estimated global market for Wireless Sensors from 2022 to 2032 [98].

In a similar context, the global Industrial IoT market benefits from technological advancements in new products within semiconductors and wireless electronic devices. As an example, applications in the fields of logistics, transportation, and healthcare involve solutions encompassing remote monitoring, data management and analysis, and security. In addition, the easy availability of low-cost sensors and processors at an affordable cost aids in providing access to real-time information.

The global Industrial IoT market size was estimated at 320.9 billion dollars in 2022 and is projected to reach approximately 1,562.35 billion of dollars by 2032 during the forecast period from 2023 to 2032. The logistics and transportation sector absorbed the highest share of Industrial IoT in 2022 as companies embraced smart transportation, real-time monitoring, and tracking. Fig.2.22 also illustrates the growth of this market until 2032. It is noteworthy that these two areas are complementary and have been evolving together. As new sensors become available, they are quickly integrated into wireless applications. Simultaneously, with the emergence of more effective reader architectures and techniques, new sensors are also developed to meet this demand. North America asserted its dominance in the industrial IoT market in 2022. Countries in the Asia-Pacific region, especially China, have emerged as global industrial hubs. Similarly, India is experiencing significant opportunities for the industrial sector, with cost-effective labor and infrastructure conducive to establishing industrial units [99].

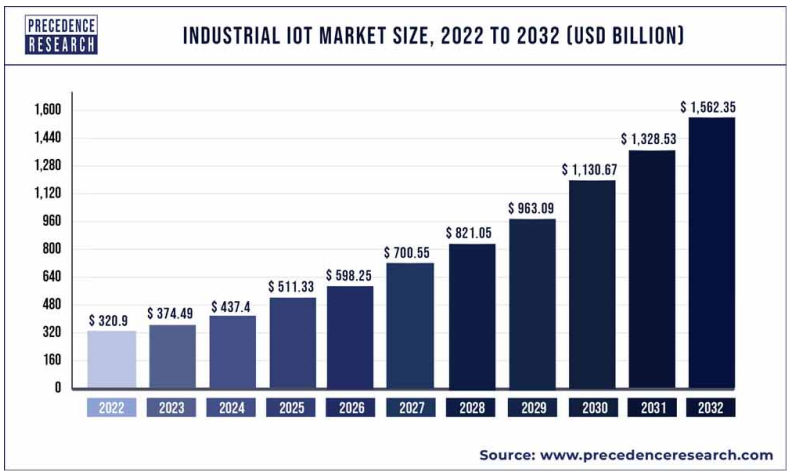

Figure 2.22: Estimated global industrial IoT market size from 2022 to 2032 [99].

A variety of architectures and techniques can be employed to interrogate these sensors, in the time domain, frequency domain, and hybrid approaches. In the next subsection, we will elaborate on some of these techniques.

2.3 Interrogation methods

Currently, SAW interrogator architectures are divided into two categories: Time Domain Sampling (TDS), also known as wideband or wideband sampling, and Frequency Domain Sampling (FDS), also known as narrowband sampling or partial. There is an additional subdivision based on the hybrid concepts of FDS and TDS to consider recent developments, such as the use of Stepped

Frequency Continuous Wave (S-FSCW), pulsed and continuous Frequency Modulation (FM) and Amplitude Modulation (AM). Both architectures have influences from TDS and FDS in terms of concept, front-end and signal processing. The Fig. 2.23 provides an overview of wireless interrogation techniques for SAW delay lines and resonators, based on time or frequency domain, or hybridizing both of them. Each sensor type and interrogator architecture has advantages and disadvantages. Depending on the application, an analysis is necessary to select the most suitable type of interrogator [100], [101].

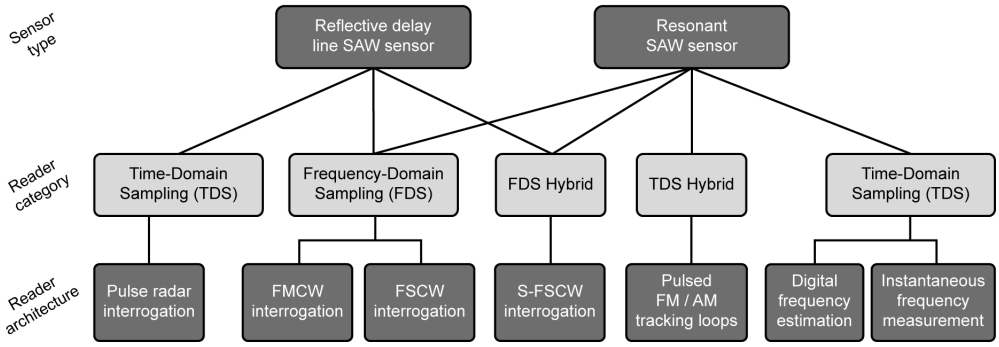

Figure 2.23: Current SAW sensor and interrogator architectures and their classification for wireless detection [102].

For TDS, the read signal spans the entire system bandwidth at once. Therefore, fast sampling on the interrogator and high measurement update rates are required. With FDS, the sensor frequency band is sampled in several steps. Thus, the baseband bandwidth can be narrow, resulting in a simpler, cheaper hardware design with significantly longer interrogation periods than with TDS. Utilizing a FSCW interrogation signal, the FDS technique is comparable to a single-port using the S_{11} (monostatic) or two-ports using the S_{21} measurement (bi-static) in a VNA. When a Frequency-Modulated Continuous Wave (FMCW) interrogation signal is used, the measurement is similar to common FMCW radar systems. Both excitation signals can be used for resonant as well as reflective delay line SAWs devices [102].

For passive sensors based on the resonator-type acoustic transduction principle, the works [103]–[105] used the time domain interrogator category, with a pulse in the UHF band and for an interrogation distance up to 5 m. The transmit power of the reader was 10 dBm and the sensitivity was related to the variation of the resonance frequency or of the insertion losses, applied to the measurement of torque or impedance variation. Other works using a resonator type SAW device used the interrogator category in the frequency domain. For these, the interrogation was carried out with an FPGA module by pulse and with FMCW, in the HF, VHF and UHF bands and for

an interrogation distance also up to 5 m [106], [107].

2.3.1 Time domain

The first generation of interrogators for SAW delay lines was based on the pulse radar principle. A fixed frequency transmitter with RF switches generates a short burst of RF, usually only a few tens of nanoseconds, which is transmitted to the sensor. At the sensor, it is partially reflected and transmitted and leads to a train of delayed non-ovelapping pulses as a response signal [100], [108]. The main advantage of this architecture is that dynamic measurements are possible due to the short interrogation times [109]. However, the high bandwidth is also its disadvantage: the architecture is quite expensive and complex due to the fast sampling and switching circuits required, and the required broadband excitation is not always compatible with the strict limits of the ISM band [110]. Some prototypes were built and evaluated in the works [108], [111]–[115].

In 2017, [81], [116] proposed a wireless interrogation system for SAW delay lines sensors using the time domain interrogator category. In these cases, interrogation with pulsed signals in the UHF range has been employed for temperature measurement (ranging from -20 °C to 40 °C) of SAW sensors at distances of up to 5 m with a maximum transmission power of 10 dBm.

Almost all of today's interrogators for delay line sensors use one of the FDS or hybrid architectures, as they are easier and more cost-effective to implement. However, this may change in the future when the progressive integration of RF chips, software-defined radio solutions, and faster analog-to-digital converters offers more cost-effective implementation options [102].

2.3.2 Frequency domain and hybrid frequency domain

With FDS, the sensor frequency band is sampled in several steps and the sensor response is determined from the amplitude, phase and frequency differences between the transmitted and received signals. The baseband bandwidth can be low, resulting in a simpler and cheaper hardware design. However, they have longer interrogation times than with TDS. The FDS technique can be used for both delay lines and resonant SAW sensors. In addition, there are two possible interrogation signals: FMCW, in which a frequency-modulated linear transmission signal is used, and FSCW, in which discrete frequencies are measured one after the other [117]. Frequency domain sampling with FMCW or FSCW interrogation is ultimately a distance measurement with a radar system that detects a SAW resonant or R-DL.

Radars are used in many applications such as level measurement, obstacle detection, meteorology, military, etc. They are mainly based on pulsed or Continuous Wave (CW) technologies, including FMCW [25], [103], [118]–[125]. In the CW family of radars, the FMCW radar transmits and receives a signal continuously, but the frequency of the transmitted signal changes as a function of time, and therefore the frequency of the received signal can be used to measure a delay. In the study carried out in [126], a FMCW radar was developed to interrogate a passive sensor for gas detection using the structure (sensor) and antenna cable considered as a delay line. By this principle, sensor measurement is optimal and different line lengths allow identifying multiple sensors with adjacent spectral lines in the radar beating signal. This identification technique is useful for measuring a physical quantity, regardless of the interrogation distance. For example, a sensor and its reference (pressure or gas detection) are connected to a single antenna by two lines of different lengths.

Depending on specific application requirements (such as accuracy, speed and cost) frequency synthesis can be achieved by a Voltage Controlled Oscillator (VCO), a Phase Locked Loop (PLL) circuit, a Direct Digital Synthesis (DDS) or a combination of these. A detailed comparison of FSCW, S-FSCW and FMCW interrogators in the same environment and with the same SAW delay-lines in the 2.4 GHz ISM frequency band is reported in this study conducted by Binder *et al.* [127].

The Software Defined Radio (SDR) platforms are particularly popular due to their flexibility and easy customization. SDR hardware is too expensive for large-scale commercial use, but new interrogation algorithms and strategies can be evaluated quickly and efficiently. In [128], a SAW interrogator based on a PXIe that can operate in any frequency band between 85 MHz and 6.6 GHz was presented. Likewise, the radio platform defined by software, was programmed as the interrogator for OFC SAW sensor interrogation [129], [130]. The front-end of the RDS B200 platform can process RF signals between 70 MHz and 6 GHz. In the works [131], [132], the SAW delay-lines were interrogated using a SDR in UHF band (915 MHz and 380 MHz, respectively) for temperature and mass measurement. The first one was used for an interrogation distance between 20 and 30 m using a PCB antenna and a transmission power of 6 dBm, the second for a shorter interrogation distance, between 1 and 5 m. Based on resonators and delay lines, the works of [130], [133], [134] highlighted the interrogation of passive sensors at a distance between 10 and 20 m, in UHF band (920 MHz) and using FMCW, in order to measure distance and mechanical vibration from the phase shift and reception signal amplitude..

FMCW radars were designed to interrogate passive sensors, from 20 to 30 m, for distance and

temperature measurement based on the RCS of the antennas coupled to the passive sensor. These interrogations were carried out in the K and Ka bands using horn antennas and satellite dishes with a gain of 13 dBi. It is shown that wireless measurement of various physical quantities is possible from the analysis of the variability of cross-sections of passive sensors. In addition, the same FMCW radar can be used to identify passive sensors in a wireless network [135], [136].

In the works in [94], [95], interrogation of a wireless biosensor based on LW sensors is performed using a guiding layer of PMMA and protein receptor layers on a piezoelectric substrate based on $LiNbO_3$ for immunoglobulin detection. A 440 MHz R-DL composed of unidirectional transducers and three reflectors was fabricated as sensing element. A theoretical modeling was carried out to describe the propagation of Love waves in the piezoelectric substrate with high piezoelectricity. Manufactured devices were wirelessly characterized using the network analyzer as the reading unit. The binding of IgG to the protein in a receptor layer induced phase shifts of the reflection peaks due to the mass loading effect. The changes of the reflected peak in terms of time were slow and it took approximately 10 minutes to reach the saturation. Good linearity, reproducibility, and high sensitivity were observed. This highlights a simple wireless measurement method over other currently available ones. Again, various interrogator architectures exhibit their own advantages and drawbacks and they can be selected depending on the application.

In summary, passive sensors have been the subject of study in recent years, primarily due to their advantages for use in harsh environments and with energy autonomy. Acoustic wave sensors, in particular, have garnered attention for their applications in different environments. The detection and classification of molecule concentrations in liquids are becoming increasingly important with the advancement of acoustic wave sensor development. In this context, numerous interrogation architectures and instrumentation protocols have been suggested. The choice of hardware depends on the cost, operating frequency, and operating principle of the device, as well as the interrogation distance, energy required / available for each application, and the nature of the measurand. If the interest lies in simultaneous location and detection, frequency modulation interrogation has proven to be a viable solution. If the focus is on a more flexible system, SDR is an effective alternative because it can be quickly programmed for different frequency bands. Depending on the gain and radiation characteristics of the antennas used, impedance mismatch on the sensor side, and the sensor's operating principle, configurations in near-field and far-field should be considered, either through electromagnetic coupling, backscatter, or target RCS measurement. In studies involving feasibility and proof of concept, VNAs are preferably used because they facilitate the study of both wired and wireless sensors, offer flexibility in operating frequency, and provide good resolution.

The principle of wireless systems considering the electromagnetic response of the sensor is well established, as seen in RFID systems with no acoustic signal. Considering the acoustic response of a SAW sensor, it is possible to wirelessly detect and classify various substances. The main current challenge is to perform this reading at greater distances. In Tab. 4.5, a synthesis of the state-of-the-art wireless interrogation for passive sensors is presented, focusing on LW sensors. However, no work explores the electromagnetic response in a wireless configuration with these sensors. To date, no conclusive studies are available and further research is necessary. The challenge is to demonstrate the feasibility and proof of concept of wireless reading using the electromagnetic response of the LW sensor in a liquid medium.

Table 2.2: Wireless interrogation for passive sensors: characteristics and applications

Work	Device	Analytes and Applications	Frequency (MHz)	Reader	Distance Interrogation	Antenna Type	Transmission Power	Sensitivity
[137]	R-DL	Temperature	227	BPSK (PPGA) and FSCW (VNA)	15 cm	Monopole	x	Feasibility
[138]	R-DL	Corrosion	256	VNA	x	Dipole	5 dBm	Detection
[139]	Resonator	Strain	288	VNA - Electromagnetic Coupling	5 mm	Coils	x	0.439 ($/\mu\epsilon$)
[140]	Resonator	Strain	325	VNA - Electromagnetic Coupling	10 mm	Coils	x	-182 (Hz/$\mu\epsilon$)
[141]	R-DL	Temperature and Pression	425	ESG	x	Espiral	Pulse 1 ms	Linearity
[142]	MSAW	Temperature and Magnetic Field	433	SUSS PM5 Probe Station and VNA	x	x	x	−63 ppm/°C and −781 ppm/mT
[143]	MSAW	Temperature and Magnetic Field	433	VNA-wired**	x	x	x	-774 ppm/mT and -67.7 ppm/°C
[144]	LW - R-DL	Ice	433	VNA/Transceiver	x	x	x	Detection
[145]	LW - DL	Water contamination	433	VNA and Raspberry Pi (Active*)	700 m	Helical	10 dBm	Detection
[81]	Resonator	Electric Field	433	VNA	10 cm	Helical	13 dBm	Position
[146]	Resonator	Vibration	433	VNA	20 cm	Dipole	20 dBm	10.4 kHz/g
[89]	R-DL	Dimethylmethylphosphonate (DMMP)	434	SCM: C8051F065 and FSCW-based	20 cm	Planar (18 cm x 5 cm)	x	20.1°/(mg/m3)
[87]	R-DL	Dimethyl methylphosphonate (DMMP)	434	SCM: C8051F065 and FSCW-based STM32	20 cm	x	x	4.63°/(mg/m3)
[147]	R-DL	Temperature	434	FSCW-based	50 cm	Planar	x	36.5°/°C
[82]	R-DL	Soil Impedance	434	VNA	50 cm	Microstrip FR4 PCB (5.6 cm x 1.8 cm)	10 dBm	Feasibility
[94]	LW - R-DL	Imunoglobulina G	440	VNA	50 cm	Planar (10 cm x 10 cm)	10 dBm	17.5°/nM.
[95]	LW - R-DL	Imunoglobulina G and Anti-DPN	440	VNA	20 cm	Planar (10 cm x 10 cm)	10 dBm	167.9 deg $\mu g^{-1} ml^{-1}$
[148]	LW - R-DL	CO_2	440	VNA	25 cm	Planar (10 cm x 10 cm)	10 dBm	7.07° ppm^{-1}
[96]	LW - R-DL	Imunoglobulina G and Cartilage Oligomeric Matrix Protein (COMP)	440	VNA	20 cm	Planar (10 cm x 10 cm)	10 dBm	15 deg/μg/mL(IgG) and 1.8 deg/ng/mL (COMP)
[149]	LW - R-DL	Imunoglobulina and Anti-DPN	440	VNA	1 m	Planar (10 cm x 10 cm)	10 dBm	2700 deg for 0.2mg/ml
[150]	LW - R-DL	Imunoglobulina and Anti-DPN	440	VNA	x	Planar (10 cm x 10 cm)	x	167.9°/μg/ml and 44.8°/μg/ml
[151]	LW - R-DL	CO_2	440	VNA	50 cm	Planar (10 cm x 10 cm)	10 dBm	7 deg/ppm
[36]	R-DL	CO_2 and NO_2	440	VNA	20 cm	Planar (10 cm x 10 cm)	10 dBm	2.12°/ppm (CO_2) and 51.5°/ppm (NO_2)
[88]	R-DL	CO_2	440	VNA	50 cm	Planar (10 cm x 10 cm)	10 dBm	1.98°ppm^{-1}
[152]	Resonator	Pression	865	DSP (TMS320C6746)	6 cm	Dipole	x	200 Hz/mmHg
[90]	Resonator	Blood Pression Detection	868	DDS	x	Helical	Pulse	x
[153]	SAW-RFID	Temperature and Strain	915	FMCW-based - Agilent 8648D - Wavetek 395	15 cm	Microstrip FR4 PCB (5.6 cm x 1.8 cm)	Pulse 10 ns	75ppm/°C and 1 ppm/$\mu\epsilon$
[154]	SAW-RFID	Temperature	915	OFC - USRP - FPGA	2 m	PCB (11.43 cm × 3.81 cm)	x	Concept proof
[134]	R-DL	Temperature	915	OFC - USRP - FPGA	23 cm	Dipole e Yagi	10 dBm	Feasibility
[91]	Resonator	Temperatura and Strain	2450	Comercial Reader	2.5 cm	Patch Comercial	x	Feasibility
[126]	EM	Gas Concentration	2880	Radar FMCW	1 m a 5 m	Horn	x	Feasibility
[155]	EM	Pression	26000	Radar FMCW	20 m - 30 m	Satellite Dish and Horn	YY	YY

2.4 Motivation and challenges

Based on the synthesis regarding wireless interrogators and surface acoustic wave sensors, the objective of this work is to contribute to the advancement of a passive sensor protocol, focusing on LW, encompassing both wired and wireless interrogation systems, tailored for liquid environments. Given the increasing importance of these interrogators in communication systems, our proposal involves the development of a remote reading link that allows the detection and extraction of information about the liquid deposited on the surface of the LW sensor.

The proposed steps for this work are as follows. First, a testing platform and protocol are established with our existing LW sensor in the wired configuration. From this sequence, we estimate the energy flow in the sensor based on S-parameters. Although the LW sensor is designed for applications in liquid media, to date, only the acoustic response of the sensor has been utilized. In this regard, an electromagnetic approach has proven being viable as another possible sensitivity path specific to the electrical parameters of the liquid, given its multiparametric characteristics. The main idea is to investigate the feasibility of classifying a saline solution (as a buffer electrical sample) and facilitating wireless reading based on this response. Based on that, we study a model of this system for predicting and reproducing experimental results.

Considering the wired sensor response, operating frequency, interrogation distance, the parameter to be read, will help to identify the key characteristics of a wireless link and transmission and reception circuits adapted for the VHF range. Interrogation techniques are then proposed, and experimental tests are designed to evaluate the sensor response, initially for the detection of liquids with extreme characteristics, and then refining the system to enable the classification of concentrations of saline solutions.

Several challenges will be faced, such as implementing a wireless reading system at the sensor's operating frequency in a compact form and dealing with noise associated with this frequency band. Furthermore, considering the passive nature of the sensor, the interrogation distance that can be performed. Overall, recent works have interrogated sensors based on the same principle, albeit at a higher frequency, at distances on the order of centimeters. In this regard, a state-of-the-art review is necessary concerning the architecture used with SAW and LW sensors. Finally, we investigate further to propose appropriate physical explanations for what occurs at the system and sensor levels.

2.5 Chapter conclusion

This chapter introduced the main techniques for wireless reading of passive and chipless sensors. A brief analysis of the current and future markets allowed establishing the importance of detection in liquid environments, particularly with optimistic forecasts in the field of biosensors in the medical sector. It presented the advantage of using a wireless system instead of a wired one, especially when applied in hazardous and harsh environments, explained the key techniques for wireless reading of passive and chipless tags, focusing on radar systems and electromagnetic coupling. In this context, on the sensor side, it was explored how the impedance change affects the system matching, enabling the reading of a physical quantity.

Prominent works in both wired and wireless interrogation involving SAW sensors have been presented, with a focus on the state of the art in the application of LW sensors for the detection and classification of substances in liquid environments. It is evident that the development for this application is still in its early stages, creating both scientific and market opportunities. The LW sensor was introduced along with the possibility of investigating the electromagnetic signal separately from the acoustic signal. Therefore, it is proposed to explore whether it is possible to remotely monitor variations in the sensor's electrical parameters from variations in the electrical parameters of the liquid deposited across the sensor's surface, capitalizing on the temporal distinction between the electrical and acoustic nature of the sensor.

Finally, a global comparison was provided for the most significant works using SAW sensors. Wireless link characteristics, such as antenna features, distance, interrogation power, measured parameter, and utilized architectures, were highlighted. It leads us to conclude by suggesting the use of two wireless system configurations. The first one aims to employ the radar system and RCS measurement to detect variations in the target. The second one involves using the VNA and evaluating the reflection coefficient S_{11}, focusing solely on the electromagnetic response of the sensor.

2

3

The Love Wave Device and Characterization in Saline Solution

Contents

LW acoustic sensors are recognized for their enhanced sensitivity in the detection of biochemical substances in liquid environments. Additionally, the LW sensors have the capability to simultaneously measure multiple parameters. While their applications in liquid media pertaining to the mechanical properties of complex liquids have progressed, their utility in the detection of electrical parameters, such as conductivity and permittivity, remains relatively unexplored. This underexplored aspect can present an advantageous potential for LW sensors, particularly given the high cost of commercial probes and limited range of operation used in electrochemistry [156]. Among other applications, they may be of interest in water quality measurement, as salinity represents one of the observable variables in this case. The focus here is on electrical quantities, especially the electrical conductivity of solutions. In this context, a wide range of applications could be addressed, spanning from medicine and biology to environmental monitoring.

The first part of this chapter goes deeper in the structure and the operating principle of SAW sensors, moving to the LW sensors used in our work along with their key characteristics. The second part outlines the wired experimental setup for these LW sensors and presents results related to the detection and classification of saline solutions. Finally, the chapter ends with an electrical model elaborated in the Quite Universal Circuit Simulators (QUCS) studio environment. This analysis aims to characterize the sensor behaviour in terms of input impedance, based on wired measurements, and highlights a sufficiently significant variation to be detected passively in further wireless measurements, aligning with the central focus of this thesis.

3.1 SAW devices

As introduced in the previous chapter, eletroacoustic systems for sensor applications have been the subject of numerous studies for several decades. The literature is abundant with works describing the use of various electroacoustic transducers based on piezoelectric substrates for many applications, enabling the production of physical and biochemical sensors for use in gaseous and liquid environments [63], [76], [80]. The objective of this section is specifically to revisit the definitions and general characteristics of SAW devices capable of functioning as sensors. Given that this class of sensors is already well-known, we will not delve into detailed and exhaustive presentations of these concepts. However, we will provide essential information to understand the operation of LW sensors applied in a liquid medium. The section on piezoelectricity and the generation of acoustic waves within the material is presented in the Annex 4.4.

3.1.1 The operating principles

In this context of application in liquid and gaseous environments, miniaturization, and measurement, relevant SAW devices have increasingly become the focus of study, ranging from their design and manufacturing aspects to the development of wireless systems. Due to their multiparametric characteristics, they find applications in various fields of knowledge, spanning from physical concepts to notions of biology and chemistry [157]. Certain phenomena, such as piezoelectricity or the generation of acoustic waves, are closely linked to them.

The manufacturing of SAW devices in planar technology is particularly well established, which has attracted significant interest in the RF community [80], [158]. By employing an interdigitated array as a transducer, a cumulative effect can be achieved. The application of an alternating voltage at the input transducer generates alternating compressions and expansions that can propagate along the substrate, as shown in Fig.3.1. The principle of these devices is based on the use of IDTs, whose periodicity determines the acoustic wavelength in a piezoelectric material with a specific phase velocity, thus establishing an optimal frequency for wave propagation.

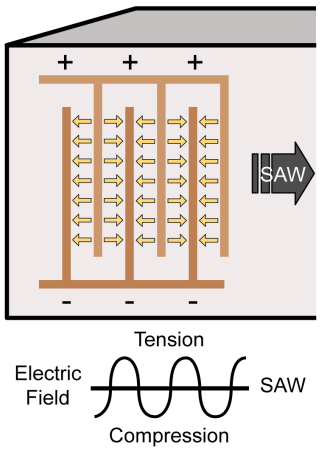

Figure 3.1: SAW generation phenomenon in piezoelectric wafer [76].

This thesis work focuses on the study of LWs, due to their well-known property of being compatible with an adjacent liquid medium and sensitive to its characteristics. The design aspects and additional details of these transducers will be detailed in the following subsections.

3.1.2 Design aspects

A comprehensive understanding of SAW devices requires the study of their fundamental elements, such as the substrate, materials, IDTs, configurations, electroacoustic coupling coefficient, and some applications.

The substrate

The piezoelectric substrate is essential for generating surface acoustic waves. Typically obtained by cutting a bulk piezoelectric crystal into slices (wafers), the substrates are characterized by the resulting crystallographic orientation. This cut angle and the orientation of the IDTs on the surface determine the waves than can be generated, in terms of direction and polarization. The Euler angles (φ,θ,ψ) characterize the crystallographic orientation, including the crystal surface and its direction perpendicular to the IDTs. They are defined based on elementary transformations of the reference axes (XYZ) [86], [159]. In this work, a LW sensor with a AT-cut quartz substrate was used. $LiNbO_3$ is another material extensively used in the literature for the design of such devices. The substrates and cuts widely used in SAW applications are characterized based on different properties. First of all, the full set of electromechanical constants characteristic of the material and its orientation have to be calculated after rotations according to the Euler angles, from a basic set defined in the reference axes (XYZ). Then, some parameters associated to the acoustic waves generation and propagation are defined, especially:

- The velocity of surface acoustic waves v, which determines the device's operating frequency f in relation with the wavelength λ according to:

$$f = \frac{v}{\lambda}. \tag{3.1}$$

- The electromechanical coupling coefficient (k^2) which characterizes the efficiency of conversion between electrical and mechanical energy. The value of k^2 is typically calculated using the expression:

$$k^2 = 2\frac{v_o - v_m}{v_o}. \tag{3.2}$$

  Here, v_o and v_m are the velocities of the surface acoustic wave in the case of a free surface or a metalized surface, respectively [160]. For experimental determination, the approximation

involving the resonance f_r and anti-resonance f_a frequencies is often preferred and given by [161]

$$k^2 = 2\frac{f_r - f_a}{f_r}. \tag{3.3}$$

Other substrate properties are also considered, among them, the temperature coefficient of frequency Temperature/Frequency Coefficient (TCF) can be of importance, which quantifies the device frequency variation in response to a temperature change. The power-flow angle Power-Flow Angle (PFA) is also considered, which is the angle between the wave propagation direction and the energy radiation. It is also interesting to specify that the constants (elastic stiffness, dielectric, piezoelectric constants, for example) depend on the propagation medium and the crystallographic section. [162], [163].

For example, quartz substrates are interesting due to their temperature stability but have a low electroacoustic coupling coefficient compared to the others substrates. The properties of the most commonly used cuts can be seen in Tab. 3.1. More details can also be seen in [76].

Table 3.1: Properties of the most used substrates

Substrate	Cut	Direction	Euler Angle	v (m/s)	k^2	TCF (ppm/°C)	Ref.
Quartz	AT	Perpendicular	(0;121.5°;90°)	5098	*	0* (25* °C)	[162]
Quartz	ST	X	(0;-47,25°;0)	3159	0.12	0 (at 25 °C)	[86], [160]
$LiNbO_3$	Y + 128°	X	(0;38°;0)	3992	5.3	-75	[86], [160]

SAW devices are not limited to the use of monocrystalline piezoelectric substrates. Piezoelectric films can be deposited on non-piezoelectric substrates, and structures such as ZnO / Si, AlN / Sapphire, and AlN / Diamond have already been studied [161], [164], [165].

The IDTs

The IDTs deposited on the piezoelectric material, as shown in Fig. 3.2, allow the generation and detection of acoustic surface waves from the alternation of positive and negative electrical potentials applied, thanks to direct and reverse piezoelectricity. They also define the wavelength from their spatial periodicity [166].

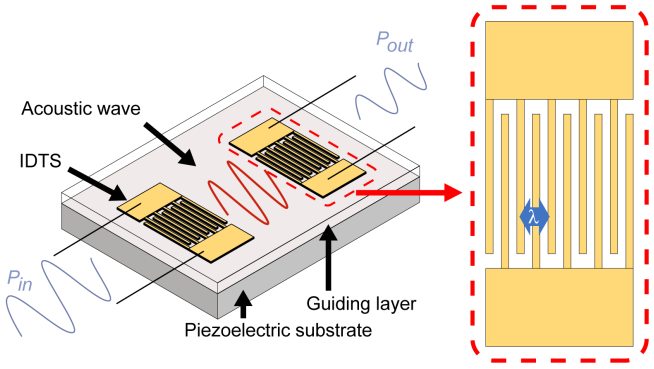

Figure 3.2: Electrode deposited on a piezoelectric substrate [5]

With respect to constituent materials, aluminum, gold, platinum, titanium, and copper are the most commonly used. Aluminum is the most used because it has the advantage of being a good conductor and low density, limiting the attenuation of waves during their propagation, as it is also easier to manufacture and better compared to quartz. Another possible material is gold, used because it is chemically more stable than aluminum. However, it is more difficult to manufacture and has a higher density and acoustic impedance compared to quartz.

Furthermore, beyond the substrate and IDTs materials and orientation, the design of the IDTs plays a major role in the device characteristics, both in terms of electrical and mechanical behaviors. For example, the quality factor of the system can be increased by increasing the number of IDT‘s fingers or the full shape of the acoustic filtering response can be adjusted with specific geometries. Split electrodes is a way to limit acoustic reflections when the acoustic signal passes under the output IDT, by limiting the acoustic impedance breakdown at each + and – electrical center [76], [80].

Detection principle

Based on such so obtained device, the output electrical signal is delayed and attenuated relative to the input one. Variations in every parameter of the structure disturbs the wave by altering the characteristics of wave generation, wave propagation velocity, and attenuation. In this way, external parameters such as temperature, pressure, driven mass, viscosity, permittivity and conductivity can influence the state of these devices. For application as chemical sensors or biosensors targeting specific compounds, an additional sensitive film deposited on the surface is a way to increase the specific immobilization or interaction, thus amplifying the sensor sensitivity and selectivity,

provided the interaction results in a change in one of the above parameters. This gives these devices a multiparameter detection capability, with a sensitivity associated to each one. Finally, if v is the velocity and Δv represents this change, v can be expressed in a general way by

$$v = f(\sigma, \epsilon, T, P, m, \eta ...) \tag{3.4}$$

and

$$\frac{\Delta v}{v_0} = \frac{1}{v_o}\left\{\frac{\delta v}{\delta \sigma}\Delta\sigma + \frac{\delta v}{\delta \epsilon}\Delta\epsilon + \frac{\delta v}{\delta T}\Delta T + \frac{\delta v}{\delta P}\Delta P + \frac{\delta v}{\delta m}\Delta m + \frac{\delta v}{\delta \eta}\Delta\eta + ...\right\}. \tag{3.5}$$

Here, σ is the electrical conductivity, ϵ is the dielectric permittivity, T is the temperature, P is the pressure, m is the mass, and η is the viscosity. Measuring this disturbance allows for the detection of specific chemical species and determination of their characteristics, such as concentration, for example. Based on the wave generated in these devices, they can be more sensitive to gases or liquids [2], [76], [80], [160]. Fig. 3.3 proposes a classification of the different configurations most explored in SAW sensors and possible modifications in the wave, all participating to the sensitivity.

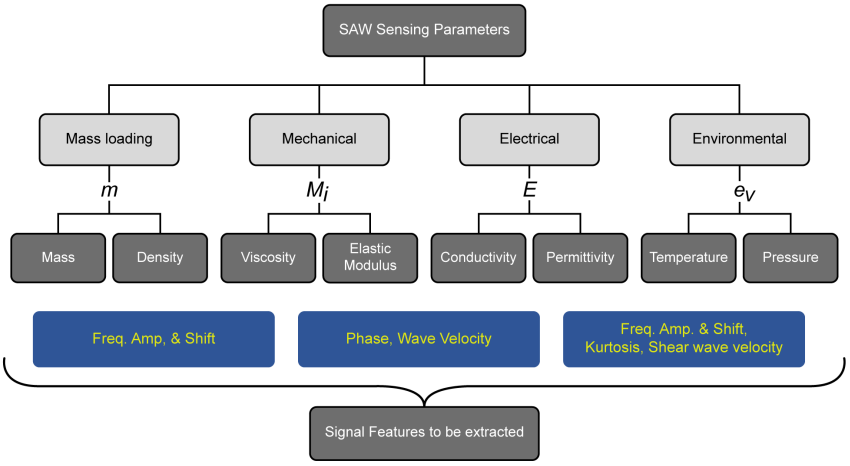

Figure 3.3: Classification of the SAW sensing parameters [76].

An antenna can be connected to the IDT of the sensors (input IDT in the case of a 2-port device), enabling wireless interrogation without the need for power battery. The interrogation unit sends a RF interrogation signal that provides the energy to excite the passive sensor through the antenna-IDT element. Along with converting electrical into acoustic energy and *vice-versa*, the IDT can be also influenced electromagnetically depending on changes of its near environment, such as a material deposited on its surface. Thus, both the IDTs (electrical parameters) and the acoustic propagation path (mechanical parameters) can be considered as sensitive regions. In the case of a

single antenna at the input IDT, the interrogation unit will solely receive the reflected signal, with information to be extracted about these changes. Using the measurement protocol (particularly in the liquid deposition across the sensor surface), we will elucidate the electromagnetic response of the sensor and neglect the acoustic one in wireless reading, due to the very low level of reflected acoustic energy and as a focus is expected on the electromagnetic signal, complementary to the acoustic one. However, it is important to note that this is not a general characteristic of these devices. Other SAW sensors built with substrates of different materials have good energy conversion and low transmission loss, and several studies have managed to detect this signal, based on 1-port devices specifically designed, as previously presented.

Thus, in our case, when dealing later with wireless interrogation, the sensor will be regarded as an electrical impedance on which the liquid will exert an influence, focusing on the influence on the input IDT only, directly and via the insertion loss due to wave emission, apart from the interactions along the acoustic wave propagation itself, that would have to be considered in further works as additional signals.

Furthermore, our works targeting liquid media are carried out based on LW sensors, which have already demonstrated their viability and sensitivity for liquid applications [50], [63]. The next subsection will present this LW sensor itself and the experimental setup using them as well as the methodology applied in the detection and classification of NaCl solutions associated with the testing platform.

3.2 The Love wave sensor

A device with vertically polarized transverse acoustic waves suffers from excessive propagation losses with an adjacent liquid medium, due to radiation of energy into the liquid. In contrast, transverse horizontal and longitudinal polarizations can be operated with an adjacent liquid medium, whose properties will affect their propagation, provided the mechanical parameters such as viscosity are within a range compatible with acceptable losses induced. Besides, the mechanical deformation of the acoustic wave is combined with an electrical field due to electroacoustic coupling, inducing a sensitivity to the dielectric characteristics of the medium encountered along its propagation. The so-induced electric field in an adjacent aqueous solution induces energy radiattion in the liquid, and consequently leads to energy losses [167]–[169].

LWs are considered as surface waves with shear horizontal polarization, initially generated as SH

bulk waves and trapped along a thin layer deposited on the surface, with appropriate parameters. In the case of an AT-cut quartz substrate, a SiO_2 thin film on the entire substrate allows the propagation of this type of acoustic wave. Acoustic energy is then confined in the thin layer, which serves as a waveguide and is therefore called the guiding layer, as represented on Fig. 3.2. Thus, the transducer is protected from the external environment by this layer, making the sensor compatible for use in liquid medium [170], [171]. In this sense, applications for the detection and classification of liquids are shown in the Tab. 2.1 become viable.

3.2.1 Measurement parameters of interest

LW devices are commonly electrically characterized through their scattering parameters (S - parameters), denoted as S_{ij}. These parameters represent the ratio of the output power at port i to the input power at port j. A typical result of the characterization of a LW delay line as used in this work (two-port device) measured with a VNA in the frequency domain (S_{11} and S_{21}) is shown in Fig. 3.4.

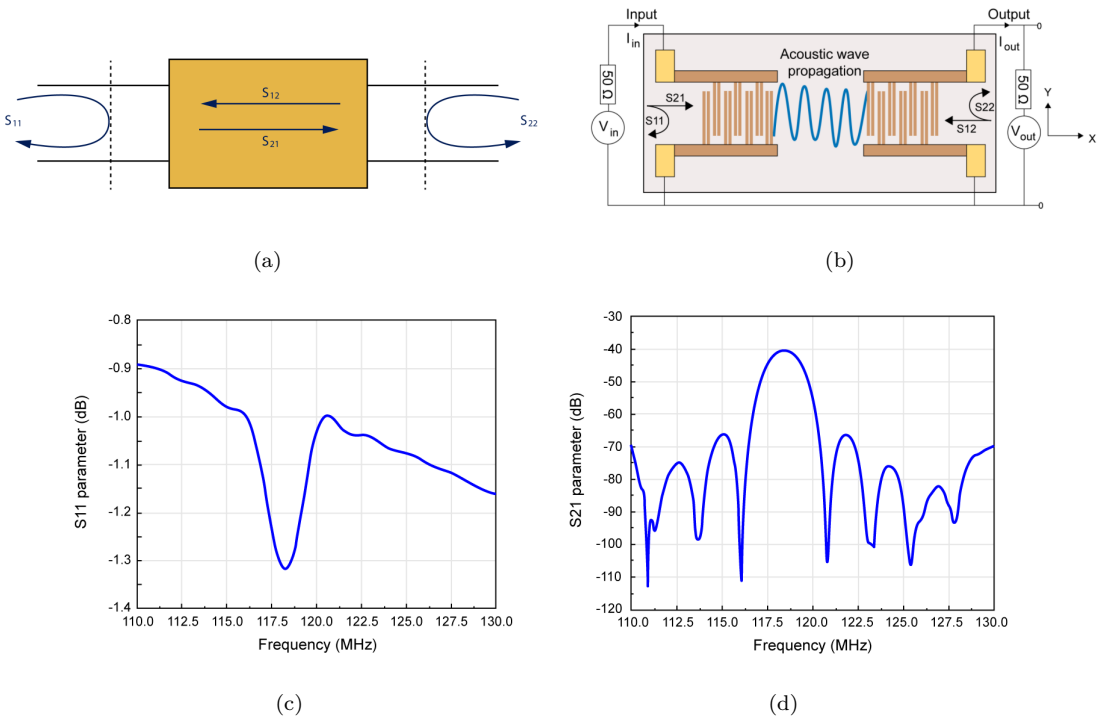

(a) (b)

(c) (d)

Figure 3.4: (a) S-parameters of a two-port device; (b) Principle of an open loop measurement system of LW sensors; (c) S_{11} and (d) S_{21} parameters of a typical LW device frequency response [172].

.

Fig.3.4 (d) illustrates that the transmission coefficient of the delay line is comparable to the absolute value of a cardinal sinus centered at f_r as

$$S_{21} = A.(\frac{sin(N.2\pi(f-f_r)/f_r)}{N.2\pi(f-f_r)/f_r})^2, \tag{3.6}$$

with N the number of fingers (or finger pairs), f_r the resonance frequency at which the electromechanical transduction occurs (here around 118 MHz), f the frequency and A the magnitude. The bandwidth (at -3 dB) and quality factor are directly linked to the constructive aspects of the IDTs. The resonance corresponding to the peak in the magnitude of the transmission coefficient S_{21} is associated to a decrease in the magnitude of the reflection coefficient S_{11}.

The electrical input impedance Z_{11} of the device can be derived from S_{11}, as indicated by

$$Z_{11} = Z_0 \frac{1+S_{11}}{1-S_{11}} \tag{3.7}$$

or

$$S_{11} = \frac{Z_{11}-Z_0}{Z_{11}+Z_0}. \tag{3.8}$$

Here, Z_0 is the transmission line characteristic impedance, typically 50 Ω for a VNA [173]. As described in [5], in the presence of a liquid facing the IDTs, the input impedance of the device is modified according to the dielectric properties of the fluid over the full frequency range, while liquid above the acoustic path between the IDTs mainly modifies the mechanical wave propagation. The magnitude of the reflection coefficient S_{11} and the impedance of the device Z_{11} are key elements in this study, as the deposition of another layer of material on top of the substrate and the guiding layer affect the wave propagation, the energy distribution in the system, the resonance frequency, and magnitude coefficient. In this context, aiming for wireless detection, the measurement of the reflection coefficient is the focus of analysis.

3.2.2 The Love wave transducer

The device used in this work is illustrated in Fig. 3.5. This LW delay line is based on a AT-cut quartz piezoelectric substrate with 500 μm in thickness, IDTs with 40 μm wavelength and a 6.4 μm SiO_2 guiding layer. The geometry has been previously described in detail in references [4], [174].

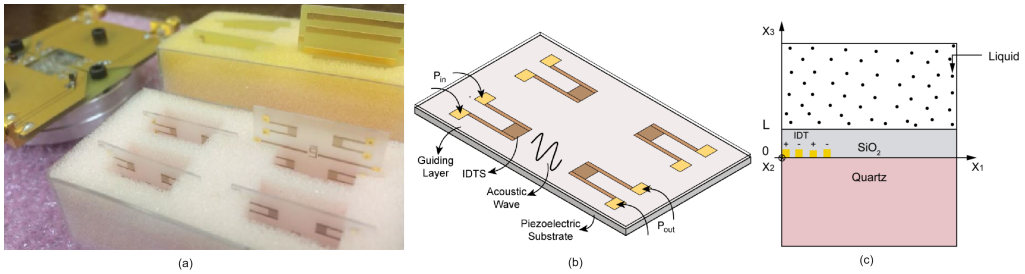

Figure 3.5: (a) Photo of 4 LW sensors manufactured by IMS and LAAS; (b) Structure of the LW sensor; (c) Cross-sectional view of the sensor and added liquid.

Based on previous descriptions, the electric field contained within each period of an IDT, acting as a planar capacitor, is at the origin of the primary energy conduction path that can be perturbed by the medium of detection. Thus, the electrical parameters of an adjacent liquid affect not only the reflected electrical energy, but also the energy transfer from the input to the output IDT, and consequently the S_{11} parameter, thus the input impedance, and the S_{21} parameter, as described previously and illustrated in Fig.2.15.

Since the liquid inserted on the sensor's surface has mechanical and electrical properties (viscosity, density, conductivity, permittivity), isolating the acoustic and electromagnetic energies by time gating of the S_{21} parameter at times of a few microseconds and inferior to tenths of microseconds respectively, as presented in [5], will allow an analysis of these properties. Similarly, by depositing the liquid over the entire sensor surface, including over the IDTs, any change of the liquid electric and dielectric properties and of the induced double layer formed by the liquid and the sensor surface, will alter the capacitive electrical impedance of the device's input, as extracted from the S_{11} parameter. Thus, the impedimetric approach of the LW sensor and an equivalent circuit model based on resistance and capacitance can provide us with a good approximation of how the liquid interacts with the LW sensor. The relationship between the capacitance and liquid parameters, although seemingly simple, still presents scientific challenges related to the experimental reproducibility, appropriate electrical circuit models, effective materials and geometries of substrates, guiding layers and electrodes, surface insulation, surface cleaning and adsorption. Therefore, it is necessary to investigate how the liquid's parameters influence both the reflection and transmission of the LW sensor. In this sense, there are several alternatives for liquid deposition protocols and geometries of cavities made of PDMS to isolate some of these effects and facilitate data processing and analysis. This will help to determine the level of influence of a liquid's parameters on each type of energy flow, firstly in a wired configuration in order to establish a setup adapted for a passive wireless system.

In Fig. 3.6 an overview of the experiments carried out is shown: wired and wireless interrogations, both with the liquid deposited onto the entire sensor surface (acoustic path and IDTs). Based on the results with the wired configuration, an equivalent electrical circuit was constructed using the QUCS simulator. For the wireless interrogation, different transmission and reception circuit strategies were employed, first, with antennas in the far field, then with the circuits. In the next sections, the wired experiments are detailed and the circuit model in QUCS is presented.

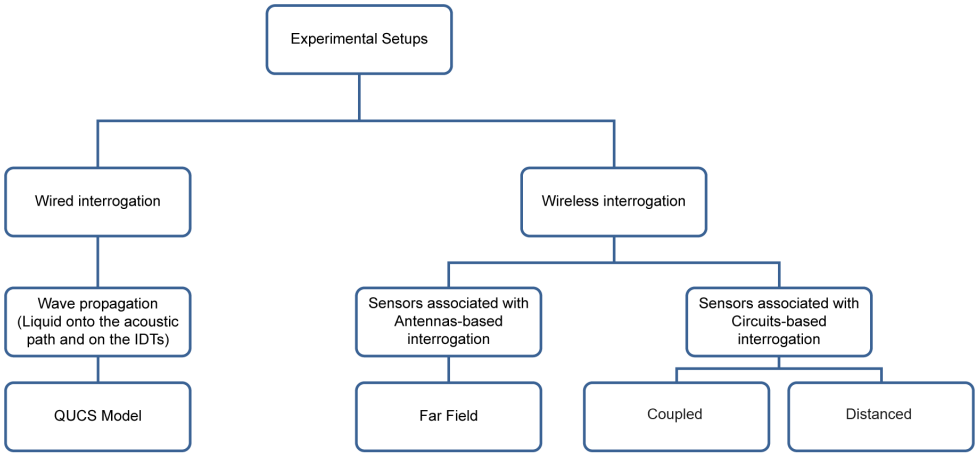

Figure 3.6: Overview of experiments performed: Strategies wired and wireless.

The next subsection is dedicated to describing how the sensor is inserted into the measurement cell and the protocol used to introduce solutions onto the sensor surface.

3.2.3 Test cell and experimental protocols

Test cell

The experimental setup consists of a sensor unit with a LW sensor and a test cell, allowing electrical connections to ensure sensor operation. A PDMS chip was used to localize the aqueous sample onto the sensor surface and prevent any direct contact with the electrical connections. Measurements were performed using a microfluidic PDMS chips with open cavity, allowing the injection of a liquid sample onto the sensor surface using a micropipette. A ”long chamber” chip was used to localize the liquid sample both on the acoustic path and over the input and output IDTs electrically protected by the SiO_2 guiding layer, while a ”short chamber” chip limits the liquid region to the acoustic path between the IDTs, similar to most common methods. In this way, the electrical effects are

superimposed on the mechanical ones and can influence the input and output reflected signals, as well as the transmitted one through the electromagnetic energy flow and thus the coupling capacitance between the IDTs, depending on the liquid conduction properties.

The components of the test cell can be assembled manually and sealed by screws that keep the assembly secure, as shown in Fig 3.7. The test cell is assembled for the measurement of the reference S parameters with the bare sensor in a dry state (air only), the use of the VNA making it possible to observe each parameter (S_{11} and S_{21}) to seek to decorrelate the different mechanisms involved.

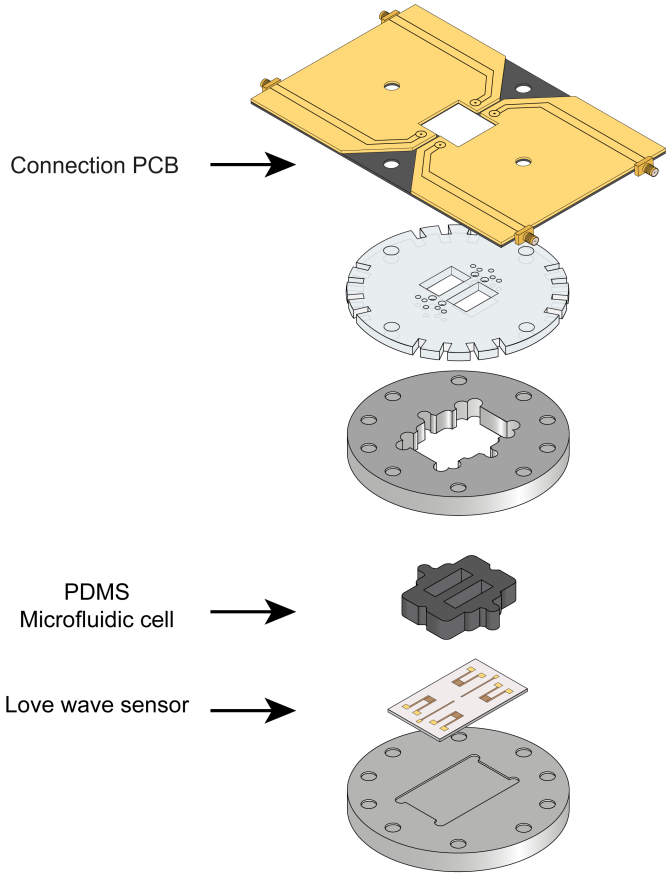

Figure 3.7: Test cell with LW sensor and PDMS chip [5].

Typical experimentation protocol

For all measurements, a SOLT calibration was performed first at the cables terminations. After assembly of the sensor setup, 150 μL of liquid sample are deposited into the PDMS long chamber open cavity onto the sensor surface (including the IDTs and the acoustic path) using a micropipette, as shown in Fig. 3.8.

The use of micropipettes was proved to be robust and allowing sufficient reproducibility, and each measurement was carried out five times [59]. For measurements with a soluted compound at different concentrations, a typical series of measurement started with measurements in air, then in DI water, then in successive samples of increasing concentration, after removing the previous sample carefully with the micropipette at each step. To minimize errors, after each measurement series, the experimental setup was disassembled, and the sensor and PDMS chip were thoroughly cleaned with distilled water, isopropyl alcohol, and acetone.

From the measurement of the S parameters, Matlab and Python (SCIKIT-RF, open source licensed package for RF/Microwave engineering) scripts were used to study and analyze the resistance and capacitance, resonance frequencies, phase and magnitude of the signals.

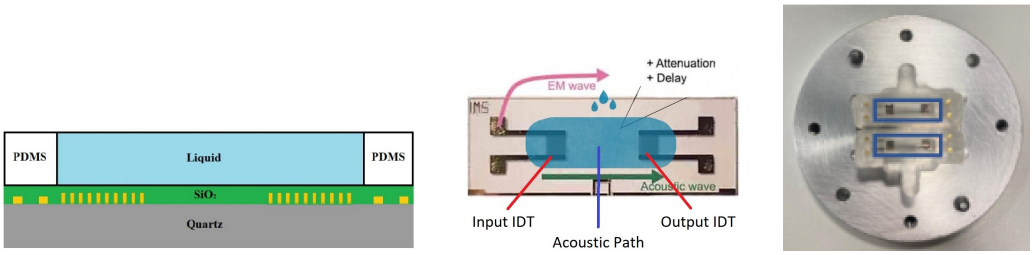

(a) (b) (c)

Figure 3.8: (a) The 2-D cross-section illustrates the structure of the LW sensor and the surface in contact with the liquid; (b) Illustration of the electromagnetic (EM) and acoustic waves in the sensor; (c) Long chamber microfluidic PDMS chip designed for precise and reproducible liquid sample localization onto the sensor surface.

Saline solutions preparation and characterization

The saline solution of NaCl was chosen for this work due to its high conductivity, which most affected the S_{11} parameter among other solutions such as DI water, glycerol and ethanol, thus facilitating further investigation and feasibility demonstration.

The preparation of sodium chloride (NaCl) solutions was carried out using a Sartorius CP225D analytical balance, ensuring the precision and consistency required for the experiments. In this regard, common salt, DI water, a beaker, and a spatula for salt manipulation were employed. A fixed volume of DI water was added to the beaker, and the analytical balance was calibrated. The mass of NaCl to be added to the water was then measured, and the salt was dissolved until a homogeneous mixture was achieved. A total of 8 solutions were prepared, comprising 4 with low concentrations (< 5 g/L) and 4 with high concentrations (30-360 g/L). Subsequently,

using the HI98129 Conductivity Meter from Hannah Instruments, and following cleaning and calibration procedures, the conductivity's of the low-concentration saline solutions and DI water were measured, as shown in Fig.3.9. Due to the conductivity meter's reading limit of 3999 μS/cm, the conductivity values for the highest concentration solutions (30-360 g/L) were estimated from the NaCl concentration (in mol/L) present in Tab. A.1 for at a temperature of 20°C. Permittivity, viscosity, and density were fully estimated from Tables A.1,A.2 and A.3. The characteristics of the solutions are consolidated in Tab. 3.2 and more details can be observed in Appendix A [175]–[177].

Figure 3.9: NaCl solutions preparation setup: precision balance, HI98129 conductivity meter and its cleaning and calibration solutions.

As described previously, the solutions were always deposited on the entire surface of the sensor by using the long chamber PDMS chip, starting with measurements in air, then in DI water, passing through the first 4 solutions of low concentrations and ending with the last 4 of highest concentrations.

Table 3.2: Characteristics of analysis media: air, DI water and NaCl solutions

Medium	Concentration (mol/L)	Conductivity (μS/cm)	Permittivity	Viscosity (cP)	Density (g/cm3)
Air	x	0.009	1	0.01722	0.00129
DI Water	x	10	80.6	0.89	0.9982
NaCl Solution (0.465 g/L)	0.0080	912	80.2	0.94	1.00087
NaCl Solution (0.800 g/L)	0.0137	1525	80.1	0.99	1.00093
NaCl Solution (1.240 g/L)	0.0212	2388	80.08	1.01	1.00098
NaCl Solution (2.456 g/L)	0.042	3856	80	1.03	1.00116
NaCl Solution (30 g/L)	0.513	41700	74.0	1.05	1.01709
NaCl Solution (120 g/L)	2.053	132200	60.9	1.25	1.07227
NaCl Solution (240 g/L)	4.106	205100	48.5	1.51	1.13709
NaCl Solution (360 g/L)	6.159	240000	39.8	1.93	1.19412

3.3 Wired interrogation

Preliminary measurements were conducted to investigate the impact of depositing a saturated NaCl solution (high conductivity) on two sensors operating at respective frequencies of 113 MHz and 145 MHz. Subsequently, new measurements were performed using the 8 NaCl solutions of different concentrations, thereby providing results and analyses in both the frequency and time domains. The results will be used to propose a QUCS electrical model of the circuit based on the mechanical and electromagnetic responses of the sensor. This sequence is illustrated in Fig. 3.10.

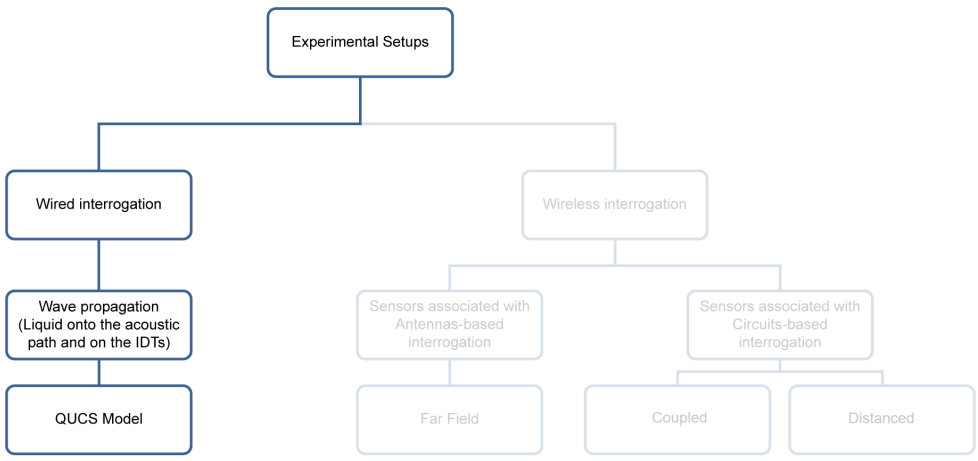

Figure 3.10: Overview of wired experiments performed and QUCS Model.

For wired measurements, the LW sensor unit described in the Subsection 3.2.3 was connected to a computer-controlled VNA (Copper Mountain TR1300/1) to measure the Scattering (S) parameters, as illustrated in Fig. 3.11. Given our final interest in conducting remote measurements,

our objective was to achieve maximum variation in S_{11} and, consequently, in input impedance, justifying the use of the long chamber PDMS chip for liquid across the entire sensor surface, particularly over the input IDT.

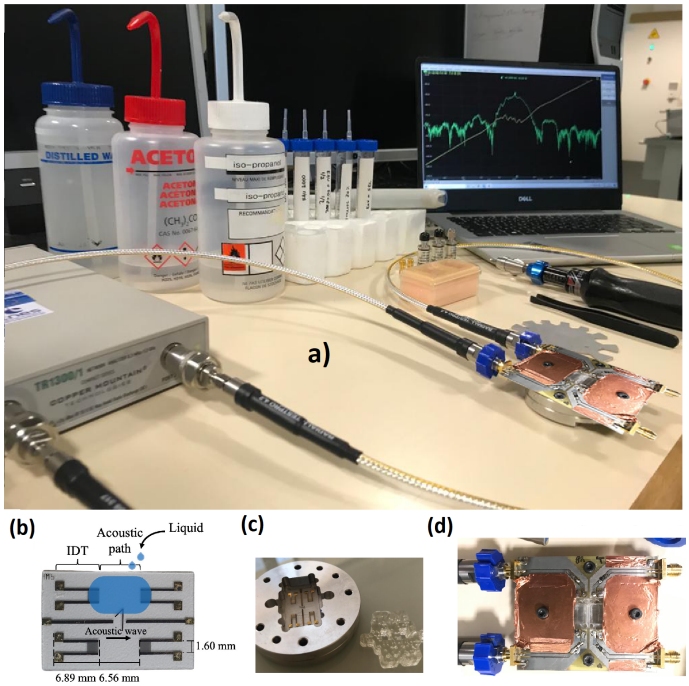

Figure 3.11: (a) Experimental setup for the sensor in wired configuration; (b) LW dual delay-line; (c) Device test cell with microfluidic chip; (d) Full test cell.

3.3.1 LW sensor response in liquid medium: preliminary results

The experimental reflection and transmission characteristics of the sensors in a wired configuration, with and without liquid deposited onto its surface, are presented in Fig. 3.12. With liquid, it can be observed a significant shift in the magnitude of the reflection coefficient (S_{11}) over the full frequency range for both devices (10 or 20 MHz around the acoustic resonance), as well as a slight shift in frequency. The magnitude of the transmission coefficient (S_{21}) was also highly affected by the liquid, resulting in the disappearance of the acoustic peak drowned into the baseline, which shifted due to the electromagnetic transmission from the input IDT to the output through the liquid itself. In this case, a shift in resonance frequency cannot be detected any more, though it is still visible on the S_{11} parameter.

Indeed, the addition of the highly concentrated saline solution decreased the reflected energy S_{11} of several dB, and increased the transmission of energy S_{21} from the input to the output of the sensor by several tens of dB. This energy balance can be attributed to the electrical short circuit

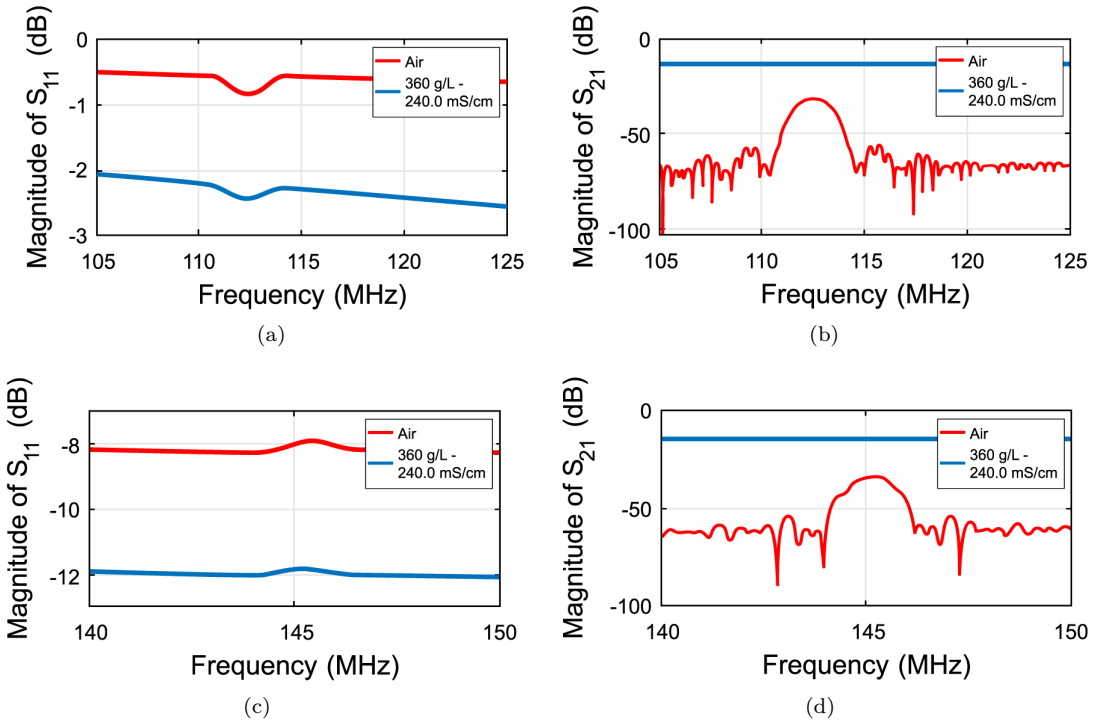

Figure 3.12: Preliminary results comparing the devices S parameters with air and NaCl solution with high conductivity (24 S/m): S_{11} (a, c) and S_{21} (b, d) for sensors operating at frequencies of 113 MHz (a, b) and 145 MHz (c, d).

behavior of the conductive liquid on the SiO_2 guide layer. This leads to a substantial modification in input impedance which will be further correlated with the parameters of the saturated NaCl solution, with a permittivity of 39.8 and a conductivity of 240000 μS/cm, as shown in Tab. 3.9. From a physical point of view, this change in permittivity and conductivity alters the distribution of the electric field on the sensor's surface as well as the conduction of energy from the input IDT. These results suggest further investigation using NaCl solutions with intermediate concentrations to explore the sensor's behavior with respect to the liquid parameters.

3.3.2 LW sensor response in liquid medium: response in NaCl solutions

Using the solutions described in Tab. 3.9 and employing the experimental setup illustrated in Fig. 3.13, different NaCl solutions were applied onto the sensor surface. Electromagnetic and acoustic responses were then captured in both the frequency and time domains. Finally, the assessment of sensitivity to the electrical and mechanical parameters of the liquid was conducted.

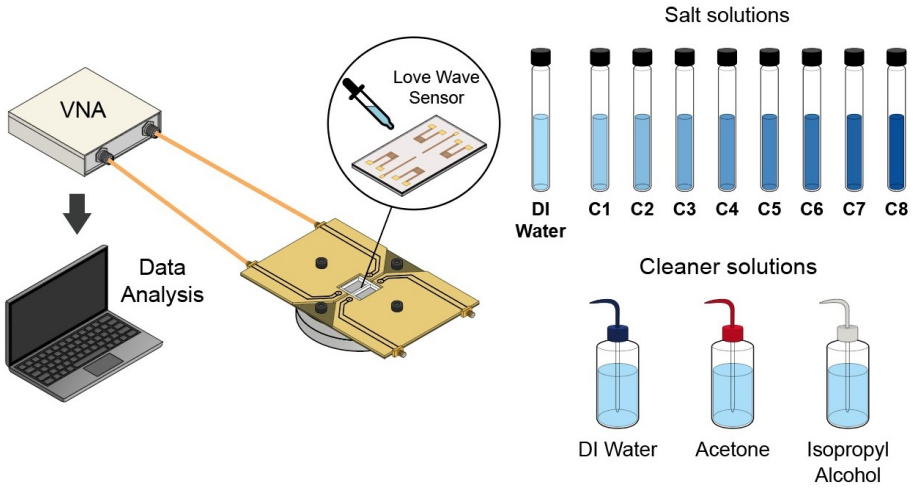

Figure 3.13: LW sensor-based liquid characterization protocol: saline solutions at various concentrations and cleaning solutions.

Frequency domain responses

Figures 3.14 and 3.15 depict the spectrum of parameters S_{11} and S_{21} in the frequency domain for the LW sensor response in air, DI water, and various concentrations of NaCl solutions. It is evident that there is a decrease in reflection and an increase in transmission with increasing solution concentration. Additionally, it is noteworthy that the change in S_{11} and S_{21} is not linear with concentration. Therefore, it is feasible not only to detect a saturated solution but also to classify the solution based on the configured setup.

Preliminary tests in subsection 3.3.1 culminated in the choice of a saline solution as the liquid most appropriate to substantially modify the sensor response. After this choice, numerous campaigns were carried out to confirm the experimental reproducibility. As a result, there was physical damage to the test cell. After several assembly and disassembly procedures, problems emerged such as screw corrosion, oxidation, and salt residue on the board, even after thorough cleaning. For this reason, the results of S_{11} and S_{21} presented in Figures 3.14 and 3.15 and Fig.3.12 present the same expected pattern but not exactly the same response.

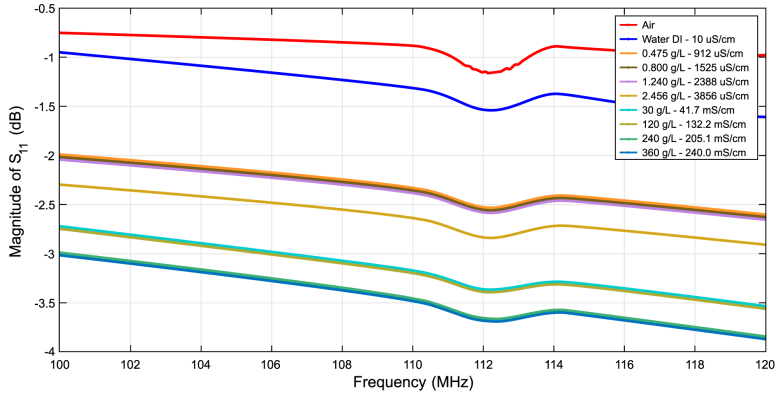

Figure 3.14: S_{11} in the frequency domain.

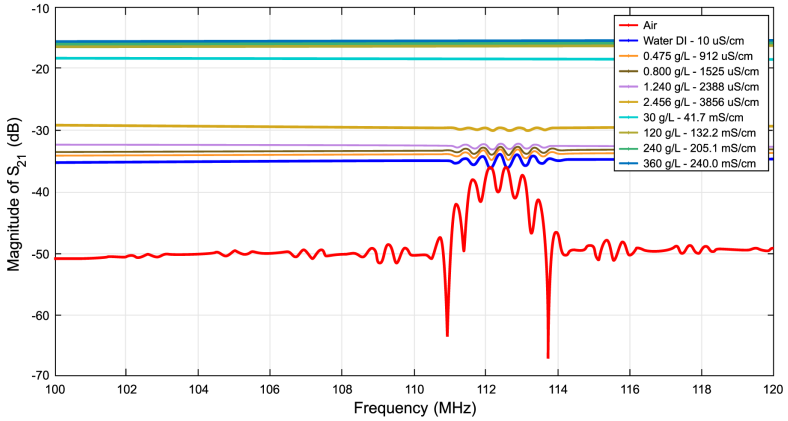

Figure 3.15: S_{21} in the frequency domain.

Time domain responses

The S_{11} response of the LW sensor in time domain, calculated from the frequency domain with an inverse Fourier transform, can be observed in Fig. 3.16. Two energy regions can be observed. The first region, centered at 0 s, corresponds to electromagnetic energy. The second one, related to acoustic energy, exhibits some influence around $\Delta t \approx$ 3.7, 4.7 and 6.5 μs, attributable to transit reflections from the IDTs. Since these energies are significantly smaller compared to the electromagnetic energy at 0 s, their effect will be neglected for the remainder of the study.

Similarly, the S_{21} response of the LW sensor in the time domain can be observed in Fig. 3.17. Several peaks are noticeable in this time domain response. The first peak at $\Delta t \approx 0$ μs corresponds to the electromagnetic coupling between the input and output of the IDTs (electromagnetic response), while the first acoustic peak at $\Delta t \approx$ 2.2 μs corresponds to the propagation time

of the LW acoustic energy from input to output (main acoustic signal). The second acoustic peak at $\Delta t \approx 4.5\ \mu$s and $\Delta t \approx 6.5\ \mu$s correspond to acoustic reflections, on the quartz edge(s) and on the IDTs respectively, the latter known as the triple transit echo (TTE) [80]. In this context, this response can be temporally controlled through time gating to separate electromagnetic energy from acoustic energy, subsequently returning to the frequency domain with a specified time window.

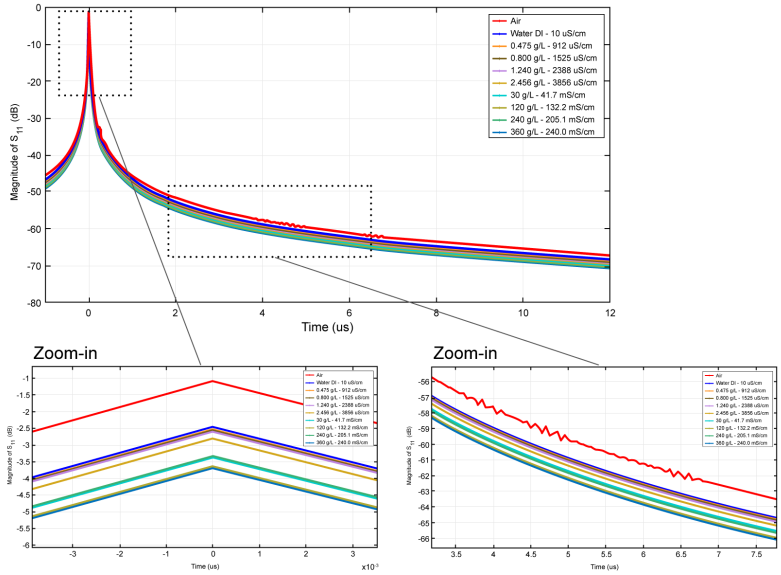

Figure 3.16: S_{11} in the time domain.

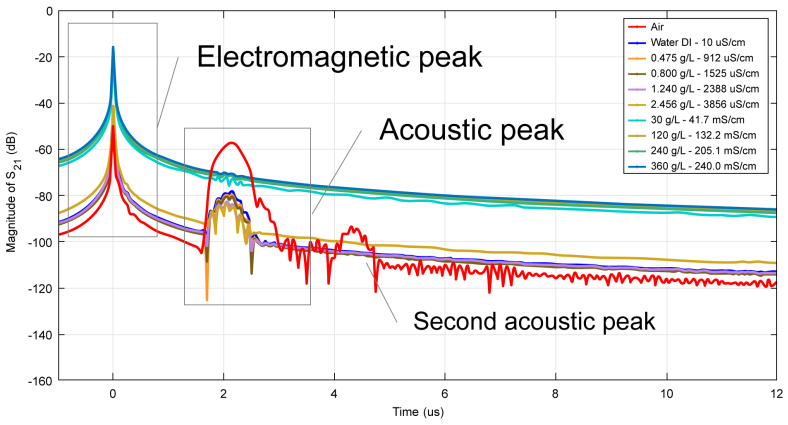

Figure 3.17: S_{21} in the time domain.

Time gating

In order to conduct an individual analysis of the responses related to each energy flow in the frequency domain, excluding the influence of other energies, such time gating technique (time-domain filtering) was employed, restricting the analysis window to the selected peak. This simple

method that enables the observation of the temporal spectrum in a specified range [178] offers a good mean to mitigate the impact of noise associated with the electromagnetic coupling in the frequency domain.

Figures 3.18 and 3.19 illustrate the frequency spectrum of the S_{21} parameter after applying time gating. Fig. 3.18 illustrates the time interval from 0 μs to 1.2 μs to isolate the electromagnetic energy only. It appears clearly that as the concentration of the solution increases, resulting in a higher quantity of dissolved ions, the transmission of electromagnetic energy also increases. Fig. 3.19, resulting from a time gating span from 1.2 μs to 3.2 μs, is utilized to focus on the main flow of acoustic energy without the influence of electromagnetic energy nor of the reflected acoustic one. With increasing viscosity and density of the liquid, greater shifts in frequency (Δf) and in S_{21} magnitude (ΔdB) can be observed. The filtered signal resembles a squared sinc function, as previously demonstrated in Subsection 3.2.1, Eq. 3.6, and consistent with the literature [80], [179]. This signal serves as the basis for analyzing our experiments concerning the S_{21} response of the sensor. It enables the establishment of the relationship between the mechanical parameters of the liquid, frequency shift, and sensitivity estimation through the linearization of the acoustic response. Moreover, by separating electromagnetic and acoustic energy, it becomes feasible to derive a QUCS electrical model from the descriptive equations, incorporating resistances and capacitances.

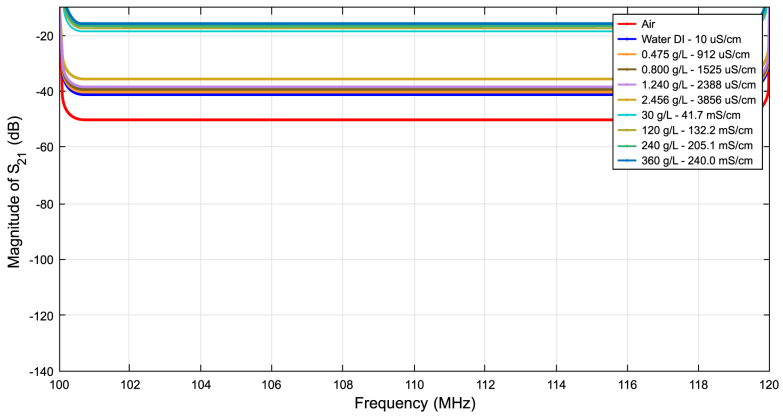

Figure 3.18: S_{21} in the frequency domain after time gating between 0 μs and 1.2 μs.

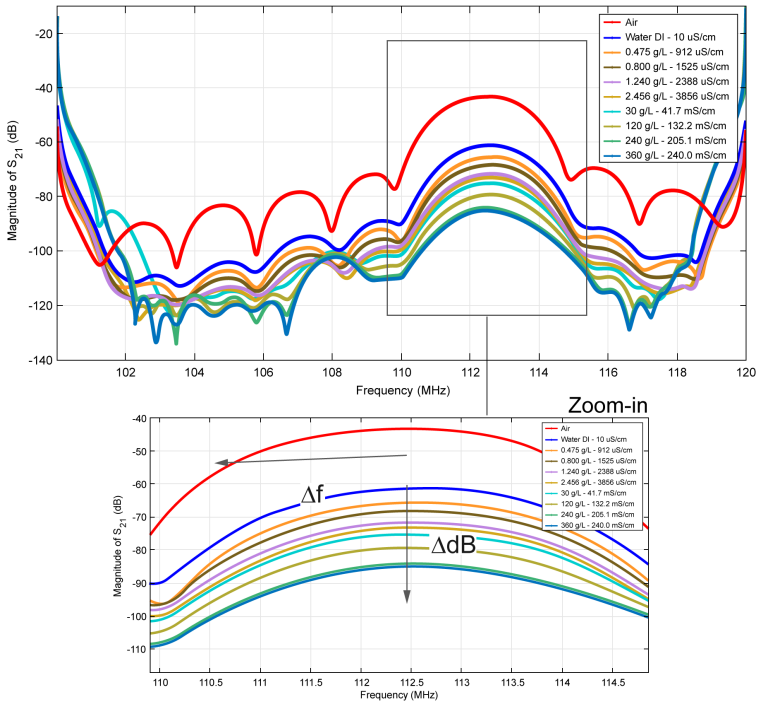

Figure 3.19: S_{21} in the frequency domain after time gating between 1.2 μs and 3.2 μs.

3.3.3 Sensitivity: linearization of the acoustic response

Several methods can be applied to estimate the behavior of LWs with adjacent liquid media. Some authors use the theory developed by [180], valid only for thicknesses much smaller than the wavelength, to estimate the variation in wave propagation in terms of frequency and attenuation. In the approach developed by [181], the influence of the liquid is observed from changes in the defined complex propagation constant (γ) from the equation

$$\gamma = \alpha + i\beta. \tag{3.9}$$

Here, the attenuation is represented by α, and β is the phase constant, given by $\beta = 2\pi/\lambda$, where λ is the wavelength determined by the spatial periodicity of the IDT. The propagation constant is modified by a liquid loading on the guide layer by

$$\frac{\Delta\alpha}{\beta} + i\frac{\Delta\beta}{\beta} = S\sqrt{\rho\frac{i\omega\eta}{1+i\omega\tau}}. \tag{3.10}$$

Here, S is the sensitivity of the device due to the surface mass charge effect, η is the flow viscosity of the liquid (Pa.s, 1 cP = 1 m.Pa.s), ρ is its density (kg.m^{-3}) and τ is defined as the shear relaxation

time of liquid [181]–[183]. The relative frequency shift related to the propagation constant can be calculated by

$$\frac{\Delta f}{f_r} = -(\frac{V_g}{V_p})\frac{\Delta \beta}{\beta} = -(\frac{V_g}{V_p})S_c\sqrt{\frac{\omega\eta\rho}{2}}. \tag{3.11}$$

Here, $V_g = \partial\omega/\partial\beta$ is the group velocity, and $V_p = \omega/\beta$ is the phase velocity. In equation 3.11, the quantity V_g/V_p is assumed to be constant by [184], as is the sensitivity S_s. The relationship between the frequency variation and the physical properties of the liquid ($\sqrt{\eta\rho}$) is given by

$$(f - f_r)/f_r = S_c.\sqrt{\eta\rho}. \tag{3.12}$$

Here, f_r is the resonance frequency. Moreover, a direct relation, expressed in equation (3.13), links the acoustic wave attenuation ΔA to the relative celerity shift

$$\Delta A = e^{2\pi S_c.p.LAP}. \tag{3.13}$$

Here, LAP is the number of wavelengths between the IDTs (from input transducer center to output transducer center) and $p = \sqrt{\eta\rho}$ [181], [185]. It can be noted that, when there is a change in viscosity and/or density, there is also a variation in the frequency [186].

Based on Eq. 3.12 and the results of the experimental frequency domain after time gating (Fig. 3.19), it is possible to observe in Fig. 3.20 the relative frequency shift due to changes in viscosity and density. As the acoustic energy was isolated, this variation is mainly caused by the mechanical characteristics of the liquid. A general linearization (I) or a two-interval linearization (II and III) can be performed. The second option was chosen for its greater realism with the results, allowing for a better correlation between experimental data and outcomes in the circuit modeling tool. In this context, $S_{c(II)} = -985.10^{-6}$ $\mathrm{mL}^{-1/2} \cdot \mathrm{cP}^{1/2} \cdot \mathrm{g}^{1/2}$ is obtained for low concentrations, $S_{c(III)} = -221.10^{-6}$ $\mathrm{mL}^{-1/2} \cdot \mathrm{cP}^{1/2} \cdot \mathrm{g}^{1/2}$ for high concentrations. In the next section, we will detail the descriptive equations and the circuit model performed in QUCS.

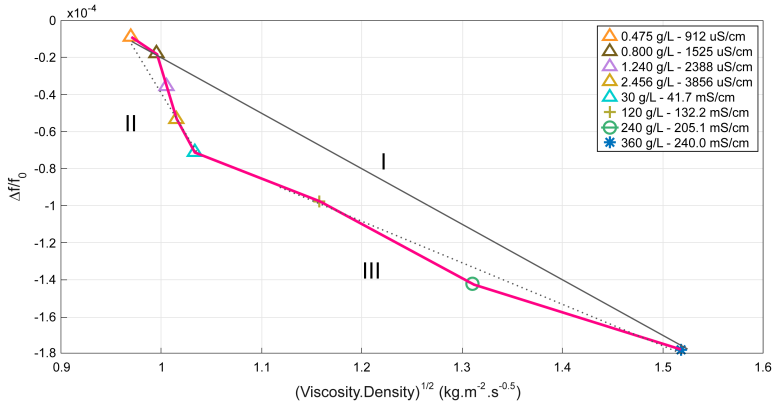

Figure 3.20: Variation of the S_{21} parameter of the electroacoustic wave after time gating as a function of the mechanical parameters of the liquid (reference: DI water).

3.4 QUCS model

In this section, a behavioral model for the LW sensor using QUCS is proposed to develop the LW sensor model in a liquid medium. The use of the QUCS tool has gained popularity in academia and industry due to its open-source nature, allowing RF work [187]. Moreover, it serves as a cost-effective alternative to other tools capable of modeling electrical and acoustic systems, such as ADS. The main idea was to replicate an existing SAW-LW sensor model based on descriptive equations and adapt it to the LW sensor used in experiments in the air medium. Building upon this initial behavior, the final goal is to propose a circuit model for the liquid that represents the influence on S-parameters of the sensor when saline solutions are introduced onto its surface.

3.4.1 Equivalent electrical model

The behavior exhibited by the LW sensor response can be effectively modeled using the QUCS tool, employing equations and circuit representations. In the work carried out by [185], this approach was proposed using the QUCS tool and descriptive equations to simulate the acoustic response of the LW sensor. Here, we contribute to a more global model involving electrical parameters. Initially, the electrical input impedance of the sensor is characterized by a capacitance (C_{idt}) in series with a resistance (R_{idt}) at both the input and output terminals of the sensor. Additionally, a capacitance (C_3) interconnects the input and output ports to shape the electromagnetic coupling surrounding the device. The values of capacitance and resistance were determined through retrosimulation until

they aligned with the experimental values obtained in the air medium. Fig. 3.21 illustrates this LW sensor model (highlighted in green).

In electrochemical devices, equivalent circuit models have been extensively employed to analyze device performance in liquid medium, providing an understanding of the contribution of various components [188]. Two of these circuits widely used to model conductive liquids are Randles and Debye, based on RC circuit configurations [189]–[191]. Based on these models, the model of the liquid deposited on the sensor surface was adjusted by introducing a circuit featuring a resistance (R_{liq}) in parallel with the input/output IDTs and a capacitance (C_{liq}) in parallel with the coupling capacitor C_3, as depicted in the configuration presented in Fig. 3.21 (red blocks). However, R_{liq} in the output IDT does not substantially influence the sensor input impedance. The components are connected to the LW sensor from the switches S_R, S_{R1} and S_C.

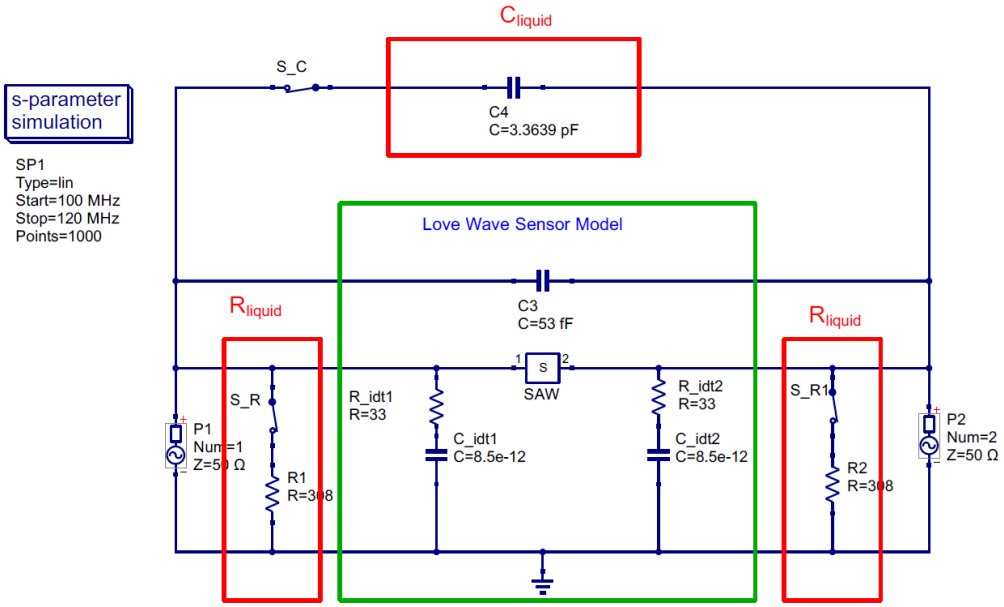

Figure 3.21: QUCS model of the LW device fitting in liquid medium.

3.4.2 Descriptive equations

The acoustic part (SAW block based on equations) at the input can be modeled by

$$S_{11_{ac}} = 1 - A_{S_{11}} sinc^2(c_t \pi N(f - f_r)/f_r). \tag{3.14}$$

Here, c_t is a fitting parameter and N is the number of generation acoustic wavelengths. The transmission acoustic energy can be modeled by

$$S_{21_{ac}} = A_{S_{21}} sinc^2(c_t \pi N(f - f_r)/f_r).e^{-j\omega t_d}. \quad (3.15)$$

Here, t_d is the wave delay time, which is linked to the LAP and the resonance frequency f_r with $t_d = LAP/f_r$. $A_{S_{11}}$ and $A_{S_{21}}$ are respectively the acoustic absorption and the insertion loss at the resonance frequency of the S_{11} and S_{21} responses.

All parameters incorporated in equations 3.14 and 3.15 and employed to fit the experimental results with the simulated outcomes are depicted in Fig. 3.22.

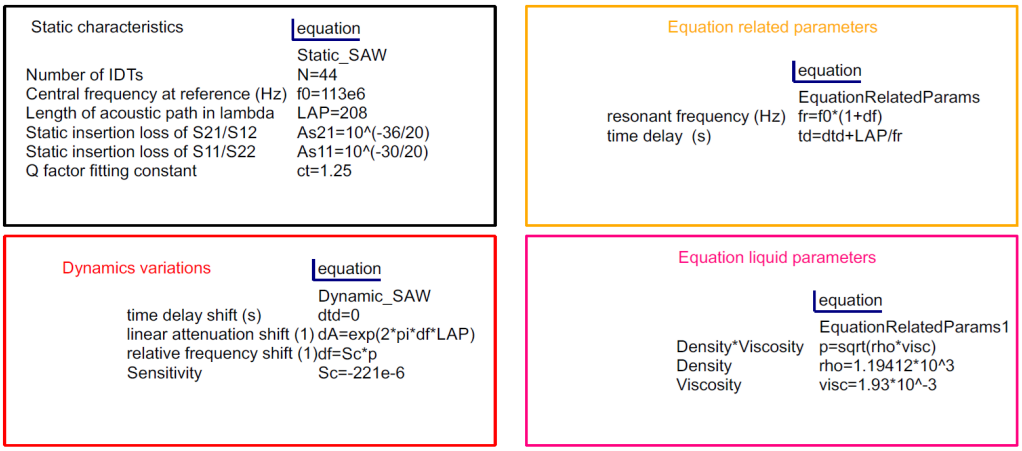

Figure 3.22: LW QUCS model descriptive parameters.

Fig.3.23 and Fig.3.24 show the comparison between the simulated spectrum (S_{11} and S_{21}) of the LW QUCS model (dashed lines) and the measurement (solid lines). The simulated results are close to the measurements, although the fit can be improved for S_{11} in the sense that the measured responses present a more pronounced capacitive behavior, especially for the highest concentrations.

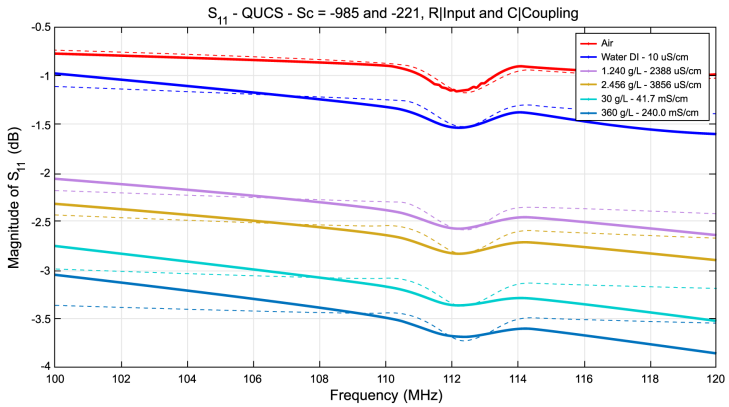

Figure 3.23: S_{11} parameters: a comparison between wired measurement (solid lines) and QUCS estimation (dashed lines) for variations in the electrical and mechanical parameters of the solutions

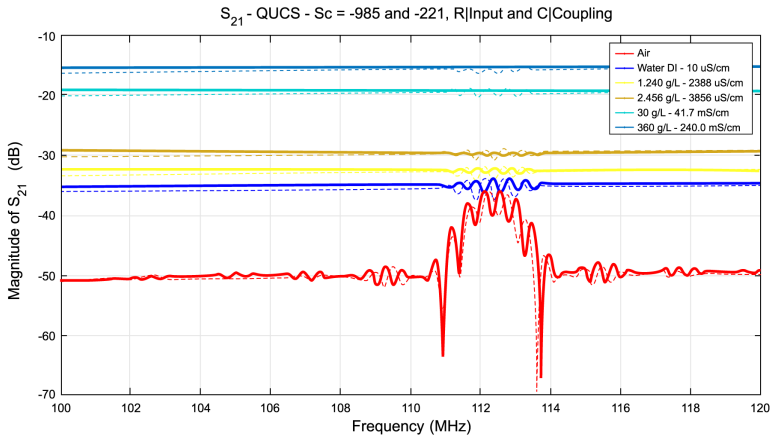

Figure 3.24: S_{21} parameters: a comparison between wired measurement (solid lines) and QUCS estimation (dashed lines) for variations in the electrical and mechanical parameters of the solutions

In the Tab.3.3 and Fig.3.25, the resistance R and capacitance C values of the solutions that optimally fit with the experimental results are presented. Each pair (R, C) of the electrical model is associated to a pair of viscosity and density (η, ρ) representing the mechanical parameters of the liquid and a pair of conductivity and permittivity (σ, ϵ) representing the electrical parameters, as corroborated by Tab. 3.2 and as shown in Section 3.2.3. The proposed QUCS model is in good agreement with both measurements and theory. This provides us with a frequency response to electromagnetic effects when the solution is added to its surface, complementing the state of the art that has so far only used mechanical parameters (such as viscosity and density) to describe its behavior [185].

Table 3.3: Resistance and capacitance values for the liquid in the LW sensor

Medium	**Resistance (Ω)**	**Capacitance (pF)**
Air	Infinite (open switch)	Infinite (open switch)
Water DI	2203	0.2449
NaCl Solution (0.465 g/L)	580	0.2999
NaCl Solution (0.800 g/L)	574	0.3196
NaCl Solution (1.240 g/L)	565	0.3724
NaCl Solution (2.456 g/L)	479	0.5713
NaCl Solution (30 g/L)	358	2.052
NaCl Solution (120 g/L)	352	2.9663
NaCl Solution (240 g/L)	313	3.0856
NaCl Solution (360 g/L)	308	3.3639

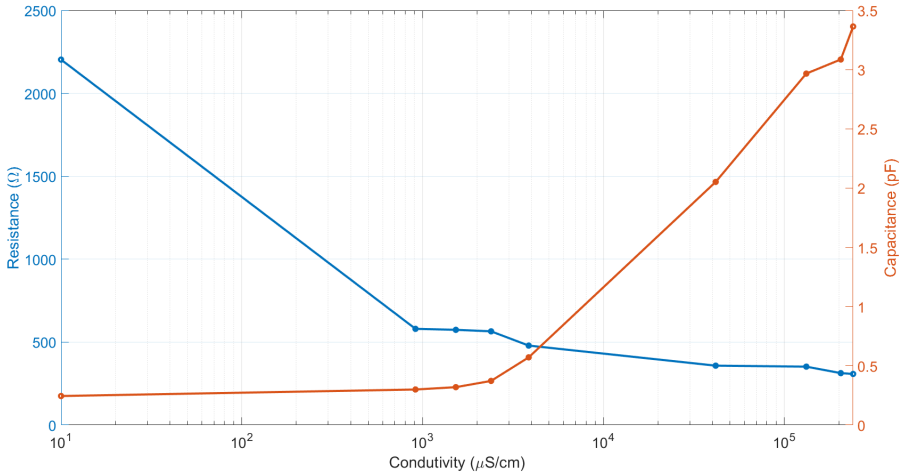

Figure 3.25: Relationship between the resistance and capacitance of the LW sensor in the QUCS simulation as a function of the conductivity of the solution.

In the next chapter, wireless experiments will be presented and discussed.

3.5 Chapter conclusion

While SAW devices have traditionally been utilized as filters in mobile communication devices, their application as sensors is currently expanding. The sensitivity of wave propagation velocity to external disturbances, along with the electromagnetic aspect of the sensor's response, particularly influenced by the medium above its IDTs, highlights the sensor's potential to concurrently measure various physical parameters. Through the experimental setup, we examined and correlated the sensor's responses S_{11} and S_{21} with the electrical and mechanical properties of NaCl solutions of different concentrations. The protocol employed demonstrated reproducibility, and the use of time-gating allowed for the separation of the sensor's electromagnetic and acoustic responses, consolidating recent works with this sensor. In particular, we focus on the influence of the liquid on the parameter S_{11}, which is dependent on the input impedance Z_{11} of the device, and adapted established liquid models from the literature and based on RC circuits for our LW sensor experiment. A close agreement was observed between the measured and simulated results obtained using the open-source simulation software QUCS. Specifically emphasizing the variation in S_{11}, we have the necessary components to utilize the sensor as a tag and detect it in a wireless configuration. This chapter elucidated various aspects and challenges associated with SAW sensors, particularly the LW sensor, for applications in liquid environments. We demonstrated the feasibility of detecting and classifying saline solutions in a wired setup, paving the way for wireless reading, which serves as the primary objective of this thesis.

4 Passive Wireless Love Wave Sensor System

Contents

In the context of wireless systems, the type of reader, link characteristics, transmission and reception, free space losses, and the type and response of the sensor to be read are crucial elements that significantly influence what can be extracted as information, especially those mentioned in the previous chapter related to input impedance. In this chapter, we demonstrate how the electromagnetic response of these passive sensors can be obtained from various experimental configurations and dedicated calibration processes. The feasibility of wireless reading using LW sensors will be assessed from setups including antennas and circuits, as well as experimental configurations based on Radar Cross Section (RCS) measurements and electromagnetic coupling. The initial experiments were conducted using commercial antennas. Following this, the design of a transmission circuit with dimensions compatible with the test cell and our LW sensor in its frequency range will be presented. Subsequently, the feasibility and ability of detection using these transmission and reception circuits will be investigated, culminating in remote detection of the electrical parameters of a liquid at different concentrations. Continuing, the results obtained regarding the design of a wireless system capable of detecting and classifying NaCl solutions present on the surface of the LW sensor will be presented. The issues, advantages, and drawbacks of the experimental setups will be addressed. Finally, a comparison will be conducted between the proposed solutions and prospects as a complementary approach to the use of wireless sensing with LW sensors, particularly focusing on the measurement of input IDT impedance, which has not been utilized in the literature, will be presented.

4.1 Experimental setups

Several wireless techniques and systems capable of communicating with devices, especially passive sensors, have been deployed in different configurations. These systems are designed based on the characteristics of the transduction type, such as electromagnetic and acoustic wave propagation, geometry, materials, recommended sensitivity depending on the application and the frequency range to be monitored. In a typical wireless setup, a sensor sensitive to a measurand (such as physical parameters of water) is connected to an antenna [102], [139], [152].

As shown in Fig. 4.1, the schematic setup includes a transmission (T_x) and reception (R_x) circuit connected to the reader (electronic reading device). The target consists of another backscatter circuit connected to the test cell containing the LW sensor. The backscattered signal depends on the properties of the medium in which the sensor is inserted. To analyze the response of the target (*i.e.* the sensor) as a function of the T_x and R_x signals, techniques based on backscattering and

RCS measurements can be used.

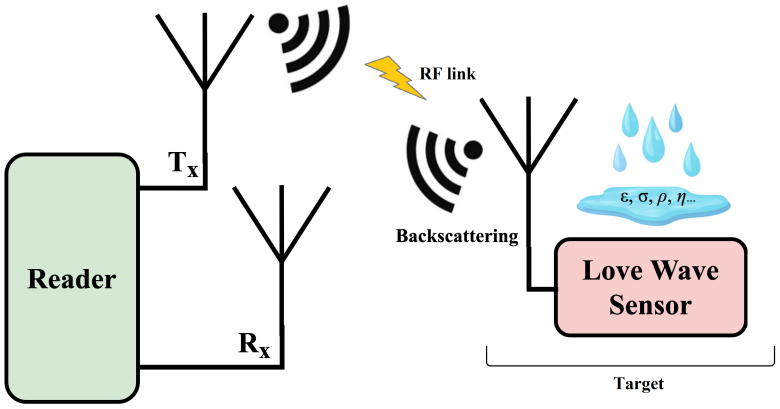

Figure 4.1: Synoptic schematic in bistatic configuration of a teledetection system.

.

In these techniques the target (sensing element) consists of a receiving antenna connected to sensors such as multiresonant transmission lines, spiral or split-ring resonators, or a SAW device [192]–[195]. The RCS signature of the target (including the sensor) can also be measured from the change in the resonance frequency or magnitude of the backscattered signal that carries the information of the parameter to be detected [25], [126], [196]–[198].

The work presented in this section demonstrates the use of a Love wave sensor configured for the wireless detection of various concentrations of saturated NaCl solution present on its surface. As discussed in the preceding chapters, given the high insertion losses of the sensor, it is challenging to extract its mechanical characteristics through wireless interrogation. Here, we are not concerned with the sensor's acoustic response regarding the liquid's mechanical parameters but rather its electromagnetic response and its relation to the liquid's electrical characteristics. In this context, we focus on leveraging its input impedance and reflection characteristics. In addition, a sensor-side measurement protocol was conducted to explore its electromagnetic response. Indeed, for remote detection, the relationship between the emitted and received power by the reader depends on the characteristics of the RF link balance parameters and variations in the sensor impedance response due to the properties of the liquid deposited on its surface [197], [199]–[201]. Thus, the resonance frequency or amplitude of the backscattered signal considers the liquid medium parameter to be monitored. Furthermore, the operating frequency of the LW sensor and the sensor type are crucial parameters for selecting the reader architecture and the remote interrogation method to be deployed.

In the preceding chapter, it was shown how the addition of NaCl solutions affects the energy

flow and modifies the sensor's impedance in wired experiments. This difference in electromagnetic energy was measured and serves as the primary indicator for potential wireless detection. In Fig.4.2, we provide an overview of the experiments conducted in this chapter, highlighting the wireless approaches. Moving forward, we will address wireless configurations in two different setups. The first one utilizes commercial omnidirectional antennas associated with the vector network analyzer (VNA) reader and the sensor. The second setup uses rectangular spiral circuits made of FR-4 for transmission, reception, and sensor connection.

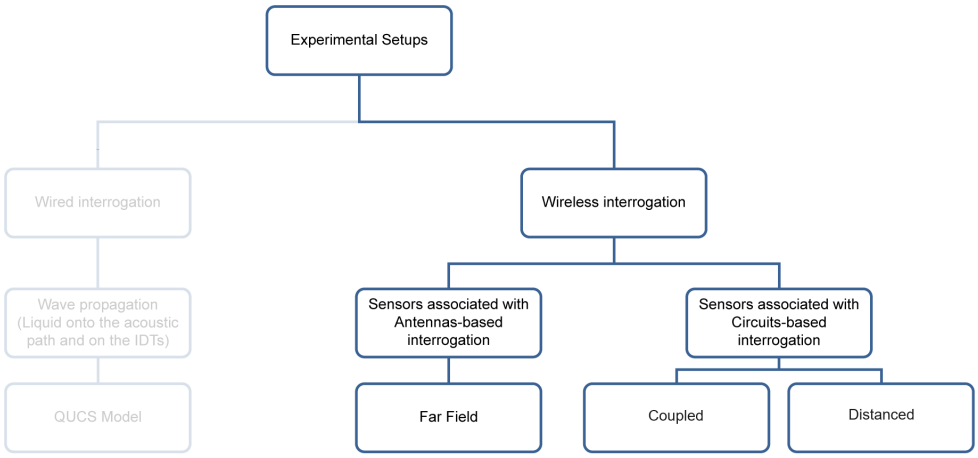

Figure 4.2: Overview of wireless experiments performed: Sensors associated with antennas and circuits.

Initially, the feasibility of the measurement was determined. Based on the results of the initial experiments, we progressed to the experimental setup for the RCS measurement. These approaches will be detailed in the following subsections, along with the characterization of the antennas used and others relevant points of the RF link. In the next section, we will focus on the configurations with the reader and the sensor associated with the antennas.

4.2 Love Wave sensor associated with antennas

In Fig.4.3, an overview of the initial tests conducted with the LW sensor is presented. Initially, the aim is to demonstrate the feasibility of remote measurements, based on cost-effective antennas with easily adjustable frequency. This led us to choose telescopic antennas, which offer flexibility in adjusting the resonance frequency by varying the dimensions of its sections. They also present some drawbacks for our application, such as a poor stability in achieving a fixed

resonance frequency and being omni-directional, thus non-directive and subject to environmental interferences. Nevertheless, it is a viable option when considering feasibility and when the objective is not to achieve classification with high sensitivity. To achieve this, two experimental setups were employed: one with two antennas and the other with three antennas. For this application of remote sensing of passive sensors, the frequency band of interest is in VHF, more specifically in 113 MHz and possibly adjustable to 145 MHz. The selected antenna is an omnidirectional telescopic type with 7 adjustable sections from 16.2 cm to 1.15 m, 50 Ω, VSWR<2.0 and operating in the frequency range of 25-1200 MHz [202]. Typically the gain of these antennas is 2.0 dBi [203]. On the sensor side, a saturated NaCl solution, consequently with high electrical conductivity, was added onto its surface. Before conducting the initial tests, antenna characterization was performed to ensure energy transmission centered at the sensor's operating frequency. In the next subsection, the frequency response of the antenna used and the experiments demonstrating the feasibility of remote detection are detailed.

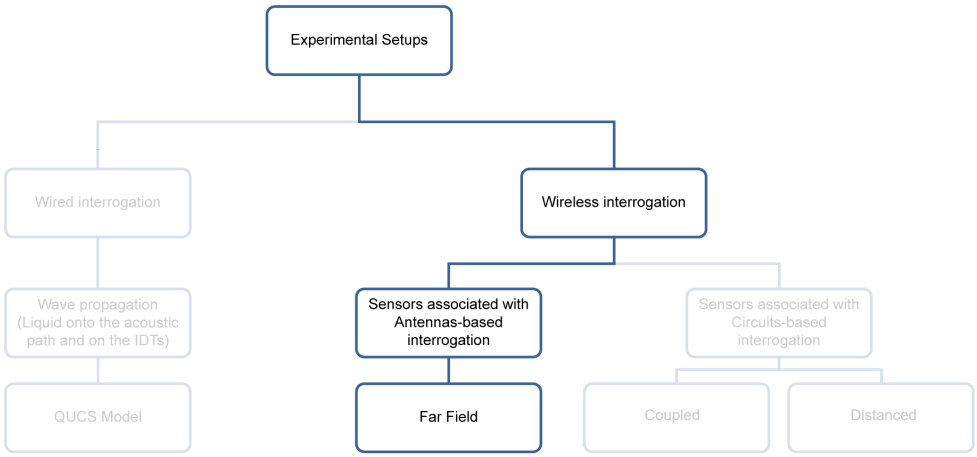

Figure 4.3: Overview of wireless preliminary experiments in far field performed with two and three antennas.

Antennas characterization

The setup of the antenna experimental characterization is shown in Fig. 4.4(a). A computer was connected to the VNA via a USB cable, and port 1 of the VNA was connected to the telescopic antenna for S_{11} measurement and length adjustment to achieve the desired operating frequency. Theoretically, the length of the antenna should be equal to $\lambda/4$, thus close to 62 cm to fit with a sensor resonance frequency of 113 MHz. Practically, the antennas were aligned at identical positions (same height and perpendicular to the surface) using laser as means of improving link

efficiency. The magnitude of the reflection coefficient (S_{11} = 9.04 dB) for the T_x (which is also the R_x) antenna can be seen in Fig. 4.4. Here, f_0 = 113 MHz is the antenna resonance frequency for a length of D = 62 cm on all antennas. It can be observed a quite good adjustment of the antennas around 113 MHz, they also exhibit a bandwidth that ensures that the sensor receives maximum energy at its operating frequency. However, due to the tripod structure and antenna support, it was not possible to obtain a stable configuration at the desired frequency from -10 dB (in which at least 90% of the energy is radiated). Even so, we have good agreement between the energy transmitted by the antenna and the wired response of the LW sensor at its operating frequency.

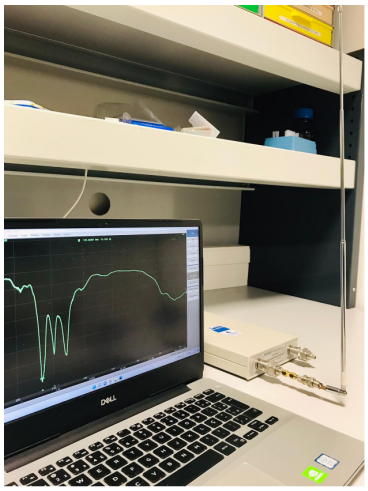

(a)

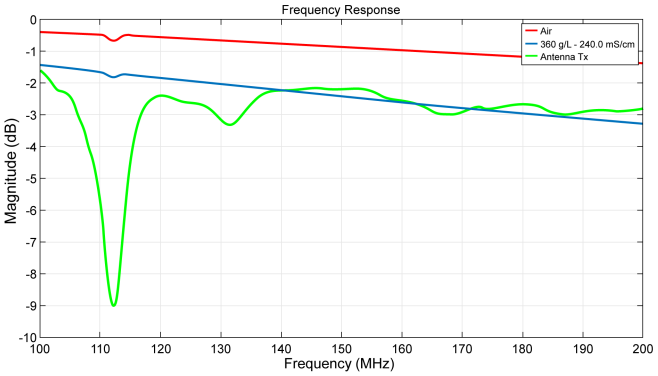

(b)

Figure 4.4: (a) Schematic of the experimental setup for the characterization of the telescopic antenna; (b) S_{11} measurement results of the three antennas with 62 cm in length and comparison with the wired response of the LW sensor in air and NaCl saturated solution.

Power estimation

For further analysis, it was necessary to have a power budget for several frequencies close to the operating frequency of the LW sensor. Therefore, we can use the radar equation to estimate the powers transmitted and received by the VNA with the power reflected by the sensor. The transmitted and received powers are correlated with the RCS of the sensor by

$$\frac{P_r}{P_t} = \frac{G_t G_r \lambda^2}{(4\pi)^3 R^4} \sigma \tag{4.1}$$

and the maximum detection distance estimated by

$$R_{max} = \sqrt[4]{\frac{P_t G_t G_r \lambda^2 \sigma}{P_{r,min}(4\pi)^3}}. \tag{4.2}$$

Here, P_t and P_r are the power transmitted and received in W, G_t and G_r are the respective gains of the antennas in dBi, λ is the wavelength in m, σ is the RCS in m^2 and R is the distance in m between the transmitter and the target. For frequency-based remote sensing systems, the information is related to the variation of the RCS as a function of frequency. Reader reception must be able to detect a minimum RCS value. This is the threshold value that sets, for a given frequency and distance, the transmit power and the receive sensitivity. From these values, including the characteristics of the antennas, we can estimate the maximum detection distance as a function of a particular bandwidth for different RCS values. The typical values of RCS for these applications are in the range of -10 to -60 dBsm [13], [25], [29], [197]. Using a Continuous Wave (CW) based detection system, which consists of a stable frequency wave, radio energy is transmitted and then received from any reflective objects. CW sets transmit a high-frequency signal continuously. The echo signal is received and processed on a ongoing basis. The power sensitivity $P_{r,min}$ of -75.23 dBm is chosen to be equal to three times the noise level and detection limit of the VNA in use as a reader, measured at -80 dBm. As the antennas are identical, the transmit antenna gain has the same value as the receive one, $G_t = G_r = 2$ dBi. From these values we have an estimation of the reading distance that we can be obtained according to the European Telecommunications Standards Institute (ETSI) standard of a radar emitting CW from the characteristics of the detection system [22]. In Fig. 4.5 the theoretical detection range chart is calculated and shown as a function of the frequency, and for RCS values set to -60, -50, -40, -30, -20, -10 dBsm. The output power transmission is set to P_t = 3 dBm and the power sensitivity is $P_{r,min}$ = -75.23 dBm.

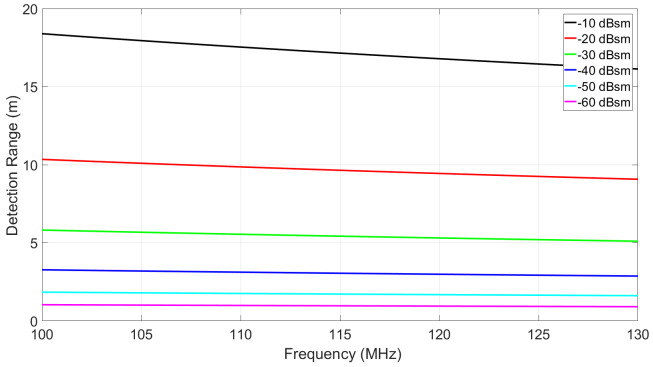

Figure 4.5: Maximum reading distance as a function of frequency for different RCS values of the sensor setup (@ $G_t = G_r = 2$ dBi, $P_t = 3$ dBm, $P_{r,min}$ = - 75.23 dBm).

In Fig. 4.6 the theoretical detection range is represented as a function of the transmission power,

and for RCS values set to -60, -50, -40, -30, -20, -10 dBsm. The frequency is set to 113 MHz, and the power sensitivity is $P_{r,min}$ = - 75.23 dBm. According to the calculations performed, the theoretical maximum reading distance does not exceed 17.3 meters, assuming a lossless and interference-free system. 40 cm was the shortest distance in the far field, and it was chosen for the initial detection tests by

$$R = \frac{2D^2}{\lambda}. \tag{4.3}$$

Here, R is the minimum distance corresponding to the the far field region (Fraunhofer region), D is the maximum antenna dimension and λ the wavelength [22]. In the next subsection, we will detail the configurations used, firstly to identify the influence of the liquid on S_{11}, then focusing on the RCS measurement considering both the S_{11} of the sensor and the S_{21} of the system.

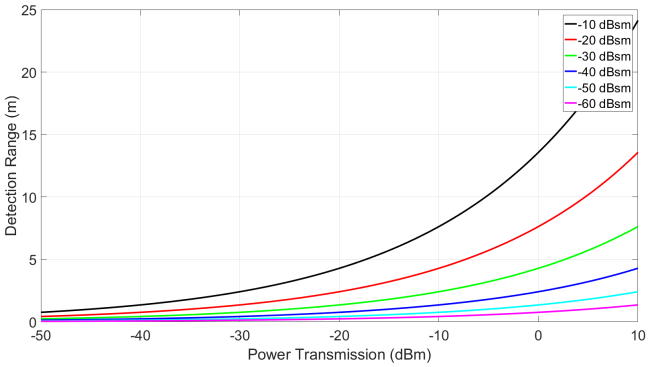

Figure 4.6: Maximum reading distance as a function of transmission power for different sensor RCS values (@ $G_t = G_r$ = 2 dBi and $P_{r,min}$ = - 75.23 dBm).

4.2.1 Monostatic configuration

The experimental bench proposed for the S_{11} remote measurements with air and liquid is shown in Fig. 4.7: a laptop computer (1), which controls the VNA (3) with USB cable interconnection (2); the VNA delivers the radiofrequency signal to feed the transmitting antenna (5) via a coaxial cable (4); the backscattering antenna (8) was connected directly to the cell with the sensor (9). The transmission and reception of the signals were carried out inside the anechoic chamber kindly provided by ENSEIRB-MATMECA - Bordeaux INP. It has dimensions of 7 × 3 ×3 m^3, constructed using C-RAM SFC absorptive material in pyramid-shaped blocks of 60 × 60 cm^2 base area, each containing pyramids with an attenuation of -30 dB for the sensor's operating frequency (-25 dB at 20 MHz up to -48 dB at 1.2 GHz). C-RAM SFC is a series of high-performance broadband RF absorbers made from treated polyurethane foam. Two wooden tripods (6) with a height of 1.2 m

are used as support for the 1.5 m metallic rail (7) in order to fix the antennas so that they do not move during the measurements and that provide a facilitated adjustment of the distance between the antennas.

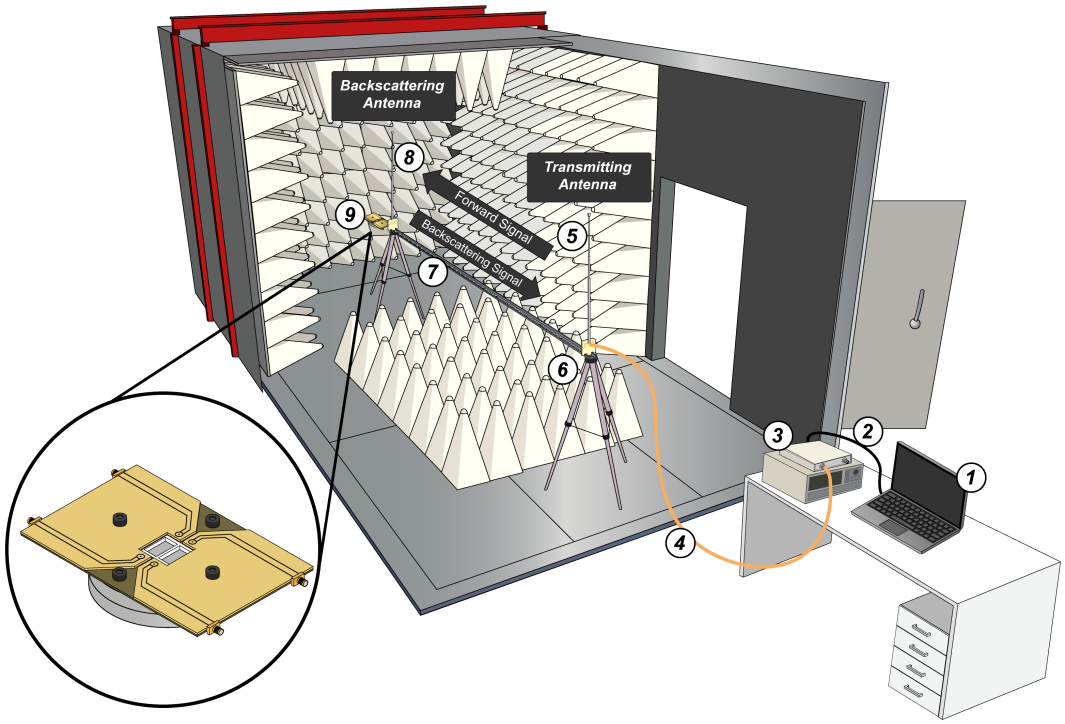

(a)

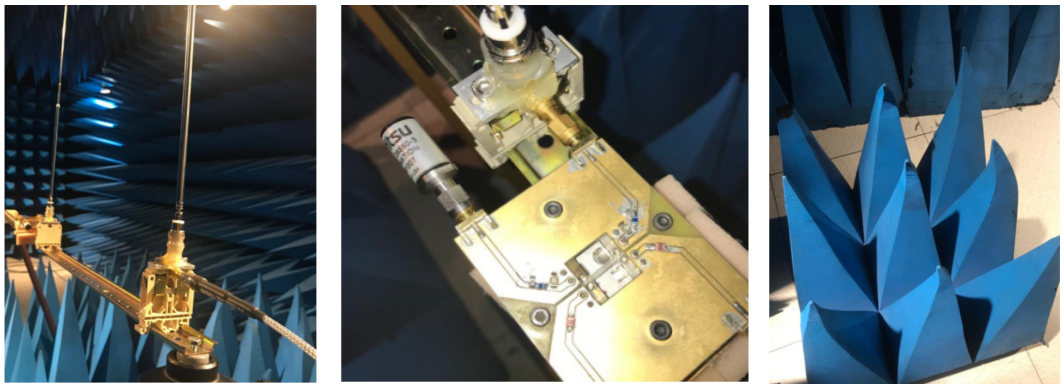

(b)

Figure 4.7: (a) Schematic of the experimental setup for wireless LW sensor interrogation in reflection; (b) Measurement in the anechoic chamber (ENSEIRB-MATMECA - Bordeaux INP), details of the test cell and absorbers.

Two identical Bingfu telescopic antennas were used. For example, a length of 62 cm allowed tuning the transmit and backscattering antenna resonances with a first mode close to the sensor operating frequency, and an experimental magnitude of -9.3 dB at 113 MHz was measured. The difference between the previously measured S_{11} in the subsection 4.2 and those in this configuration

is due to the fact that in this setup, the antenna is mounted on a support and aligned with the tripod, substantially altering the transmitted energy. However, with this value of -9.3 dB for S_{11} at the sensor's operating frequency, it is still possible to ensure that a significant portion of the energy will be transmitted. For each series of measurements, a Short-Open-Load (SOL) calibration at the end of the cable (4) was performed before connecting the antenna (5). A minimum distance of 39 cm at 113 MHz was estimated from the far field equation [33]. Therefore, a distance of 40 cm between the transmission and backscattering antennas was chosen to perform the experiment. After SOL calibration and antennas tuning, the test cell and sensor assembly described in Fig. 4.7 were connected to the backscattering antenna. Given the instability of the supports to mechanical touch in this configuration, the test cell was not disassembled and the LW sensor was not cleaned during the liquid measurement sequences. The prepared solution was inserted into the sensor surface with the micropipette in order to control the liquid volume and reduce systematic and random errors caused by this. The solution has a conductivity of 240 mS/cm.

In Fig. 4.8 (a) the measurement of the reflection characteristics at the transmit antenna is shown over a 1.2 GHz bandwidth without (blue curves) and with liquid (red curves) on the sensor surface. As it can be seen, a quite good reproducibility is obtained. Moreover, as shown in Fig. 4.8 (a) and (b), a measurable and repeatable shift of the response from ambient air to salted water can be observed only at the lower resonance of the antenna, which was tuned to be close to the sensor operating frequency. The other antenna resonance modes remained almost unchanged (up to about 800 MHz) or led to non reproducible variations at higher frequencies. An average reflection coefficient and a frequency with standard deviation of -9.39 dB (σ = 0.09 dB) and 126.701 MHz (σ = 0.41 MHz), respectively, were obtained at ambient air conditions and -9.76 dB (σ = 0.12 dB) and 126.101 MHz (σ = 0.0075 MHz) in the presence of salted water, as shown in Tab. 4.1.

Table 4.1: Monostatic configuration results

2 antennas FM				
Medium	**Frequency (MHz)**	**σ (MHz)**	**Magnitude S_{11} (dB)**	**σ (dB)**
Air	126.701	0.41	-9.39	0.09
360 g/L - NaCl	126.101	0.0075	-9.76	0.12

Thus, the addition of salted water on the sensor induced a change in its impedance and therefore a change in the reflection coefficient, reproducible around the working frequency of the LW device. In this way, this setup demonstrated the possibility of wirelessly detect the NaCl solution insertion's

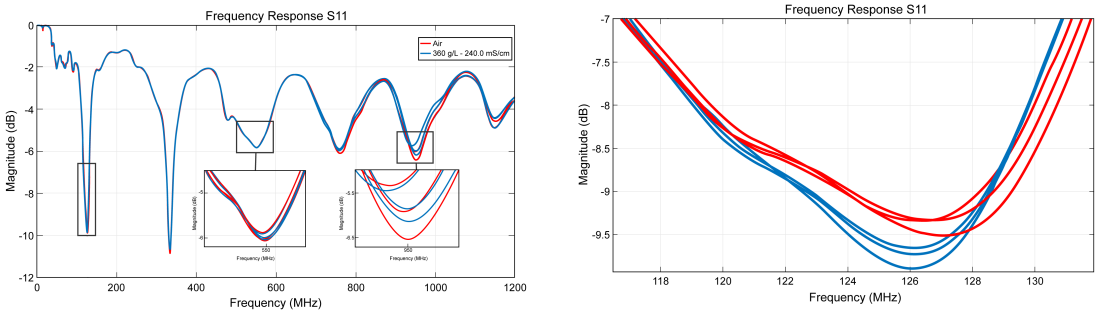

(a) (b)

Figure 4.8: LW sensor responses based on 3 wireless measurements of S_{11}, with air (red curves) and salted water (blue curves): (a) Wide frequency range and zoom in on two antenna resonance frequencies (ranges 500-590 MHz and 920-980 MHz); (b) Focus on the shift of the lowest resonance mode close to the sensor operation frequency.

influence on S_{11}, compared to a bare device. The addition of the backscattering antenna caused a change in the resonance frequency of the transmission antenna, moving its resonance frequency to 126 MHz. Each element added at reception (backscattering antenna, test cell and liquid) caused a change in the S_{11} signal. Though this initial measurement pointed out some issues, such as in the adjustment of the experimental setup with several sources of errors, it was considered encouraging as a first step towards remote measurement of the physical parameters of liquid media. Based on this initial result, an experimental configuration with three antennas was performed, which will be discussed in the next subsection.

4.2.2 Bistatic configuration

In this section, we employed a bistatic antenna setup for RCS measurements using the transmission parameter (S_{21}). The experimental configuration proposed for remote measurements under both air and liquid conditions is depicted in Fig. 4.9. This experimental setup follows a similar configuration to the previous one, with the addition of a third antenna and a Short-Open-Load-Through (SOLT) calibration performed at the end of cables (4) before connecting transmitting antenna (5) and receiving one (6). Following the SOLT calibration and antenna tuning, the test cell and sensor assembly described in Fig. 4.9 were connected to the backscattering antenna (8).

In Fig. 4.10 (a) the measurement of the magnitude transmission characteristics of the system is shown over a bandwidth of 1.2 GHz without (red curves) and with liquid (blue curves) on the sensor surface. Again, as depicted on Fig. 4.10, a measurable and repeatable shift of the response from ambient air to salted water can be observed only at the antenna lower resonance,

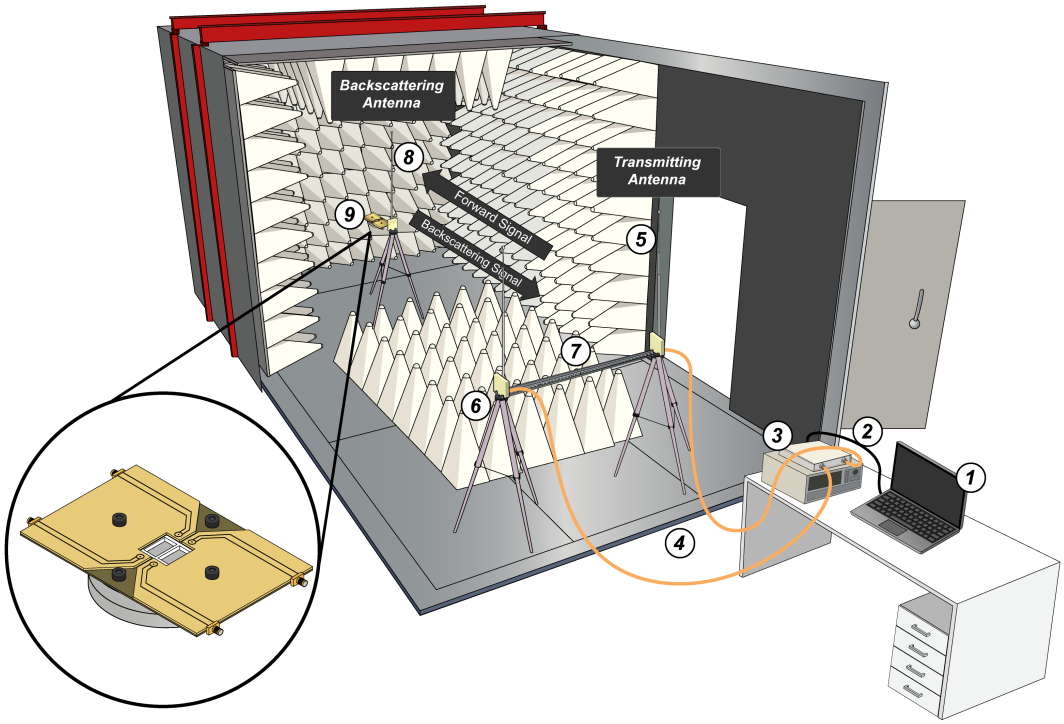

(a)

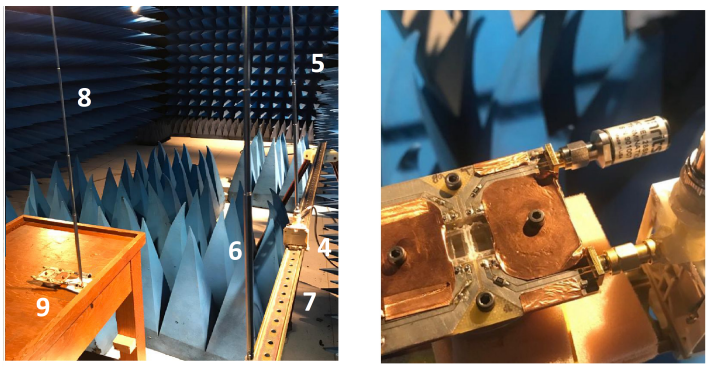

(b)

Figure 4.9: Experimental bistatic setup for LW sensor interrogation: (a) Experimental diagram overview; (b) Pictures of the experiment performed in the anechoic chamber and details of the device under test (measuring cell) containing the sensor and the aperture where the liquid was inserted.

which was tuned to be close to the sensor operating frequency. The other antenna resonance modes remained almost unchanged or led to non reproducible variations not allowing the reliable distinction between the curves with air and with the liquid. This supports the conclusion of an effect specifically attributed to the sensor near its resonance frequency. Average transmission coefficient and frequency of −18.93 dB and 117.571 MHz, respectively, were obtained at ambient air conditions and −19.10 dB and 117.350 MHz in the presence of salted water. These results led to estimate a mean variation and a standard deviation in magnitude and frequency of the order of −0.17 dB ($\sigma = 0.04$ dB) and - 221 kHz ($\sigma = 27.3$ kHz) from the bare sensor to the sensor with salted water. The RCS can be calculated from the transmission coefficient by

$$RCS_{(tgt)} = RCS_{(std)}.10^{\frac{S_{21}(tgt)-S_{21}(sdt)}{10}}. \tag{4.4}$$

Here, the indices (tgt) and (std) refer respectively to the target and to a standard metal plate, respectively [204], [205]. The standard metal plate used as a reference was made of FR-4 with a dimension of 20 cm x 30 cm and theoretical RCS of −11.37 dBsm, as in [205]. The calculated average RCS values are −10.32 dBsm in ambient air condition and −10.45 dBsm in presence of the liquid, leading to a shift of - 0.13 dBsm, as shown in Tab. 4.2. From these results, we can deduce that the addition of the salted water on the sensor induced a change in its IDT impedance measured as a change in the reflection coefficient, consequently in its RCS and in the transmission coefficient of the wireless system, which was reproducible around the working frequency of the LW sensor.

For this setup, for a transmitted power of 3 dBm, the received power was −16.09 dBm considering the bare sensor and −15.92 dBm when liquid was added. From the results of RCS, antennas gain, transmission power, considering -75 dBm as the minimum detectable signal and using the radar equation in [22]. The magnitude levels of the transmission coefficient and the RCS values calculated in this configuration have the same order of magnitude as works in the literature, used as a reference though not based on SAW devices [25], [206], [207].

In general, studies involving passive sensors and RFID tags have measured RCS in the range between -10 dBsm to -50 dBsm. For instance, the work by [198] calculates the RCS of an RFID tag located 60 cm away from the reader around -35 dBsm. Typically, with passive sensors and RCS measurements, these systems are applied to measure temperature, humidity, gas concentration, and pressure [206], [208].

Finally, we show experimentally that the difference in the magnitude of the transmission

coefficient measured with port 2 of the VNA is related to the change in impedance of the sensor when salted water is added onto its surface. Therefore, it is possible to perform remote sensing for two very extreme environments (in this case air and saturated NaCl solution) by measuring the RCS using the bistatic configuration, which allows a separation between transmitted and backscattered interrogation signals.

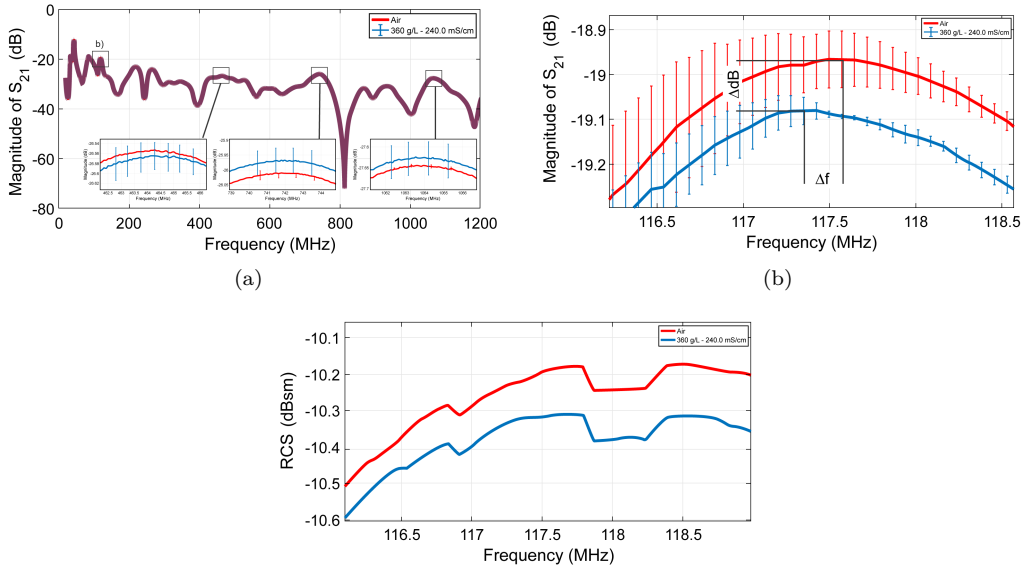

Figure 4.10: LW sensor responses based on 6 wireless measurements of S_{21}, with air (red curves) and salted water (blue curves). (a) Wide frequency range and zoom-in on three antenna resonance frequencies (ranges 462-466 MHz, 739-744 MHz and 1062-1066 MHz); (b) Focus on the shift of the lowest resonance mode close to the sensor operation frequency and (c) the corresponding RCS values.

Table 4.2: Bistatic configuration results

3 antennas FM Configuration					
Medium	**Frequency (MHz)**	σ **(MHz)**	**Magnitude of** S_{21} **(dB)**	σ **(dB)**	**RCS (dBsm)**
Air	117.571	0.0273	-18.93	0.04	-10.32
360 g/L - NaCl	117.350	0.0273	-19.10	0.04	-10.45

Nevertheless, though the shift in average RCS values at ambient air condition and in presence of the liquid could be detected, and this effect of the liquid presence was observed with a quite good repeatability only around the working frequency of the sensor, the variations of the parameters are still very small. Additionally, the system needs to be more robust to achieve better reproducibility in order to further distinguish not only highly concentrated salted solutions compared to air, but also several media with closer properties.

Indeed, as shown in the summary Tab.4.1 and 4.2 highlighting the measurements through reflection parameters S_{11} (monostatic configuration) and transmission parameters S_{21} (bistatic configuration), several challenges arise in reproducing and interpreting the measurements, even when conducted in an anechoic chamber. The commercial antennas such as those used, despite advantages such as flexible use and low-cost, also exhibit robustness limitations, with significant variations in their operating frequency adjustment and transmitted energy, as well as susceptibility to interference and size. Consequently, a new solution is described in the following section, which involved the design and implementation of a FR-4 circuit to access the sensor's parameters S_{11} and S_{21}, aiming to achieve measurements with enhanced reproducibility.

4.3 Sensor associated with circuits

In this section, we propose the same two experimental configurations as previously presented, based on S_{11} and S_{21} measurements of the wireless link and estimation of associated characteristics of the sensor input port and their variation depending on the fluid on the sensor, but replacing commercial antennas with resonant circuits for wireless interrogation. This is represented in Fig. 4.11, coupled and also distanced here will be considered for practical reasons related to the sensor low frequency range. We will first outline the steps from circuit design to characterization, which will be validated to ensure energy transmission centered on the sensor's operating frequency. Subsequently, the configurations will be implemented, and experiments demonstrating remote detection with various concentrations of the NaCl solution will be detailed.

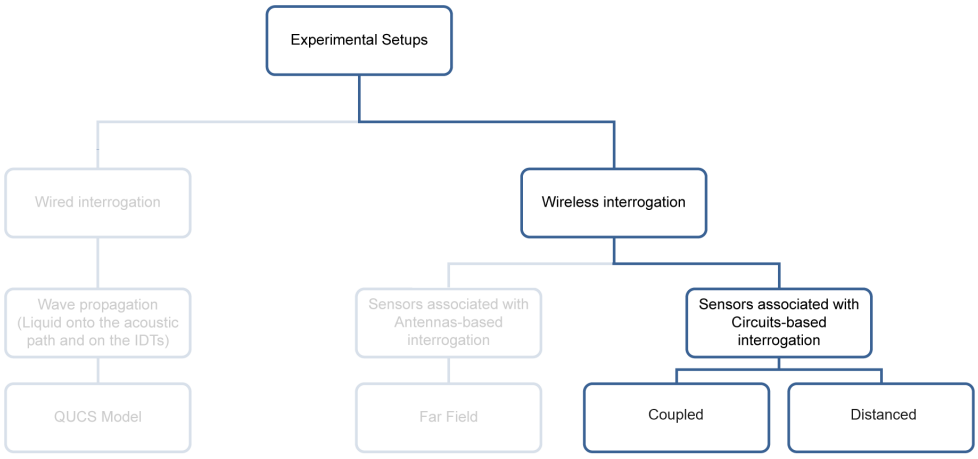

Figure 4.11: Overview of wireless experiments performed with circuits.

Circuits characterization

Microstrip rectangular spiral patch circuit can assume different geometric shapes, can be easily fabricated with low-cost material, allow a design with reduced dimensions and are used in several applications [33], [209]. Compared to other commercial antennas in the same operating frequency range close to 100 MHz, such as telescopic, Yagi-Uda or helical antennas, we will see that a microstrip patch can have the same order of size compared to the devices to be interrogated in a passive remote sensing system [94], the so-facilitated manipulation can also minimize random errors of measurement, thus improving the reproducibility of the experiments. A compromise was required between the size, directivity and radiation pattern of the irradiating element. The Yagi-Uda and helical antennas are more directive and typically have higher gain but are large in size to be connected to the sensor. The telescopic antenna has an omnidirectional radiation pattern and low gain but has low cost and variable frequency adjustment.

Spiral microstrip patch antenna circuits were used in many works. Among them, [210] developed a circularly polarized wide-band printed square spiral antenna operating in Ku-band (8 GHz - 12 GHz), applied to small satellites such as microsatellites and CubeSats. In [211] was simulated and measured a spiral antenna, built on Duroid 5880, with bandwidth of 400 MHz, resonance frequency of 1.69 GHz and area of 10.58 cm^2. A square microstrip spiral patch antenna, feeded by coaxial cable, for radio frequency microelectromechanical system applications, was developed in [212]. A wide band square spiral antenna with truncated corner, operating at 5 GHz, with bandwidth of 1.2 GHz and maximum experimental gain of 7.3 dBi was developed in [213]. In [214] was developed a circular spiral patch antenna with circular polarization operating in frequencies of 1.2 GHz, 1.5 GHz, 2.4 GHz, 3.3 GHz, and 5.8 GHz for vehicular mobile communications, with tests performed with a vehicle moving speed of 15 km/h. A spiral coplanar waveguide (CPW) antenna for biomedical applications, operating in GSM bands, Bluetooth, ZigBee, Wi-Fi, WLAN and LTE bands was presented in [215]. However, these developments use higher frequencies and conventional antenna circuits for the VHF band exhibit large dimensions, non appropriate to our small-size LW sensors.

The objective of this subsection is to describe a rectangular spiral microstrip patch circuit, with compact dimensions, operating frequency range of our LW devices, close to 113 MHz, in order to be used in our system. A slightly modified circuit was also realized, adapted to the other sensor resonance frequency of 145 MHz. This set of sensors and circuits (113 and 145 MHz) was used to obtain preliminary results regarding the influence of sensors on the systems and of the liquid on it.

The design method used was adapted from [213], [216] and can be divided in:

1. Choice of the circuit bandwidth: 2 MHz (111 MHz to 115 MHz with a center frequency of 113 MHz);
2. Selection of the material, including cost and characteristics parameters: FR4 substrate was chosen and characterized from 50 MHz to 170 MHz;
3. Design, simulation and fabrication according to the best simulated results;
4. Measurement and validation tests performed to compare the experimental results with the simulated ones;
5. Feedback between experimental and simulated data and fitting process to adapt the experimental circuit behaviour to the targeted values.

The electrical characterization of the material was performed with the measurement of the permittivity, loss tangent and thickness of the dielectric substrate by a probe process with the software Dielectric Probe 85070, using the VNA of Agilent Technology model E5071C (300 kHz — 20 GHz). The results of the dielectric characterization of the substrate material are shown in Fig. 4.12 [217].

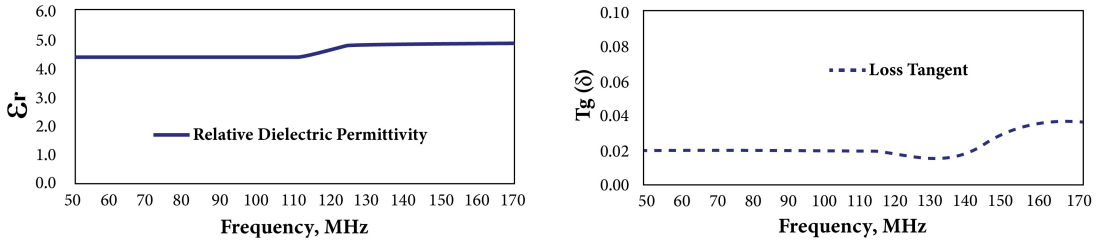

Figure 4.12: Dielectric characterization of FR4: a) Permittivity; b) Loss tangent.

This project presents a rectangular patch circuit with a spiral shape. The simulations, fabrication and measurements were performed using $Ansys^{TM}$ software, LPKF ProtoMat E33 PCB plotter and a VNA Copper Mountain TR 1300/1 (300 kHz - 1.3 GHz), respectively. The circuit structure is composed of a rectangular spiral irradiator element and a ground plane separated by FR4 dielectric substrate, thickness $h = 1.6$ mm, operating at 113 MHz with characteristics as measured: permittivity $\epsilon_r = 4.3$, loss tangent $\delta = 0.02$. The design was adapted from [218], [219] for resonance frequency compatible with the sensor, with a spiral spacing of 1 mm, lines length

calculated as fractions of the guided wavelength (λ_g) and a total area of 16.55 cm². The effective guided wavelength (λ_g) can be calculated by

$$\lambda g = \frac{c}{f_0\sqrt{\epsilon_{ffr}}}. \tag{4.5}$$

Here, $\epsilon_{ffr} = (\frac{1+\epsilon_r}{2})$, ϵ_r is the relative dielectric constant of the substrate, c is the light velocity in vacuum and f_0 is the resonance frequency [33].

Fig. 4.13 shows the simulated circuit dimensions with a resonance frequency of 113.08 MHz.

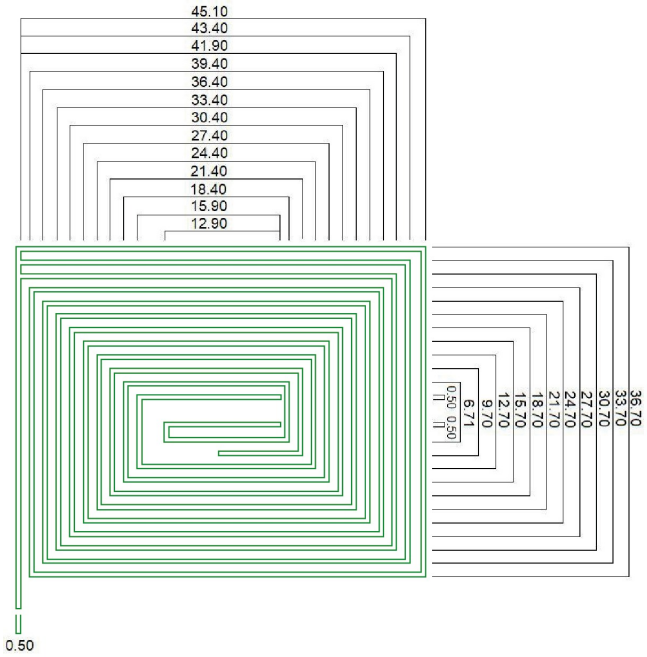

Figure 4.13: Patch circuit design @ 113MHz: patch element with fitted dimensions in millimeters.

The detection distance between the reader and the LW sensor depends on the characteristics of the link budget, transmission power, and the magnitude of the reflection coefficient of the LW sensor to the power detection threshold at reception [33]. The experimental setup used for the circuit response measurement is shown in Fig. 4.14: a computer (1) connected with a USB cable (2) to the VNA Planar TR1300/1 Copper Mountain (3); the VNA provides signals via a 30 cm RG-174 coaxial cable (4) to the patch circuit (5) connected by a SMA connector. For fixing the circuit, a metal bracket (6) is used, avoiding movement during the measurements. For each measurement, a one-port SOL (short-open-load) calibration was performed at the end of the coaxial cable (4) before connection to the circuit (5).

The comparison between the simulated and measured results of the reflection coefficient of each

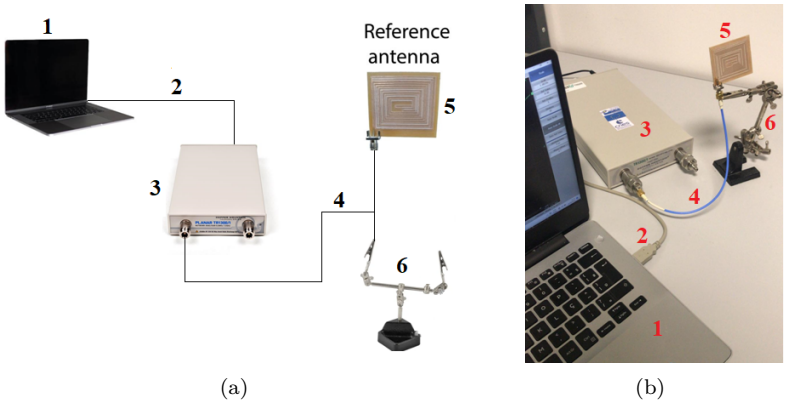

Figure 4.14: Experimental setup for characterization of the patch circuit reflection coefficient: a) Diagram; b) Picture.

one of two similar patch circuits (Rx and Tx named as their future role in the sensor interrogation) can be seen in Fig. 4.15 and in Tab.4.3, where f_0 is the resonance frequency, f_1 and f_2 are the lower and upper frequencies at -10 dB (in which at least 90% of the energy is radiated), BW is the bandwidth (f_2 - f_1) and S_{11} is the magnitude of the reflection coefficient. From the results, the difference between the resonance frequencies of the sensor and the patch circuits is very small and not critical for wireless interrogation.

Compared to the 900 MHz antenna from which our circuit was designed [220], radiation loss is observed with the increase in the dimensions of the traces to adjust to the desired frequency. In this sense, it almost completely loses its antenna characteristic and becomes a resonant circuit at the desired frequency, with radiating property. Indeed, as meeting all requirements of the initial project was physically non feasible with good efficiency, the circuit as proposed represents a technological compromise between operating frequency (113 MHz), small dimensions though quite low frequency, and good efficiency. Consequently, there is a reduction in the distance over which these circuits can be used for remote detection, which can be still interesting depending on the target application. When compared to the commercial antenna, these circuits offer the advantage of smaller dimensions, experiencing less interference, and not requiring adjustments for resonance frequency.

In Fig.4.16, the frequency response can be observed when the two circuits are positioned face to face and the S-parameters measured with the VNA Planar 304/1 Copper Mountain. Not surprisingly, the mean value of the S_{11} magnitude remains close to 0 dB, with several resonance minima, while the S_{21} magnitude is close to –30 dB over the range approximately (80 - 250 MHz), –50 dB over the full range up to 1 GHz dips, also with resonance peaks. This low value of S_{21} can

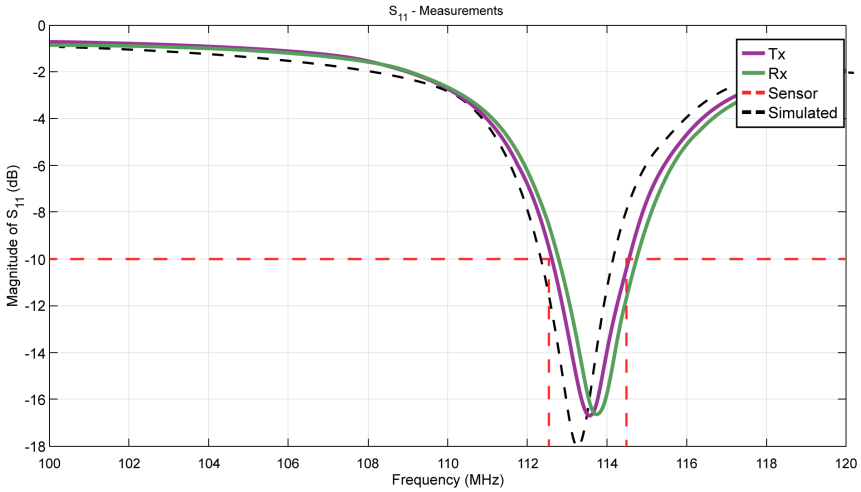

Figure 4.15: Measured and simulated results for the reflection coefficient of the rectangular spiral circuits and the sensor operating range.

Table 4.3: Measured and simulated reflection coefficient parameters of the rectangular spiral circuits

Results	**Parameters**				
	f_0	f_1	f_2	BW	$\|S_{11}\|$
	MHz				dB
Simulated	113.08	112.25	114.10	1.65	- 20.04
Measured T_x	113.55	112.58	114.52	1.94	- 16.73
Measured R_x	113.74	112.79	114.72	1.93	- 16.64

be attributed to radiated electromagnetic energy from the circuit 1 to the circuit 2. In some cases, a drop in S_{11} seems to be associated to an increase in S_{21}, which would be expected for antenna operation, though with poor quality factor for example at 900 MHz. Near the sensor's operating frequency and few other frequency points, it can be noted that both S_{11} and S_{21} parameters exhibit a drop, attributed to resonance losses, instead of a peak of energy received by circuit 2. This is not the ideal situation in terms of efficiency, but the circuits may enable remote sensor readings, based on the electromagnetic coupling between them. The greater the distance between the circuits, the lower the energy received measured with S_{21}. The maximum levels of energy transmission occur when the circuits are positioned a few centimeters apart from each other. As expected, it was observed that the preferential direction of radiation is orthogonal to its face. Little energy is radiated laterally or from its back. Experimental tests were conducted considering the variation of distance and rotating the circuits.

As there are also sensors operating at 145 MHz, similar circuits were also designed at this frequency, based on slight reduction of the conductive lines dimensions to achieve a higher resonance frequency. The experimental characterization results were satisfactory in terms of resonance

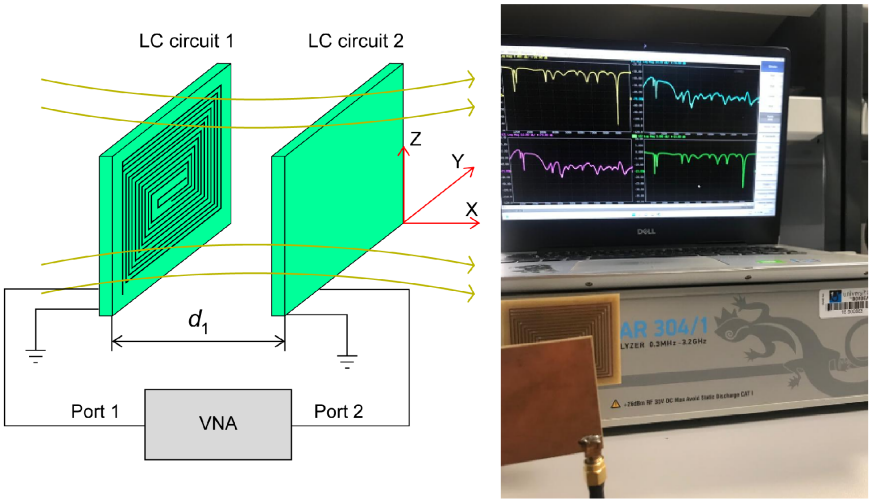

(a)

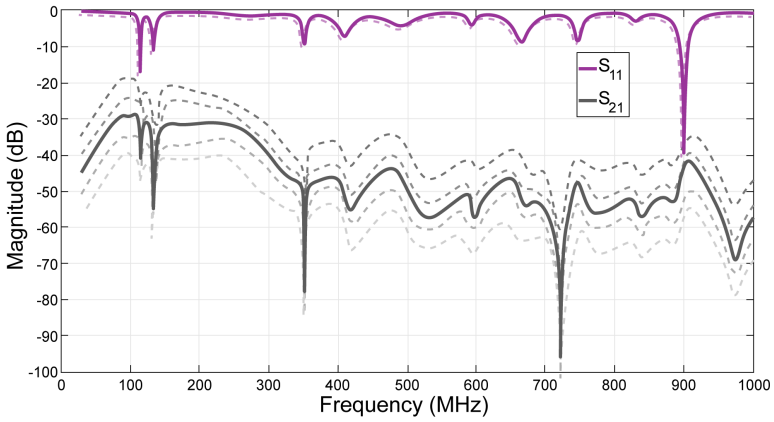

(b)

Figure 4.16: (a) Schematic and setup with the LC circuits and (b) S_{11} and S_{21} response of the T_x and R_x circuits and with the distance between them varying from 10 (dashed bottom) to 0.5 (dashed top) cm for a bandwidth of 1 GHz .

frequency, bandwidth, and magnitude of S_{11}, as shown in Fig.4.17. Finally, a good agreement can be observed between the resonance frequencies of the circuits and the frequency response (S_{11}) of the sensor.

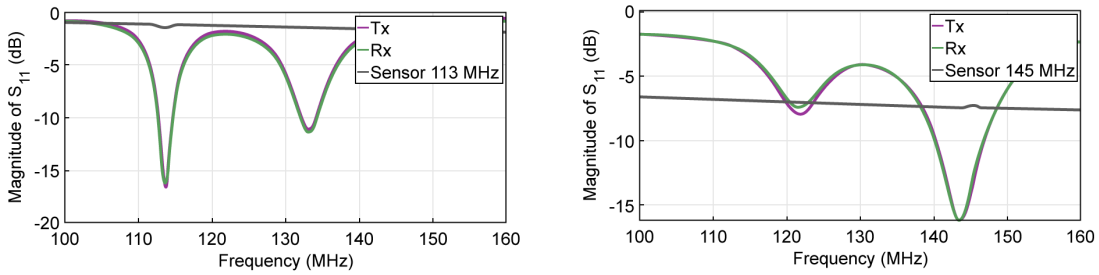

(a) (b)

Figure 4.17: Frequency response of the LW sensor and the T_x and R_x circuits at the operating frequencies of (a) 113 MHz; (b) 145 MHz and circuits and sensors operating in the same region.

It should be noted that the resonance behavior, and thus, the reading and detection system performances, is strongly influenced by the relative positions of the T_x and R_x circuits. Indeed, at far distances (from 2 cm) the resonance frequency and magnitude of S_{11} tend to remain constant, similar to the measurements above. As the circuits are closer to each other the minimum value of S_{11} decreases. The S_{21}, on the other hand, shows an increase in energy transmission as a function of distance. The closer it is, the more energy is transmitted, as seen in Fig.4.16. In the next section, the setup will be discussed with solutions of low and high NaCl concentration.

4.3.1 Coupled measurements

Preliminary results

The proposed experimental bench in coupled configuration for remote measurements with air and liquid is shown in Fig. 4.18: a computer controls the VNA by a USB cable interconnection; the port 1 of the VNA delivers the 3 dBm radiofrequency signal to feed the transmitter circuit (LC circuit 1) through a SMA adapter; the backscattering circuit (LC circuit 2) is connected directly to the load, i.e. the cell with the sensor for its wireless interrogation. The experiment was carried out in a laboratory environment, outside the anechoic chamber. Two identical rectangular planar spiral microstrip circuits T_x and R_x were used, both with the same target resonance frequency as the sensor. The distance of 2 cm between the transmitting and backscattering circuits was chosen to carry out the experiment. After SOL calibration and circuit alignment, the test cell and sensor

assembly described in the Chapter 3 were connected to the backscattering circuit R_x.

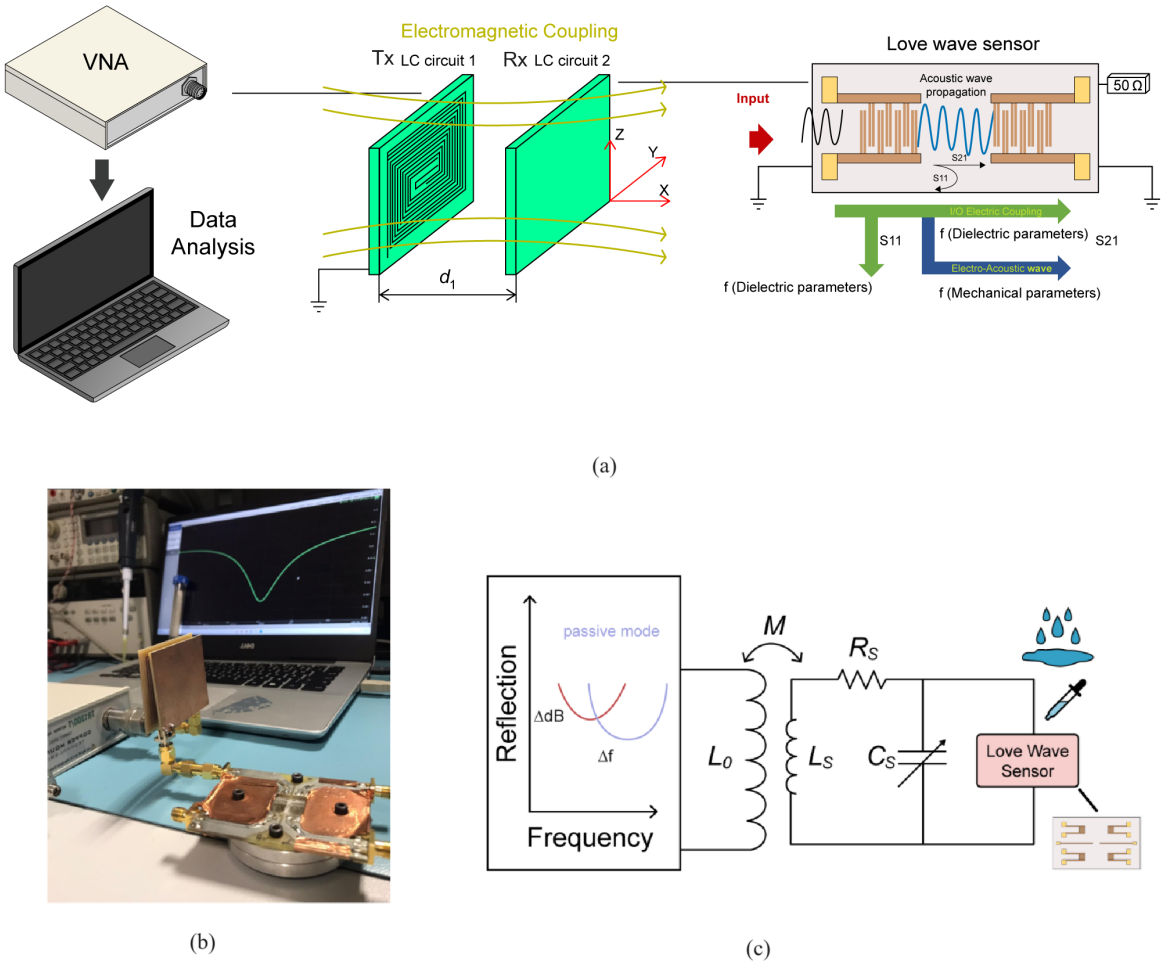

Figure 4.18: (a) Schematic of the coupled experimental setup for wireless measurement of the LW sensor; (b) Experimental setup: Two identical resonant circuits were used, one of which was connected to the test cell containing the LW sensor; (c) Illustration of the magnitude and frequency shifts in the S_{11} paramater as wirelessly measured when liquid is added in the LW sensor surface.
.

For this setup, the two sets of circuits and the two sensors at 113 MHz and 145 MHz were used. Four configurations were evaluated, based on matched and unmatched resonance frequency between the circuits and the LW sensor as shown in the Tab. 4.4, in order to understand the influence of the liquid over a wide band, including the operating range of the sensor. Five measurements were performed in two experimental sequences with air and NaCl solution for each configuration.

In this experiment, only a saturated solution with a conductivity of 240 mS/cm was employed.

Table 4.4: Coupled Measurements configurations

Setup Configurations	**Sensor 113 MHz**	**Sensor 145 MHz**
Microstrip 113 MHz	(a) Matched	(b) Mismatched
Microstrip 145 MHz	(c) Mismatched	(d) Matched

The tests with these four configurations were carried out in two sessions on two different days. All manipulations exhibited good reproducibility, provided no change in the setup such as in the distance between the circuits, which was a goal of these circuits compared to more conventional antennas. Compared to previous telescopic antennas, the use of circuits provided greater immunity to interference, gave more stability in frequency adjustment and presents a more compact system in terms of dimensions. Typical results are synthesized in Fig.4.19 and Fig.4.20. It can be observed a variation in frequency and magnitude of S_{11} due to the liquid injection, only when the set of circuits and sensor are in a matched configuration (same resonance frequency). The variation in magnitude is clearly highlighted in the dedicated curves at the low part of each figure. This conclusion related to the changes in frequency and magnitude is also clearly supported by consolidated data presented in Tab.4.5, demonstrated by another experimental sequence. This table represent the S_{11} values in terms of magnitude and frequency, with air, DI water and concentrated NaCl solution, at the two operating frequencies of the LW sensors used which a good reproducibility was achieved.

These variations upon addition of the NaCl solution are explained by the influence of the solution permittivity and conductivity, which affects the impedance on the sensor side, and consequently, the impedance seen by the reader, as previously presented. In this configuration based on the resonant circuits, it can be clearly observed that, when the circuits operate unmatched with the sensor, there is no variation in frequency, and the variation of S_{11} is smaller and not reproducible. On the basis of these preliminary results, this setup with the circuits and LW sensors at 113 MHz will be discussed in the next section.

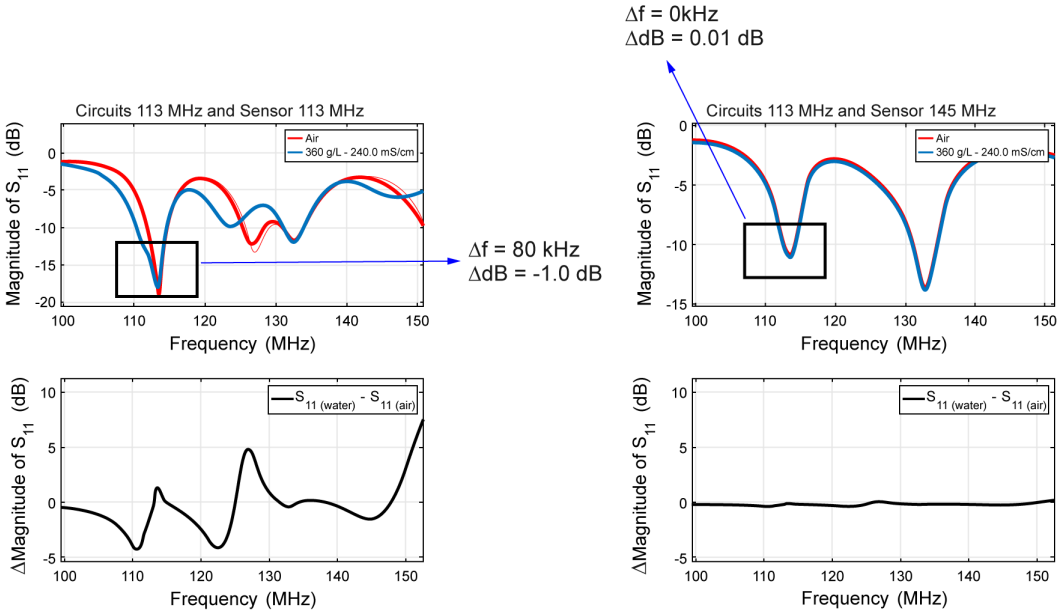

Figure 4.19: Experimental coupled wireless LW sensor characterization with two identical resonant circuits at 113 MHz, the backscattering one connected to the test cell containing the LW sensor at 113 MHz (left) and 145 MHz (right).

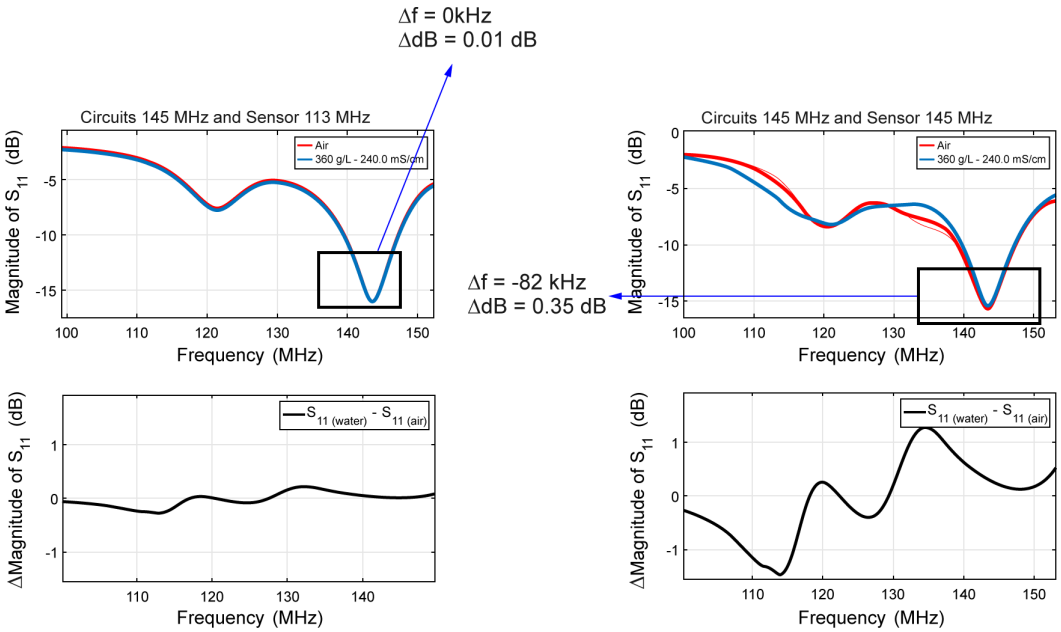

Figure 4.20: Experimental coupled wireless LW sensor characterization with two identical resonant circuits at 145 MHz, the backscattering one connected to the test cell containing the LW sensors at 113 MHz (left) and 145 MHz (right).

Table 4.5: Coupled measurements - results for all configurations (distance 2 cm between T_x and R_x circuits)

Setup Configutations	**Sensor 113 MHz**					**Sensor 145 MHz**				
Circuit 113 MHz		S_{11} **(dB)**	$\Delta_{S_{11}}$ **(dB)**	**Frequency (MHz)**	Δ_f **(MHz)**		S_{11} **(dB)**	$\Delta_{S_{11}}$ **(dB)**	**Frequency (MHz)**	Δ_f **(MHz)**
	Region 113 MHz					**Region 145 MHz**				
	Air	-15.84	0	113.943	0	**Air**	-14.12	0	114.186	0
	Water	-15.43	0.41	114.000	0.057	**Water**	-14.10	0.02	114.186	0
	Water/Salt	-15.16	0.68	114.024	0.081	**Water/Salt**	-14.09	0.03	114.186	0
Circuit 145 MHz		S_{11} **(dB)**	$\Delta_{S_{11}}$ **(dB)**	**Frequency (MHz)**	Δ_f **(MHz)**		S_{11} **(dB)**	$\Delta_{S_{11}}$ **(dB)**	**Frequency (MHz)**	Δ_f **(MHz)**
	Region 113 MHz					**Region 145 MHz**				
	Air	-18.91	0	145.866	0	**Air**	-18.06	0	145.785	0
	Water	-18.58	0.33	145.866	0	**Water**	-17.93	0.13	145.830	0.045
	Water/Salt	-18.30	0.61	145.866	0	**Water/Salt**	-17.89	0.17	145.866	0.081

Influence of NaCl concentration

The rectangular spiral patch circuit consists not only of inductance but also of parasitic resistance and capacitance, which can be represented by lumped RLC elements considering the desired resonance frequency and parasitic capacitance. The inductance of the circuit can be determined by the geometric parameters of the conductor, while its capacitance is related to the distance between the conductive traces and to the dielectric properties of the substrate. Physical measurements that alter these geometric and dielectric parameters will consequently change the values of inductance and/or capacitance of the circuit, which in turn causes a change in the magnitude and frequency of S_{11}. In this sense, when the LC-based circuit is connected to the LW sensor, the level of S_{11} can be measured by tracking the resonance frequency using another similar external reading circuit.

In the previous experiment, it was observed that the system responds with variations in frequency and magnitude of S_{11} when employing a dual-circuit configuration. Up to this point, all wireless experiments were conducted in air, D.I. water or NaCl solution with the highest conductivity. Thus far, wireless detection of the presence or absence of high conductive liquid on the sensor surface has been achievable. The set of circuits operating at 113 MHz was selected for the experiments because initial tests were conducted using telescopic antennas at the same frequency. Furthermore, the preliminary results of the wireless system with the 113 MHz circuits exhibited greater variation in the S-parameters compared to the configuration at 145 MHz when saturated NaCl solution was added onto the sensor surface. In this section, the same experimental setup is used, along with the same calibration and test protocols as described in Chapter 3, with air, DI. water and the eight prepared solutions at different NaCl concentrations with conductivity ranging from the order of μS/cm to mS/cm, as those used in wired experiments. The distance between the T_x and R_x circuits was slightly reduced to 1 cm in order to increase the S_{11} sensitivity and facilitate the results analysis. All experiments were carried out under temperature and humidity at 20°C and 53.2%, respectively. This setup is illustrated in Fig.4.21, featuring a VNA as the reader, connected to a T_x circuit. Another R_x circuit is connected to the sensor terminals. A 50 Ω load is connected to the sensor's output terminal. NaCl solutions of varying concentrations were deposited onto the sensor surface, and S_{11} measurements were conducted using the same protocol outlined in Chapter 3.

The frequency response of the system can be observed in Fig.4.22. With increasing concentration, thus increasing conductivity and decreasing permittivity of the solution, a change in frequency and magnitude of S_{11} was observed. The results demonstrate that the frequency and

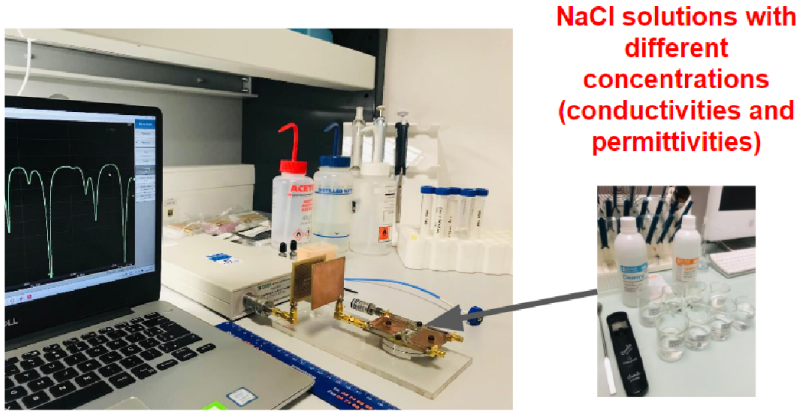

Figure 4.21: (a) LW sensor wireless measurement setup; (b) set of eight solutions of NaCl at different concentrations

.

magnitude of the system will change (with the higher conductivity solution) by approximately - 1.80 MHz and 3.12 dB, respectively. The system provides a solution for remote detection (non-contact and short-range) of NaCl solutions using the LW sensor. The system response was obtained based on the relationship between the NaCl solutions, the magnitude of S_{11} and the frequency.

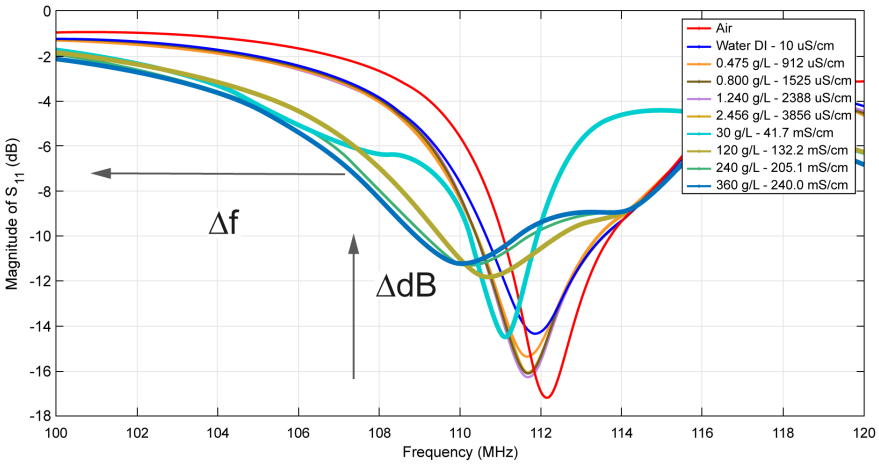

Figure 4.22: Measured S_{11} for different concentrations of NaCl sample solutions (T_x and R_x circuits and LW sensor at 113 MHz, distance 1 cm).

In Tab. 4.6, the consolidated results are presented, considering the physical characteristics of various concentrations of solutions (focus on conductivity and permittivity), along with the magnitude and frequency of S_{11} for this wireless system.

In Fig. 4.23, a comparison is presented in terms of the magnitude of S_{11} and frequency shift for the experiments as a function of the electrical conductivity of the solutions. Compared to classic wireless systems with passive sensors based on SAW signals (only the acoustic reflection signals),

Table 4.6: Coupled measurements - results

Medium	Conductivity (μS/cm)	Permittivity	S_{11} (dB)	Frequency (MHz)
Air	0.009	1	-17.25	112.164
Water DI	10	80.6	-14.36	111.846
Water/Salt (0.465 g/L)	912	80.2	-15.37	111.683
Water/Salt (0.800 g/L)	1525	80.1	-16.11	111.663
Water/Salt (1.240 g/L)	2388	80.08	-16.28	111.682
Water/Salt (2.456 g/L)	3856	80	-16.07	111.666
Water/Salt (30 g/L)	41700	74.0	-14.55	111.121
Water/Salt (120 g/L)	132200	60.9	-11.80	110.742
Water/Salt (240 g/L)	205100	48.5	-11.27	110.299
Water/Salt (360 g/L)	240000	39.8	-11.24	110.064

electromagnetically coupled wireless systems offer a simpler configuration due to the integration possibility of a low-complexity PCB-based resonator circuit. Furthermore, it can be observed more variations with the wireless configuration as the solution becomes more concentrated, thus more different from the reference medium, which may be attributed to the impact of the shape of the circuits resonance itself, added to the sensor response. However, a notable limitation is that the interrogation distance is constrained to a few centimeters, as the spiral or rectangular circuit must be positioned within the near region of the reader and considering the quite low frequency which prevents from using antennas compatible with low dimensions.

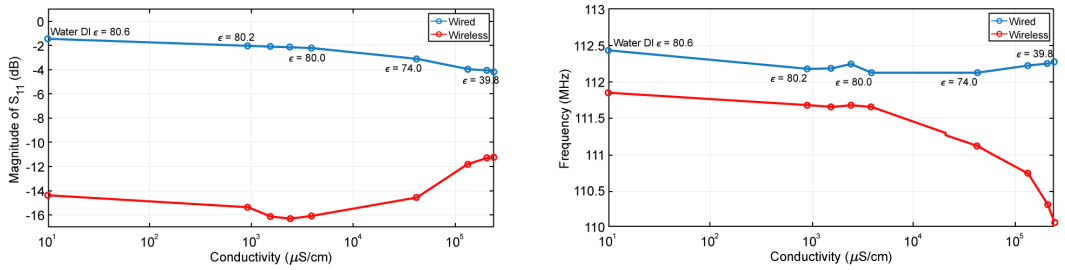

(a) (b)

Figure 4.23: Wired and wireless systems results: (a) Magnitude of S_{11}; (b) Frequency as a function of the solution electrical conductivity.

The rectangular PDMS cavity for the sensor IDTs is difficult to fill completely without introducing experimental errors. With the micropipette, although reliable, it can introduces mechanical disturbances, and even the use of DI water to dilute the residual solution leaves salt particles on the surface of the sensor. The system remains susceptible to these errors despite good fixation. However, it does not compromise the experimental reproducibility if the protocol is followed.

The experimental setup for measuring RCS, as described earlier, was also replicated, with the circuits replacing the antennas. This will be detailed in the next subsection.

4.3.2 Distanced measurements

Fig.4.24 presents the experimental setup in bistatic configuration. Similarly to previous setups, a computer (1) controls the Copper Mountain TR 1300/1 (VNA) (300 kHz - 1.3 GHz) (2). VNA port 1 sends a 3 dBm radio frequency continuous wave (CW) to the T_x circuit (3). The backscatter circuit (5) is connected directly to the test cell with the LW sensor (6), both elements constitute the target. The R_x circuit (4) is connected to port 2 of the VNA. A SOLT calibration is performed before connecting circuits (3) and (4). After SOLT calibration, the T_x and R_x circuits are connected to the VNA, the test cell and sensor are assembled and connected to the backscattering circuit (5) as presented in Fig. 4.24. To perform the experiment, a distance of 2 cm is chosen between the backscattering circuit and each one of both facing ones, T_x and R_x.

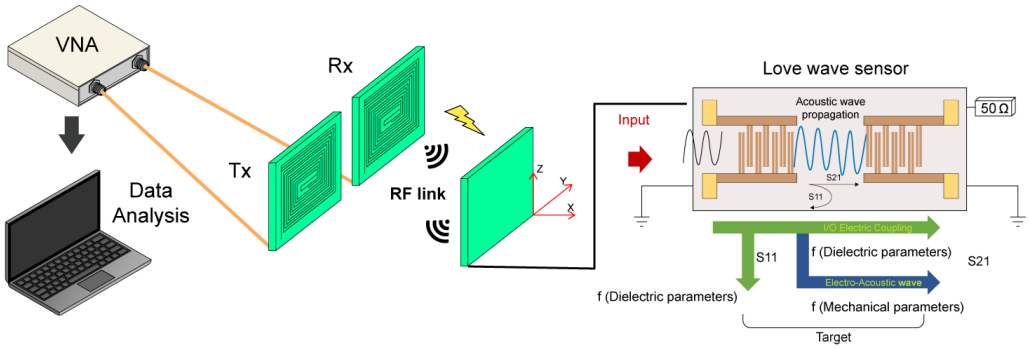

(a)

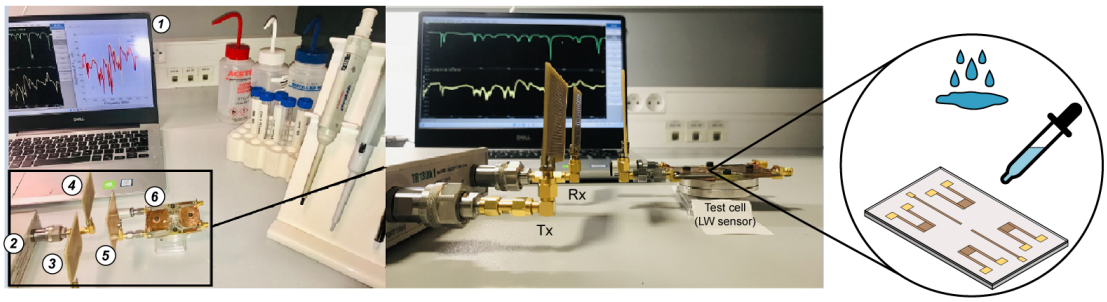

(b)

Figure 4.24: Experimental setup for bistatic configuration in CW using the VNA: (a) Schematic ; (b) Pictures of the setup with the LW-based sensor under test and illustration of liquid handling.

The magnitude of the Scattering Level (SL), defined as the S_{21} parameter measured by the VNA according to the setup presented in Fig.4.24, is shown in Fig.4.25 over a bandwidth of 1.3 GHz [221], [222]. The SL signal represents the energy reflected by the target, as measured by

VNA port 2, from the emitted energy sent by VNA port 1, thus passing through the 3 circuits. A measurable and reproducible shift of the SL from the air medium to saturated NaCl solution can be observed from the mean and standard deviation of 5 samples in the range close to the sensor operating frequency. An average shift from -73.27 dB to -73.63 dB in magnitude, and from 115.100 MHz to 114.950 MHz in frequency, was measured. Thus, a mean variation and a standard deviation in magnitude and frequency of -0.35 dB (σ = 0.05 dB) and -150 kHz (σ = 21.3 kHz) from the bare sensor to the saturated NaCl solution can be deduced, respectively. It was noticed that the addition of saline water affected other frequency bands, but this region was the only one over the full bandwidth where the SL signal was obtained with a reproducible change and with a variation in magnitude.

In order to estimate a RCS value, the standard metal plate used as a reference with dimensions of 40 cm x 10 cm has a theoretical RCS of −25.08 dBsm, as in [205]. Based on this value, and using the equation 4.4, the calculated average RCS values are −22.12 dBsm in ambient air condition and −22.42 dBsm in presence of the liquid, as shown in Fig. 4.25.

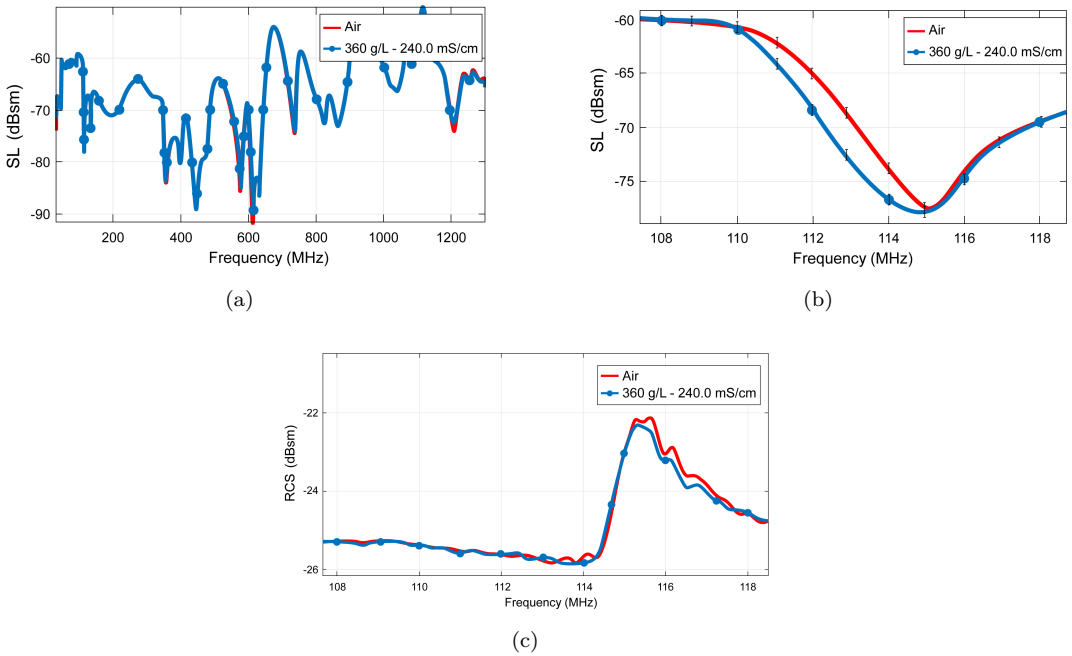

Figure 4.25: LW sensor responses based on 5 wireless measurements of SL for a distance of 2 cm between the backscattering circuit and circuits connected to the VNA, with air and saturated salt solution: (a) Wide frequency band response; (b) Focus on the shift of the lowest resonance mode close to the sensor operation frequency; (c) Magnitude of the calculated RCS.

From the results of RCS, gain of the reader, T_x power, considering −50 dBm as the minimum detectable signal, and using the radar equation in [22], we calculate the maximum reading distance

for this configuration to be around 1.2 m. Thus, the experiment was also performed with a 40 cm distance between the reader and the target. In this case, the value of RCS remained the same (ratio of energies) although the received energy decreased due to greater distance.

The addition of saline solution in this configuration with three circuits produced RCS variations in the same order of magnitude as in the configuration with three telescopic antennas, regardless of distance. Compared to the configuration with two circuits at a shorter distance using the same circuits, this configuration did not present variations in the signals that would allow the solutions to be classified. However, detection of the liquid is still possible. The addition of saturated NaCl solution onto the LW sensor modified the input impedance of the sensor with a variation similar to that found in previous experiments with different T_x and R_x circuits and antennas [197].

Table 4.7: Experimental results with three circuits

Bistatic Configuration		
Parameter/Distance	2 cm	40 cm
Magnitude of $SL_{(Air)}$	-73.27 dB	-78.16 dB
Magnitude of $SL_{(Solution)}$	-73.63 dB	-78.36 dB
ΔSL	-0.35 dB	-0.30 dB
$RCS_{(Air)}$	-22.12 dBsm	-25.50 dBsm
$RCS_{(Solution)}$	-22.42 dBsm	-25.85 dBsm
ΔRCS	0.30 dBsm	0.35 dBsm

Such circuit-based setup offers the advantages of not using coaxial cables between the reader and the sensor, being carried out outside the anechoic chamber and having more robust adjustment of the link frequency to the sensor frequency. From this, we observed a minimization of measurement errors, an improvement in reproducibility, and a decrease in the time needed to perform the experiment when compared to the previous ones.

The RCS values calculated in this work have the same order of magnitude as the works used as reference [197], [198]. In [198], for example, a chipless RFID tag was interrogated at a distance of 20 cm, which exhibited a RCS around -24.50 dBsm. Typically, with passive sensors and RCS measurements, these systems are used to measure temperature, humidity, and gas concentration. The levels of the transmission coefficient depend on the characteristics of the wireless system (T_x power of the reader, minimum value detectable by the receiver, frequency, and characteristics of the circuits). In this work, it is shown experimentally that the difference in the measured RCS is related to the addition of salted liquid onto the sensor surface, which modifies the impedance seen by the reader.

However, detecting the level of variation in the RCS is not encouraging for a more thorough

detection. Remote sensing can be performed by measuring the RCS with the bistatic configuration, although some improvements can be performed in the system, such as greater isolation between T_x and R_x, increased gain, and directivity of the T_x and R_x circuits. One of the main disadvantages of RCS-based systems is that they require a well-calibrated environment for their operation and measurement reliability. As soon as the operating frequencies are close to or contained in known commercial frequencies (such as radio, TV, Wifi, etc.), calibration becomes a challenge. If the calibration is not carried out properly or in case of interferences, a post-processing effort will be necessary.

A bistatic experimental setup was presented to measure the RCS of a LW sensor and detect liquid onto its surface. This work was performed on a laboratory bench, with interests in terms of wireless measurement, as well as without the need for an anechoic chamber. Improved reproducibility, ease of assembly, reduction of the time needed to carry out the experiment, and reduction of measurement errors were some of the advantages of this setup.

In Tab. 4.8, several characteristics can be observed from the results of the wireless reading configurations of systems with the LW sensor associated with antennas and circuits.

Table 4.8: Comparison between the experimental setups carried out

Experimental configurations used		
Characteristics	**Sensor associated with antennas**	**Sensor associated with circuits**
Reproducibility	Worse	Better
Tx/Rx Dimensions	Larger size	Smaller size
Experiment time	Longer time	Shortest time
Interferences	More interference	Less interference
Setup structure	Larger setup	Compact setup
Reading Range	Up to 40 cm	Order 1 cm
Presence of liquid	Detection	Detection up to 40 cm and Classification at 1 cm

From an experimental setup with the T_x and R_x circuits, it is possible to achieve better reproducibility, with smaller transmission and reception circuit sizes comparable to the dimension of the test cell and sensor, shorter experiment duration, with a more compact system that allows detection and classification of NaCl solutions. However, the maximum reading distance is shorter compared to the experimental setup with antennas. In the conclusions, we revisit this discussion, and in the outlook, we will outline future directions to optimize this wireless reading system for LW sensors and other passive sensors of similar nature.

4.4 Chapter conclusion

The purpose of IoT is focused on providing thousands of small devices that can work together for a common purpose. Among these devices, sensors with wireless communication capabilities are gaining ground. Many sensors have been extensively researched to monitor parameters in various environments, but their practical use has been limited due to battery power dependence. Typical wireless passive sensors can be divided into SAW, RFID, and RF-powered LC sensor. SAW sensors can be used for wireless monitoring in aggressive environments, particularly LW sensors in liquid detection. In this sense, the development of wireless measurement has attracted significant interest and with increasing prospects in the coming decades.

From experimental procedures, it was found to be possible to wirelessly detect passive LW sensors, without a battery and without the use of energy harvesting circuitry. Experimental setups based on backscattering and target RCS measurement were conducted. From these results, it was observed the capability of detecting and classifying the NaCl solutions with different conductivities and permittivities and how these physical properties modify the sensor's input impedance. It was demonstrated that it is possible to utilize the electromagnetic response of the acoustic sensor, enabling multiparametric measurement.

The proposed solutions have advantages and disadvantages. Limitation regarding operating frequency remains a challenge when aiming for wireless readings at distances of the order of meters or more, especially when aiming for a compact system with dimensions compatible with the sensor's size. Systems implemented with commercial antennas have a greater detection range, but do not allow for solution classification. In contrast, the system that uses transmission and reception resonant planar circuits has compact dimensions to be used along with the sensor, but with reduced reading distance. This configuration also allows for a reduction in the physical structure for performing experiments, improving reproducibility, handling time, and enabling operation outside the anechoic chamber. The performed systems do not employ modulation techniques, which makes them simpler, and with low levels of transmission energy. Among the experiments performed, those using circuits exhibit more consistency and robustness. Finally, it was possible to classify NaCl solutions over a wide range of conductivities based on frequency and magnitude shifts of the reflection coefficient, caused by variations in the sensor's impedance as observed by the reader.

Prospects

The LW sensor, as characterized and experimented with, exhibits promising behavior in wireless detection of electrical parameters of liquids and shows good potential for short-range applications. Meanwhile, several characteristics of the system could be improved. The system presents some limitations and prospects for improvement can still be considered, including:

- **Multiparametric wireless system**: new experimental setups can be performed to take advantage of the enriched approach (electromagnetic and acoustic responses) of the sensor and simultaneously measure the influence of the mechanical and electrical parameters of the liquid using a reflector-based LW device , as shown in Fig.4.26. This prospective system proposal consists of a LW sensor structured with a reflective delay, two antennas, and a network analyzer serving as the reader. When the input IDT on the sensor receives electromagnetic energy from the VNA via an antenna, a LW wave is generated in the waveguide layer and propagates towards the reflectors. The choice of substrate material and waveguide layer material affects the efficiency through the electromechanical coefficient k^2. The propagation of the LW wave is partially reflected by the reflectors and converted back into electromagnetic energy waves by the IDT, then transmitted to the interrogation unit through the antenna. A high value of k^2 allows for greater energy conversion efficiency, facilitating lower overall transmission loss which is of importance for both forward and backward wave travels. Consequently, this favors an increased sensitivity to the mechanical parameters of the liquid. Conversely, a low value of k^2 leads to low energy conversion efficiency at the input IDT, reflecting much of the electromagnetic energy and converting less energy into acoustic energy. This lower value favors sensitivity to the electrical parameters of the liquid. Therefore, the selection of materials and the thicknesses of the layers composing the sensor based on an intermediate value of k^2 (with both high and low efficiency aspects) and appropriate acoustic path for low acoustic losses, may enable the simultaneous detection of the electrical and mechanical properties of the liquid.

  By utilizing a PDMS chip with two distinct cavities, samples of the same liquid can be separated, allowing for the evaluation of the influence of its physical properties (electrical and

mechanical) on the sensor. With such a device, while conductivity and permittivity primarily affect the input IDT, viscosity and density induce a change in wave velocity, resulting in phase and magnitude changes of the reflected acoustic peak. By assessing the signals in magnitude and frequency at different times, the physical parameters of the liquid could be determined separately.

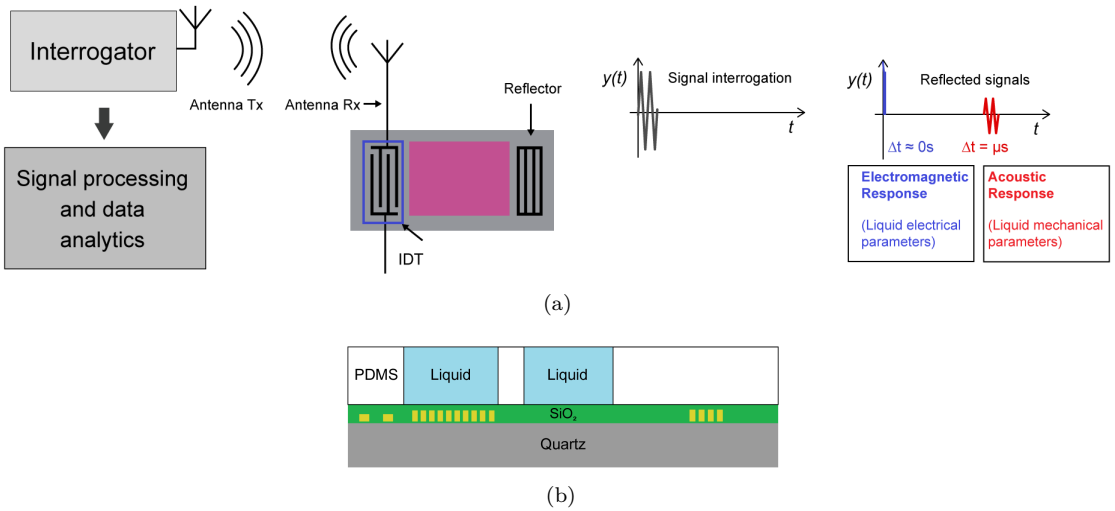

Figure 4.26: (a) Schematic of a multiparameter wireless system utilizing SAW devices. From the sensor input, it is possible to extract both the electromagnetic and mechanical responses and associate them with the corresponding properties of the measured fluid sample; (b) Cross section view of the sensor: substrate, guiding layer, PDMS chip and liquid sample.

- **Other liquids**: new experimental campaigns can explore the influence of other saline solutions on the sensor surface in order to classify which type of salt was deposited. A distinction between salts with similar conductivities but different permittivities (and vice versa) can be made. The same can be achieved by relating to the density and viscosity of the solutions. At certain intervals, the sensor can be applied as an electronic tongue, as shown in Fig.4.27. If another reflector is designed on the opposite side of the sensor, it is also possible to deposit another liquid of a different nature from the first one and verify its influence on the acoustic parameters of the wave. These signals can be separated and identified in time, where the fastest signal (the electromagnetic one) is observed approximately at ≈ 0 μ s, and the other acoustic signals can be visualized with delays of a few microseconds depending on the position where the other reflectors were built. If a third sensitive layer is added to the sensor, it can adsorb specific biomolecules. In this regard, the mechanical characterization of two liquids in the acoustic path between the IDT and the reflector and the electrical characterization of what is chosen to be deposited on the IDT could take place.

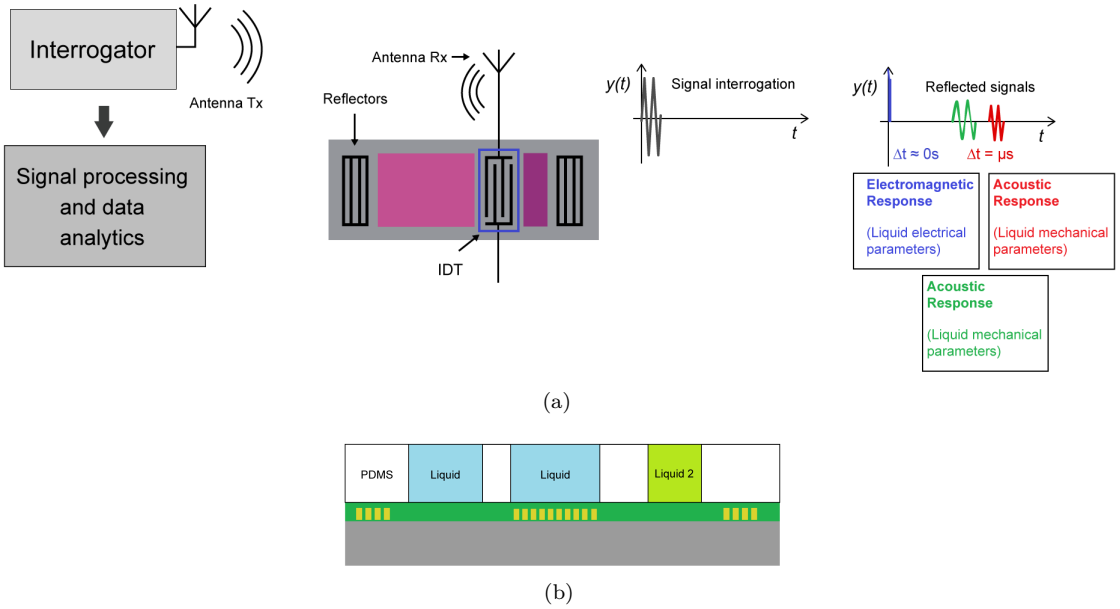

Figure 4.27: (a) Schematic view of a multiparameter wireless system for more than one liquid deposited onto the sensor surface: expected acoustic reflection peaks in relation for two different liquids in the acoustic path/reflectors and the electromagnetic reflection in the input IDT; (b) Cross section view of the sensor: substrate, guide layer, PDMS and liquid.

- **Reading Range**: the more the sensor reflects electromagnetic energy, the farther it can be remotely read. Changes in the design of IDT structures, optimization of the thin SiO_2 layer, or even in an earlier circuit to be coupled to the input IDT can improve the reflection coefficient and the sensor response.

- **Size**: although the transmission and reception circuits have dimensions compatible with those of the test cell, they have low efficiency and energy radiation. Work with a sensor at higher frequencies can reduce the size of the structure required for interrogation. Consequently, a better compromise between losses and dimensions can be found.

- **Antennas**: the operating frequency limits the compromise between antenna size and efficiency for VHF frequencies when compared to typical frequencies at 433 MHz, 900 MHz, and 2.45 GHz. A study on new antenna designs can be carried out, especially aiming at the limit of obtaining antennas compatible with the sensor dimensions and offering more power. If the target operates at a higher frequency, the use of commercial antennas becomes more viable.

- **Sensor network**: the measurements carried out were limited to interrogating a single sensor at a time. An experimental setup with two or more sensors can be considered, combining identification and measurement in the same interrogation. In this sense, the use of broadband

antennas or even antennas with reconfigurable resonance frequency may be interesting, as shown in Fig.4.28.

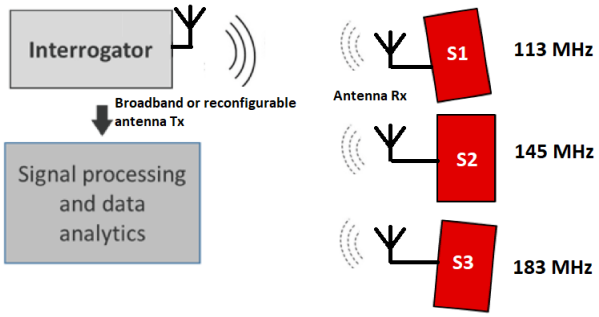

Figure 4.28: Wireless system of multiple LW sensors

.

- **Presence of restrictions**: although the wired system is robust and presents better reproducibility when compared to the wireless one, a study on mechanical impact, different measurement positions, and the use of another liquid insertion protocol into the sensor can be performed.

Conclusions

A wireless system utilizing LW sensors was at the core of this manuscript. The subject of this thesis provided a multidisciplinary approach by addressing topics of electromagnetic and acoustic nature, as well as wired and wireless instrumentation, along with physical properties of liquids. Starting from an already designed LW sensor, it was characterized and simulated in wired configuration. Based on its electromagnetic response, it was then integrated into a wireless system for passive detection when solutions of NaCl at varying concentrations were deposited onto the sensor surface. These approaches were disseminated in some scientific communications.

The IoT market is currently experiencing significant growth, particularly in domains with hostile environments and healthcare. Among these fields, sensors applied in gas detection have already demonstrated their feasibility. However, the application of sensors in liquid environments remains an area to be explored. In this context, LW sensors emerge as a relevant approach, particularly due to their passive nature. The sensitivity of wave velocity to certain external parameters gives rise to and defines the function of these sensors. Given the appropriate configuration and protocols, these devices can be passively and wirelessly interrogated. Several studies have confirmed the feasibility of wireless measurement using the sensor's acoustic response. However, no work has attempted to consider its electromagnetic response as well. LW sensors used and mentioned in the literature have already demonstrated their potential in liquid detection, especially of biochemical species, and recent work addresses their multiparametric characteristic. Only the approach using wired interrogation electronics has been verified. In this direction, a wireless system has been proposed aiming at criteria such as wireless and passive reading utilizing the LW sensor. Propositions for wireless interrogation strategies were then proposed. The selection of systems was initially justified based on the ease of implementing the wireless system, as well as the operating frequency and typical sensor response.

Constructive details of the sensor and its application in liquid media were discussed. Highlighting its multiparametric characteristic, an experimental setup and appropriate measurement protocol were proposed for extracting the acoustic and electromagnetic response of the sensor. From NaCl solutions, it was demonstrated that the LW sensor is suitable not only for providing sensitivity based on the mechanical parameters of a liquid but also as a function of

the variation in its electrical properties. These characterizations were performed using a VNA and showed a shift in the magnitude of the reflection and transmission coefficients as a function of the concentration of NaCl solutions. The liquid was deposited across the entire surface of the sensor using a long PDMS that allowed interaction with the sensor's IDTs and thus affected the input impedance. Due to the difference in the propagation time of electromagnetic and acoustic waves in the sensor, it was possible to isolate the electromagnetic wave and obtain a variation in this impedance as the main characteristic and key element for investigating the feasibility of wireless detection. The LW sensor was then validated in a wired configuration for use in the detection and classification of NaCl solutions.

The state of the art allowed for a discussion of the advantages and disadvantages of different wireless strategies. Initially, the RCS measurement strategy with commercial antennas was used for the remote detection of a liquid on the LW sensor surface. Although detection was possible, classification was not achievable, and the system lacked greater reproducibility and lower interference. In this sense, circuits were proposed and fabricated to perform this reading. With dimensions compatible with the measurement cell and sensor, they were added to the wireless system and the final measurement was obtained.

Detections were possible for distances of up to 40 cm. Sensitivity was observed to the concentration of NaCl solutions at a distance of 1 cm. The developed system stands out from the state-of-the-art because it presents some advantages:

- Wireless connection to transmission and reception circuits
- Passive, no battery required
- Operating at a frequency of 113 MHz, atypical frequency for wireless connection of objects
- Utilizing the electromagnetic response of a LW sensor, further exploring the typical acoustic response of the sensor
- Interrogation with the VNA, without the need for modulation and demodulation techniques of signals
- Instrumentation and measurement protocol validated for the application in liquid media
- Measurements carried out outside an anechoic chamber, in a real environment.

The wireless system presented here is a first step considering the LW sensor as the target. Ahead, its sensitivity to various parameters can be leveraged for broader applications involving

wireless detection of acoustic response, at different operating frequencies and longer distances. The developments made in this work can be utilized in future studies. Lastly, this system may also be useful for other applications involving different substances.

Annex 1

Piezoelectricity

The direct piezoelectric effect was predicted and verified in 1880 by the brothers P. and J. Curie in certain materials such as quartz. It is the natural ability of some materials to generate an electric voltage under the action of mechanical stress [223], [224]. The existence of the inverse effect was predicted the following year by G. Lippmann and confirmed by the Curie brothers [225]. Materials such as quartz, tourmaline, and topaz allow the observation of this phenomenon. This effect only manifests itself in crystals whose elementary cell lacks a center of symmetry. The effect of a mechanical action can thus create an electric dipole in each mesh of the material from the displacements of the barycenters of positive and negative charges, as shown in Fig.4.29.

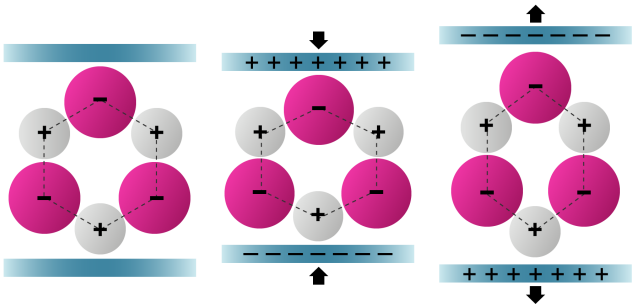

Figure 4.29: Illustration of the principle of piezoelectricity: appearance of an electrical polarization under the action of a deformation [163]

The first application of piezoelectricity took place during the First World War with the invention of the sonar by P. Langevin [226]. The first quartz oscillators were subsequently discovered by W. Cady in the 1920s, followed by extensive findings related to the phenomenon of direct and inverse piezoelectricity. A quartz oscillator is an electromechanical device and also an electronic oscillator circuit. It utilizes the mechanical resonance of a vibrating crystal, which is made of a piezoelectric material. This process enables the oscillator to generate and obtain an electrical signal with high precision frequency. To this day, these phenomena are part of our daily lives, such as in pressure sensors in the aeronautics and automotive industries. It is also possible to find their inverse effect in

the positioning systems of printers and atomic force microscopes. Finally, there are other systems that combine both direct and inverse effects, as is the case with SAW devices.

Generation of acoustic waves

In very general terms, a wave corresponds to the propagation of energy in a material or immaterial environment. In our case, we focus only on mechanical (or acoustic) waves that propagate with a velocity and an amplitude dependent on the material medium. If the material medium has an elastic (or acoustic) behavior, meaning that the disturbance generates a reversible variation in the properties of the medium, the waves are called acoustic. Vibrations in a steel string and a seismic wave are two examples.

In this sense, two main types of waves can propagate: BAW (when propagation occurs within the material) and SAW (if propagation remains at the interface). Within the family of BAW, there are still two distinct categories, as shown in Fig. 4.30:

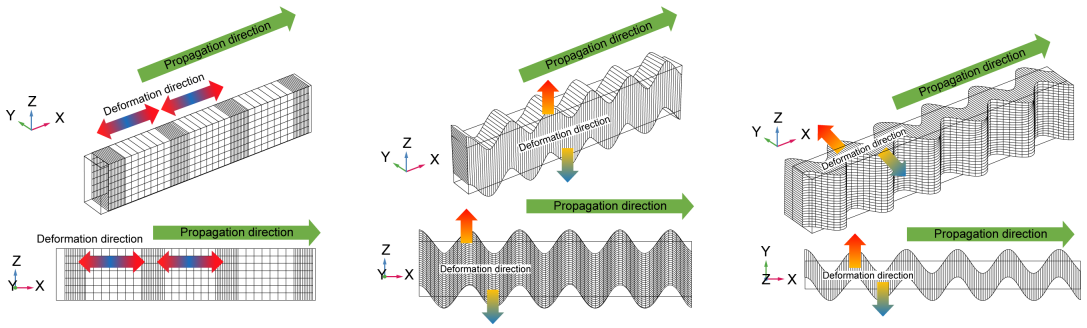

Figure 4.30: Acoustic polarization's of waves [5]

- longitudinal waves: energy moves parallel to the direction of wave propagation, creating a succession of compression-expansion zones and causing a back-and-forth motion.
- transverse or shear waves: energy moves perpendicular to the direction of wave propagation, inducing a vertical and horizontal particle movement in the medium for transverse and shear waves, respectively.

There are also other waves that can propagate on the surface, the most well-known being:

- shear horizontal waves: emanate from their equivalent volume subject to surface boundary conditions leading to damping in depth.

- Rayleigh waves: has both longitudinal and vertical shear components, resulting in an elliptical trajectory of surface particles and a rapid decay of particle oscillation with depth into the substrate.
- Love waves: correspond to a purely shear horizontal wave in a thin layer (a few µm) deposited on the surface of a semi-infinite medium, as shown in Fig. 4.31 [4].

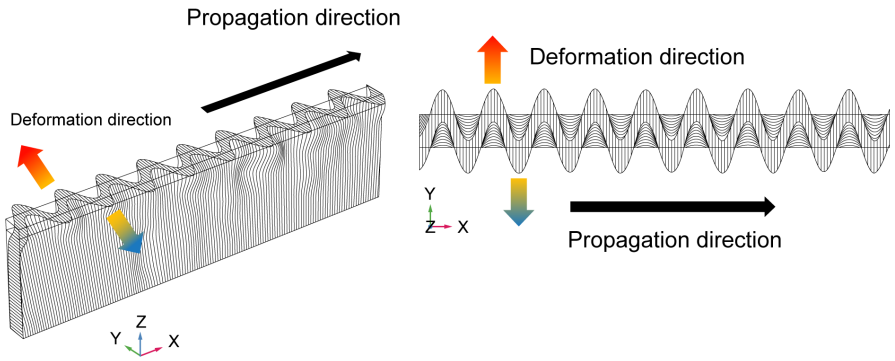

Figure 4.31: Propagation of Love waves: [185]

The propagation of surface acoustic waves in piezoelectric materials is governed by a coupling between the equations of motion and the equations of the electric field, in a relationship involving Hooke's Law and Maxwell's equations, according to

$$\begin{cases} T_{ij} = C_{ijkl} S_{kl} - e_{kij} E_k \\ D_i = e_{ikl} S_{kl} + \epsilon_{ij} E_j. \end{cases} \tag{4.6}$$

Here, T_{ij} represents the components of the mechanical stress tensor, C_{ijkl} is the elasticity tensor, e_{kij} is the piezoelectric tensor, ϵ_{ij} is the electric permittivity tensor, E_k is the electric field tensor, S_{kl} is the strain tensor, and finally, D_i is the electrical displacement tensor [160].

A

A

Some physical properties of NaCl solutions

A.1 Dielectric parameters

Concentration (mol/L)	ε_s	$\pm\varepsilon_s$*	τ (ps)	$\pm\tau$*(ps)	α	$\pm\alpha$*	σ_i (S/m)	$\pm\sigma_i$*	RMSE
0.001	80.6	0.1	9.16	0.08	0.005	0.003	0.01	0.00	0.36
0.005	80.0	0.1	9.21	0.08	0.002	0.003	0.05	0.00	0.36
0.01	80.1	0.1	9.25	0.08	0.001	0.003	0.11	0.00	0.36
0.03	80.2	0.1	9.37	0.10	0.001	0.003	0.30	0.00	0.44
0.05	80.1	0.1	9.37	0.12	0.002	0.004	0.49	0.00	0.54
0.07	78.9	0.2	9.12	0.16	0.005	0.006	0.72	0.00	0.72
0.09	78.4	0.2	9.18	0.19	0.005	0.007	0.94	0.00	0.86
0.1	78.2	0.2	9.08	0.20	0.006	0.008	0.96	0.00	0.92
0.2	77.0	0.2	8.98	0.10	0.009	0.004	1.83	0.01	0.44
0.5	74.0	0.2	8.91	0.13	0.023	0.006	4.17	0.01	0.53
0.7	72.4	0.2	8.80	0.15	0.023	0.006	5.64	0.01	0.57
0.9	70.1	0.2	8.50	0.14	0.038	0.006	7.04	0.01	0.54
1	68.7	0.2	8.55	0.16	0.038	0.006	7.76	0.01	0.61
1.5	65.3	0.3	8.44	0.21	0.040	0.009	10.54	0.01	0.72
2	60.9	0.3	8.13	0.26	0.065	0.011	13.22	0.02	0.81
2.5	56.8	0.4	8.01	0.34	0.085	0.015	15.85	0.02	0.95
3	53.8	0.4	7.95	0.41	0.104	0.018	17.53	0.02	1.04
3.5	50.5	0.5	7.86	0.51	0.125	0.022	19.48	0.02	1.14
4	48.5	0.5	7.89	0.58	0.147	0.024	20.51	0.02	1.19
4.5	46.1	0.6	7.98	0.70	0.175	0.028	21.62	0.03	1.26
5	43.9	0.7	8.13	0.85	0.207	0.032	22.33	0.03	1.31

Figure A.1: Dielectric parameters of different NaCl solutions at 20°C using the Cole-Cole Model [175]

A.2 Viscosity

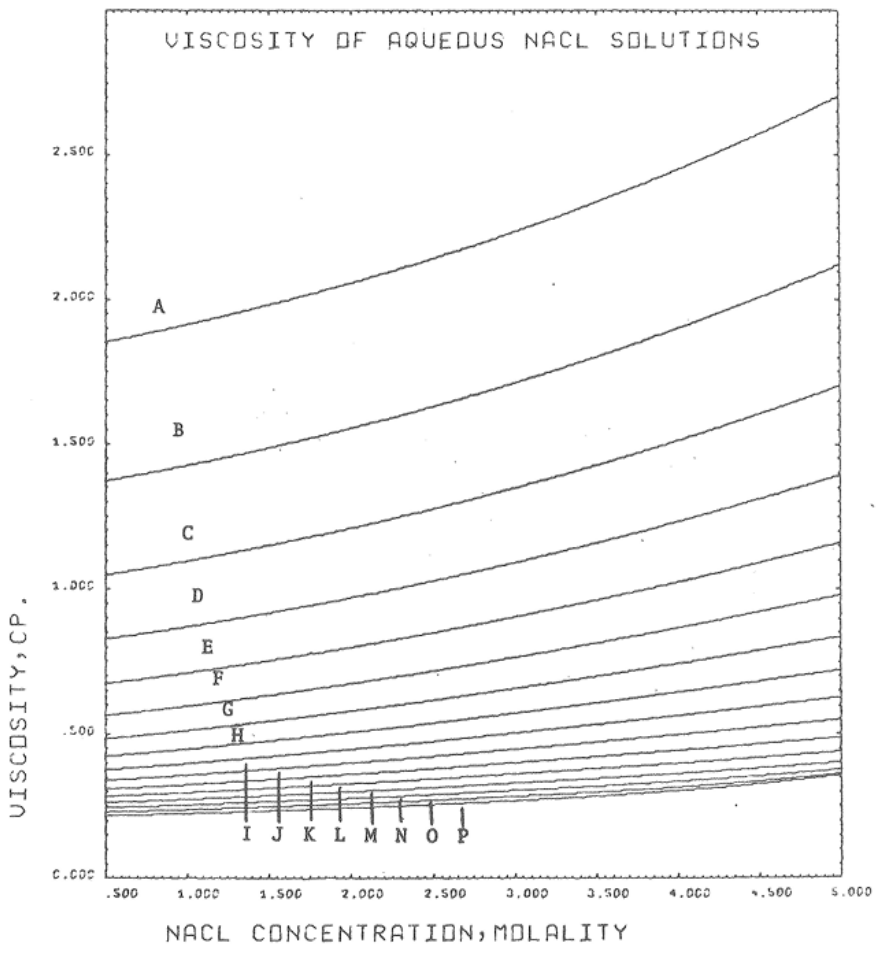

Figure A.2: Viscosity of NaCl solutions as a function of the concentration (A, B, C, D, E, F, G, H, I, J, K, L, M, N, P) = (0, 10, 20, 30, 40, 50, 60, 70, 80, 90, 100, 110, 120, 130, 140, 150) °C [176].

A.3 Density

m /mol·kg$(H_2O)^{-1}$	T = 10.0 °C	T = 25.0 °C	T = 40.0 °C	T = 55.0 °C	T = 70.0 °C	T = 85.0 °C
0.1	1.00399	1.00116	0.99622	0.98964	0.98168	0.97254
0.2	1.00822	1.00520	1.00016	0.99352	0.98554	0.97640
0.3	1.01239	1.00921	1.00406	0.99736	0.98936	0.98022
0.4	1.01651	1.01317	1.00792	1.00117	0.99315	0.98401
0.5	1.02059	1.01709	1.01175	1.00495	0.99690	0.98776
0.6	1.02463	1.02098	1.01555	1.00867	1.00062	0.99148
0.7	1.02864	1.02483	1.01931	1.01240	1.00431	0.99517
0.8	1.03260	1.02866	1.02305	1.01609	1.00797	0.99883
0.9	1.03653	1.03245	1.02676	1.01975	1.01161	1.00247
1.0	1.04043	1.03621	1.03043	1.02338	1.01522	1.00607
1.2	1.04812	1.04366	1.03771	1.03056	1.02235	1.01321
1.4	1.05569	1.05096	1.04488	1.03764	1.02939	1.02024
1.6	1.06313	1.05817	1.05194	1.04462	1.03633	1.02717
1.8	1.07044	1.06527	1.05890	1.05150	1.04317	1.03400
2.0	1.07765	1.07227	1.06577	1.05829	1.04992	1.04075
2.5	1.09517	1.08932	1.08253	1.07486	1.06640	1.05721
3.0	1.11203	1.10579	1.09873	1.09090	1.08235	1.07313
3.5	1.12829	1.12170	1.11440	1.10642	1.09778	1.08854
4.0	1.14398	1.13709	1.12958	1.12145	1.11274	1.10347
4.5	1.15915	1.15199	1.14428	1.13602	1.12724	1.11795
5.0	1.17385	1.16644	1.15854	1.15016	1.14130	1.13200
5.5	1.18811	1.18048	1.17239	1.16388	1.15496	1.14564
6.0	1.20198	1.19412	1.18585	1.17721	1.16822	1.15891

Figure A.3: Values of the density of NaCl solutions as a function of the concentration and temperature [177].

A

Publications

International conferences with proceedings

Santos, M. A., Freire, R. C. S., Hallil, H., Tamarin, O., and Dejous, C. (2022, July). Remote measurement of a VHF Love wave sensor for liquid detection. In 2022 Wireless Power Week (WPW) (pp. 536-540). IEEE.

Andrade, M., Freire, R. C., Souza, A. S., Hallil, H., Tamarin, O., and Dejous, C. (2023, August). Liquid Detection based on Radar Cross-Section Measurement of Love Wave Sensor. In 2023 7th International Symposium on Instrumentation Systems, Circuits and Transducers (INSCIT) (pp. 1-6). IEEE.

Andrade, M., Freire, R. C., Fernandes, P., Santana, E. E., Santos, E. F. D., de Souza, M. G., ... and Serres, A. J. (2020). Compact monopole antenna for smart meter applications in ISM band 900 MHz. In Proceedings of the 23rd International Workshop on ADC and DAC Modelling and Testing IMEKO TC-4.

Souza, A. S., Freire, R. C., Nobrega, L. A., **Andrade, M.**, Serres, A. J., Tamarin, O., and Dejous, C. (2023, August). Transformer Oil Viscosity Measurements Using a Love Wave Sensor. In 2023 7th International Symposium on Instrumentation Systems, Circuits and Transducers (INSCIT) (pp. 1-5). IEEE.

Bernardes, D. D. J. P., Carvalho, E. E., da Silva, P. F., Oliveira, M. A., **Andrade M.** Jean, A., Serres, R., ... and da Fonseca Silva, P. H. (2021, May). Microstrip Patch Antenna Bioinspired in Primrose Flower for WLAN and Bluetooth Applications. In 2021 IEEE International Instrumentation and Measurement Technology Conference (I2MTC) (pp. 1-4). IEEE.

Silva, M.V, **Andrade, M.**, Santana E. E.C., , Freire, R. C. S., Tamarin, O., and Dejous, C. 2023. Power Consumption Estimation of Love Wave Sensors using LTspice Measurement, Quality and Data Science 2023, 1-3

References

[1] K. Länge, B. E. Rapp, and M. Rapp, "Surface acoustic wave biosensors: A review," *Analytical and bioanalytical chemistry*, vol. 391, pp. 1509–1519, 2008.

[2] H. Hallil, C. Dejous, S. Hage-Ali, *et al.*, "Passive resonant sensors: Trends and future prospects," *IEEE Sensors Journal*, vol. 21, no. 11, pp. 12 618–12 632, 2021. DOI: 10.1109/JSEN.2021.3065734.

[3] O. Tamarin, S. Comeau, C. Dejous, *et al.*, "Real time device for biosensing: Design of a bacteriophage model using love acoustic waves," *Biosensors and Bioelectronics*, vol. 18, no. 5-6, pp. 755–763, 2003.

[4] C. Zimmermann, D. Rebiere, C. Dejous, J. Pistre, E. Chastaing, and R. Planade, "A love-wave gas sensor coated with functionalized polysiloxane for sensing organophosphorus compounds," *Sensors and Actuators B: Chemical*, vol. 76, no. 1-3, pp. 86–94, 2001. DOI: 10.1016/S0925-4005(01)00578-0.

[5] M. Rube, O. Tamarin, M. Sebeloue, *et al.*, "Unconventional protocol for saw sensor: Multi-physic response enrichment in liquid medium," *IEEE Sensors Journal*, vol. 22, no. 12, pp. 11 345–11 354, 2021.

[6] J. Janhunen, K. Mikhaylov, J. Petäjäjärvi, and M. Sonkki, "Wireless energy transfer powered wireless sensor node for green iot: Design, implementation and evaluation," *Sensors*, vol. 19, no. 1, p. 90, 2018.

[7] Y. Li, J. Yu, Y. Wei, *et al.*, "Recent progress in self-powered wireless sensors and systems based on Triboelectric Nanogenerator (TENG)," *Sensors*, vol. 23, no. 3, p. 1329, 2023.

[8] J. R. Stetter, W. R. Penrose, and S. Yao, "Sensors, chemical sensors, electrochemical sensors, and ecs," *Journal of The Electrochemical Society*, vol. 150, no. 2, S11, 2003.

[9] G. Zhu, P. Ren, J. Yang, *et al.*, "Self-powered and multi-mode flexible sensing film with patterned conductive network for wireless monitoring in healthcare," *Nano Energy*, vol. 98, p. 107 327, 2022.

[10] W. Zheng, H. Xu, M. Wang, *et al.*, "On-skin flexible pressure sensor with high sensitivity for portable pulse monitoring," *Micromachines*, vol. 13, no. 9, p. 1390, 2022.

[11] O. Galinina, K. Mikhaylov, K. Huang, S. Andreev, and Y. Koucheryavy, "Wirelessly powered urban crowd sensing over wearables: Trading energy for data," *IEEE Wireless Communications*, vol. 25, no. 2, pp. 140–149, 2018.

[12] S. Jena, A. Gupta, R. K. Pippara, P. Pal, and Adit, "Wireless sensing systems: A review," *Sensors for Automotive and Aerospace Applications*, pp. 143–192, 2019.

[13] R. Raju, "Compact passive wireless uhf sensors for packaged food monitoring," 2022.

[14] P. Mehrotra, B. Chatterjee, and S. Sen, "Em-wave biosensors: A review of rf, microwave, mm-wave and optical sensing," *Sensors*, vol. 19, no. 5, p. 1013, 2019.

[15] I. F. Akyildiz, W. Su, Y. Sankarasubramaniam, and E. Cayirci, "Wireless sensor networks: A survey," *Computer networks*, vol. 38, no. 4, pp. 393–422, 2002.

[16] J. R. Smith, A. P. Sample, P. S. Powledge, S. Roy, and A. Mamishev, "A wirelessly-powered platform for sensing and computation," in *International Conference on Ubiquitous Computing*, Springer, 2006, pp. 495–506.

[17] A. Ferrer-Vidal, A. Rida, S. Basat, L. Yang, and M. M. Tentzeris, "Integration of sensors and rfid's on ultra-low-cost paper-based substrates for wireless sensor networks applications," in *2006 2nd IEEE Workshop on Wireless Mesh Networks*, IEEE, 2006, pp. 126–128.

[18] A. Wheeler, "Commercial applications of wireless sensor networks using zigbee," *IEEE communications magazine*, vol. 45, no. 4, pp. 70–77, 2007.

[19] M. Asad and M. H. Sheikhi, "Highly sensitive wireless h2s gas sensors at room temperature based on cuo-swcnt hybrid nanomaterials," *Sensors and Actuators B: Chemical*, vol. 231, pp. 474–483, 2016.

[20] R. M. Ferdous, A. W. Reza, and M. F. Siddiqui, "Renewable energy harvesting for wireless sensors using passive rfid tag technology: A review," *Renewable and Sustainable Energy Reviews*, vol. 58, pp. 1114–1128, 2016.

[21] E. Perret, *Radio frequency identification and sensors: from RFID to chipless RFID*. John Wiley & Sons, 2014.

[22] M. I. Skolnik, "Radar handbook second edition," *McGrawHill*, 1990.

[23] J.-M. Colin, *Le radar: théorie et pratique*. Ellipses, 2002.

[24] M. Gupta, "Radar revisited (review of radar handbook, by merrill skolnik)[book reviews]," *IEEE Microwave Magazine*, vol. 9, no. 4, pp. 129–130, 2008.

[25] F. Chebila, "Lecteur radar pour capteurs passifs à transduction radio fréquence," Ph.D. dissertation, 2011.

[26] E. F. Knott, J. F. Schaeffer, and M. T. Tulley, *Radar cross section*. SciTech Publishing, 2004.

[27] D. Hotte, R. Siragusa, Y. Duroc, and S. Tedjini, "Radar cross-section measurement in millimetre-wave for passive millimetre-wave identification tags," *IET Microwaves, Antennas & Propagation*, vol. 9, no. 15, pp. 1733–1739, 2015.

[28] M. F. Sundermeier and D. Fischer, "Compact radar cross-section measurement setup and performance evaluation," *Advances in Radio Science*, vol. 19, pp. 147–152, 2021.

[29] A. Vena, "Contribution au développement de la technologie rfid sans puce à haute capacité de codage," Ph.D. dissertation, Université de Grenoble, 2012.

[30] H. Stockman, "Communication by means of reflected power," *Proceedings of the IRE*, vol. 36, no. 10, pp. 1196–1204, 1948.

[31] J. Landt, "The history of rfid," *IEEE potentials*, vol. 24, no. 4, pp. 8–11, 2005.

[32] E. Perret, S. Tedjini, and R. S. Nair, "Design of antennas for uhf rfid tags," *Proceedings of the IEEE*, vol. 100, no. 7, pp. 2330–2340, 2012.

[33] C. A. Balanis, *Antenna theory: analysis and design*. John wiley & sons, 2016.

[34] C. S. Hartmann, "A global saw id tag with large data capacity," in *2002 IEEE Ultrasonics Symposium, 2002. Proceedings.*, IEEE, vol. 1, 2002, pp. 65–69.

[35] H. Wohltjen and R. Dessy, "Surface acoustic wave probe for chemical analysis. i. introduction and instrument description," *Analytical chemistry*, vol. 51, no. 9, pp. 1458–1464, 1979.

[36] C. Lim, W. Wang, S. Yang, and K. Lee, "Development of saw-based multi-gas sensor for simultaneous detection of co2 and no2," *Sensors and Actuators B: Chemical*, vol. 154, no. 1, pp. 9–16, 2011.

[37] W. Wang, H. Hu, X. Liu, *et al.*, "Development of a room temperature saw methane gas sensor incorporating a supramolecular cryptophane a coating," *Sensors*, vol. 16, no. 1, p. 73, 2016.

[38] Z. Xu and Y. J. Yuan, "Implementation of guiding layers of surface acoustic wave devices: A review," *Biosensors and Bioelectronics*, vol. 99, pp. 500–512, 2018.

[39] R. Maxence, O. Tamarin, M. Sébéloué, *et al.*, "A dual love wave and impedance-based sensor: Response enrichment," in *2020 IEEE SENSORS*, IEEE, 2020, pp. 1–4.

[40] J. Kondoh, Y. Okiyama, S. Mikuni, Y. Matsui, H. Yatsuda, and M. Nara, "Development of sh-saw sensing system for liquids," in *2007 IEEE International Frequency Control Symposium Joint with the 21st European Frequency and Time Forum*, IEEE, 2007, pp. 20–24.

[41] Y. Hur, J. Han, J. Seon, Y. E. Pak, and Y. Roh, "Development of an sh-saw sensor for the detection of dna hybridization," *Sensors and Actuators A: Physical*, vol. 120, no. 2, pp. 462–467, 2005.

[42] S.-G. Kim, H.-J. Lee, J.-H. Lee, H.-I. Jung, and J.-G. Yook, "A highly sensitive and label free biosensing platform for wireless sensor node system," *Biosensors and Bioelectronics*, vol. 50, pp. 362–367, 2013.

[43] Y. Zhang, F. Yang, Z. Sun, Y.-T. Li, and G.-J. Zhang, "A surface acoustic wave biosensor synergizing dna-mediated in situ silver nanoparticle growth for a highly specific and signal-amplified nucleic acid assay," *Analyst*, vol. 142, no. 18, pp. 3468–3476, 2017.

[44] H.-L. Cai, Y. Yang, X. Chen, *et al.*, "A third-order mode high frequency biosensor with atomic resolution," *Biosensors and Bioelectronics*, vol. 71, pp. 261–268, 2015.

[45] M. Agostini, G. Greco, and M. Cecchini, "A rayleigh surface acoustic wave (r-saw) resonator biosensor based on positive and negative reflectors with sub-nanomolar limit of detection," *Sensors and Actuators B: Chemical*, vol. 254, pp. 1–7, 2018.

[46] Y.-S. Choi, J. Lee, Y. Lee, J. Kwak, and S. Suk Lee, "Increase in detection sensitivity of surface acoustic wave biosensor using triple transit echo wave," *Applied Physics Letters*, vol. 113, no. 8, 2018.

[47] P. Jandas, J. Luo, A. Quan, *et al.*, "Highly selective and label-free love-mode surface acoustic wave biosensor for carcinoembryonic antigen detection using a self-assembled monolayer bioreceptor," *Applied Surface Science*, vol. 518, p. 146 061, 2020.

[48] Y.-C. Peng, C.-H. Cheng, H. Yatsuda, *et al.*, "A novel rapid test to detect anti-sars-cov-2 n protein igg based on shear horizontal surface acoustic wave (sh-saw)," *Diagnostics*, vol. 11, no. 10, p. 1838, 2021.

[49] K. Suresh, V. Jeoti, M. Drieberg, *et al.*, "Simultaneous detection of multiple surface acoustic wave sensor tags for water quality monitoring utilizing cellular code-reuse approach," *IEEE Internet of Things Journal*, vol. 9, no. 16, pp. 14 385–14 399, 2021.

[50] D. B. Go, M. Z. Atashbar, Z. Ramshani, and H.-C. Chang, "Surface acoustic wave devices for chemical sensing and microfluidics: A review and perspective," *Analytical methods*, vol. 9, no. 28, pp. 4112–4134, 2017. DOI: 10.1039/C7AY00690J.

[51] T. Nomura, A. Saitoh, and Y. Horikoshi, "Measurement of acoustic properties of liquid using liquid flow sh-saw sensor system," *Sensors and Actuators B: Chemical*, vol. 76, no. 1-3, pp. 69–73, 2001.

[52] G. Sehra, M. Cole, and J. W. Gardner, "Miniature taste sensing system based on dual sh-saw sensor device: An electronic tongue," *Sensors and Actuators B: Chemical*, vol. 103, no. 1-2, pp. 233–239, 2004.

[53] J. K. J. Kondoh and S. S. S. Shiokawa, "New application of shear horizontal surface acoustic wave sensors to identifying fruit juices," *Japanese journal of applied physics*, vol. 33, no. 5S, p. 3095, 1994.

[54] Y. Wang, D. Chen, X. Chen, D. Li, C. Wu, and J. Xie, "A surface acoustic wave device for water impurity levels monitoring by measuring signal-to-perturbation ratios," *Japanese Journal of Applied Physics*, vol. 58, no. 6, p. 061 002, 2019.

[55] Y. Q. Fu, J. Luo, X. Du, *et al.*, "Recent developments on zno films for acoustic wave based bio-sensing and microfluidic applications: A review," *Sensors and Actuators B: Chemical*, vol. 143, no. 2, pp. 606–619, 2010.

[56] W. Gongi, M. Rube, H. Ben Ouada, H. Ben Ouada, O. Tamarin, and C. Dejous, "Elaboration and characterization of a new heavy metal sensor functionalized by extracellular polymeric substances isolated from a tunisian thermophilic microalga strain graesiella sp.," *Sensors*, vol. 23, no. 2, p. 803, 2023.

[57] A. S. Souza, R. C. Freire, L. A. Nobrega, *et al.*, "Transformer oil viscosity measurements using a love wave sensor," in *2023 7th International Symposium on Instrumentation Systems, Circuits and Transducers (INSCIT)*, IEEE, 2023, pp. 1–5.

[58] A. Choudhari, M. Rube, I. Sadli, M. Sebeloue, O. Tamarin, and C. Dejous, "Love wave acoustic sensor response in high turbidity liquid environment," in *2022 IEEE Sensors*, IEEE, 2022, pp. 1–4.

[59] O. Tamarin, M. Rube, J. L. Lachaud, V. Raimbault, D. Rebière, and C. Dejous, "Mobile acoustic wave platform deployment in the amazon river: Impact of the water sample on the love wave sensor response," *Sensors*, vol. 20, no. 1, p. 72, 2019.

[60] O. Tamarin, W. Ouelhazi, J.-L. Lachaud, *et al.*, "Mesoporous titania-coated love wave sensors and fem model applied to viscosity micro-measurements," in *2017 IEEE SENSORS*, IEEE, 2017, pp. 1–3.

[61] V. Raimbault, D. Rebière, C. Dejous, M. Guirardel, and J.-L. Lachaud, "Molecular weight influence study of aqueous poly (ethylene glycol) solutions with a microfluidic love wave sensor," *Sensors and Actuators B: Chemical*, vol. 144, no. 1, pp. 318–322, 2010.

[62] Y. Tian, H. Li, W. Chen, *et al.*, "A novel love wave mode sensor waveguide layer with microphononic crystals," *Applied Sciences*, vol. 11, no. 17, p. 8123, 2021.

[63] M. Gaso, Y. Jiménez, L. Francis, and A. Arnau, "Love wave biosensors: A review," *State Art Biosens. Gen. Asp*, pp. 277–310, 2013. DOI: 10.5772/53077.

[64] X. Hu and W. Yang, "Planar capacitive sensors–designs and applications," *Sensor Review*, vol. 30, no. 1, pp. 24–39, 2010.

[65] V. Tsouti, C. Boutopoulos, I. Zergioti, and S. Chatzandroulis, "Capacitive microsystems for biological sensing," *Biosensors and Bioelectronics*, vol. 27, no. 1, pp. 1–11, 2011.

[66] X. Dai, L. Fang, C. Zhang, H. Sun, *et al.*, "Design of a novel passive wireless integrated saw-based antenna sensor for structural health monitoring," *Journal of Sensors*, vol. 2020, 2020.

[67] S. Sherrit, Y. Bar-Cohen, X. Bao, S. Louyeh, and M. Badescu, "Transport powder and liquid samples by surface acoustic waves," 2009.

[68] K. Chang, Y. Pi, W. Lu, *et al.*, "Label-free and high-sensitive detection of human breast cancer cells by aptamer-based leaky surface acoustic wave biosensor array," *Biosensors and Bioelectronics*, vol. 60, pp. 318–324, 2014.

[69] D. Li, Y. Feng, L. Zhou, *et al.*, "Label-free capacitive immunosensor based on quartz crystal au electrode for rapid and sensitive detection of escherichia coli o157: H7," *Analytica chimica acta*, vol. 687, no. 1, pp. 89–96, 2011.

[70] Q. Wang, Q. Yang, and W. Wu, "Ensuring seafood safe to spoon: A brief review of biosensors for marine biotoxin monitoring," *Critical Reviews in Food Science and Nutrition*, vol. 62, no. 9, pp. 2495–2507, 2022.

[71] F. Narita, Z. Wang, H. Kurita, *et al.*, "A review of piezoelectric and magnetostrictive biosensor materials for detection of covid-19 and other viruses," *Advanced Materials*, vol. 33, no. 1, p. 2 005 448, 2021.

[72] N. Levit, D. Pestov, and G. Tepper, "High surface area polymer coatings for saw-based chemical sensor applications," *Sensors and Actuators B: Chemical*, vol. 82, no. 2-3, pp. 241–249, 2002.

[73] V. B. Raj, H. Singh, A. Nimal, M. Sharma, and V. Gupta, "Oxide thin films (zno, teo2, sno2, and tio2) based surface acoustic wave (saw) e-nose for the detection of chemical warfare agents," *Sensors and Actuators B: Chemical*, vol. 178, pp. 636–647, 2013.

[74] M. Atashbar, A. Sadek, W. Wlodarski, *et al.*, "Layered saw gas sensor based on csa synthesized polyaniline nanofiber on aln on 64 yx linbo3 for h2 sensing," *Sensors and Actuators B: Chemical*, vol. 138, no. 1, pp. 85–89, 2009.

[75] D. Matatagui, M. Fernandez, J. Fontecha, *et al.*, "Love-wave sensor array to detect, discriminate and classify chemical warfare agent simulants," *Sensors and Actuators B: Chemical*, vol. 175, pp. 173–178, 2012.

[76] D. Mandal and S. Banerjee, "Surface acoustic wave (saw) sensors: Physics, materials, and applications," *Sensors*, vol. 22, no. 3, p. 820, 2022. DOI: 10.3390/s22030820.

[77] J. Ho, M. K. Tan, D. B. Go, L. Y. Yeo, J. R. Friend, and H.-C. Chang, "Based microfluidic surface acoustic wave sample delivery and ionization source for rapid and sensitive ambient mass spectrometry," *Analytical chemistry*, vol. 83, no. 9, pp. 3260–3266, 2011.

[78] Z. Ramshani, A. S. Reddy, B. B. Narakathu, J. T. Wabeke, S. O. Obare, and M. Z. Atashbar, "Sh-saw sensor based microfluidic system for the detection of heavy metal compounds in liquid environments," *Sensors and Actuators B: Chemical*, vol. 217, pp. 72–77, 2015.

[79] A. R. Rezk, A. Qi, J. R. Friend, W. H. Li, and L. Y. Yeo, "Uniform mixing in paper-based microfluidic systems using surface acoustic waves," *Lab on a Chip*, vol. 12, no. 4, pp. 773–779, 2012.

[80] K.-y. Hashimoto and K.-Y. Hashimoto, *Surface acoustic wave devices in telecommunications*. Springer, 2000, vol. 116. DOI: 10.1007/978-3-662-04223-6.

[81] C.-c. Luan, X.-h. Yao, Q.-y. Chen, and J.-z. Fu, "Research on transmission performance of a surface acoustic wave sensing system used in manufacturing environment monitoring," *Journal of Zhejiang University-SCIENCE A*, vol. 18, no. 6, pp. 443–453, 2017.

[82] L. Reindl, C. Ruppel, A. Kirmayr, N. Slockhausen, and M. Hilhorst, "Passive radio requestable saw water content sensor," in *1999 IEEE Ultrasonics Symposium. Proceedings. International Symposium (Cat. No. 99CH37027)*, IEEE, vol. 1, 1999, pp. 461–466.

[83] "Saw components dresden gmbh." (), [Online]. Available: https://www.sawcomponents.de/en/. (Accessed on: 03.01.2023).

[84] "Transense." (), [Online]. Available: https://transense.com/sawsense/,. (Accessed on: 03.01.2023).

[85] "Senseor." (), [Online]. Available: https://senseor.com/,. (Accessed on: 03.01.2023).

[86] D. Morgan, *Surface acoustic wave filters: With applications to electronic communications and signal processing*. Academic Press, 2010.

[87] Y. Pan, C. Yan, X. Gao, *et al.*, "A passive wireless surface acoustic wave (saw) sensor system for detecting warfare agents based on fluoroalcohol polysiloxane film," *Microsystems & Nanoengineering*, vol. 10, no. 1, p. 4, 2024.

[88] W. Wang, K. Lee, T. Kim, I. Park, and S. Yang, "A novel wireless, passive co2 sensor incorporating a surface acoustic wave reflective delay line," *Smart materials and structures*, vol. 16, no. 4, p. 1382, 2007.

[89] F.-Q. Xu, W. Wang, X.-F. Xue, H.-L. Hu, X.-L. Liu, and Y. Pan, "Development of a wireless and passive saw-based chemical sensor for organophosphorous compound detection," *Sensors*, vol. 15, no. 12, pp. 30 187–30 198, 2015.

[90] O. H. Murphy, M. R. Bahmanyar, A. Borghi, *et al.*, "Continuous in vivo blood pressure measurements using a fully implantable wireless saw sensor," *Biomedical microdevices*, vol. 15, pp. 737–749, 2013.

[91] P. Jeltiri, F. Al-Mahmoud, R. Boissière, *et al.*, "Wireless strain and temperature monitoring in reinforced concrete using surface acoustic wave (saw) sensors," *IEEE Sensors Letters*, 2023.

[92] I. Leonte, M. Hunt, G. Sehra, M. Cole, and J. Gardner, "Saw bioliquids sensor with rf interrogation," in *High Frequency Postgraduate Student Colloquium, 2004*, IEEE, 2004, pp. 47–52.

[93] F. Hassani, S. Ahmadi, C. Korman, and M. Zaghloul, "A saw-based liquid sensor with identification for wireless applications," in *Proceedings of 2010 IEEE International Symposium on Circuits and Systems*, IEEE, 2010, pp. 2023–2026.

[94] H.-K. Oh, W. Wang, K. Lee, C. Min, and S. Yang, "The development of a wireless love wave biosensor on 41 yx linbo3," *Smart Materials And Structures*, vol. 18, no. 2, p. 025 008, 2009.

[95] T. Song, S. Y. Song, H. C. Yoon, and K. Lee, "Development of a wireless love wave biosensor platform for multi-functional detection," *Japanese Journal of Applied Physics*, vol. 50, no. 6S, 06GL09, 2011.

[96] H. Oh, C. Fu, K. Kim, and K. Lee, "Wireless and simultaneous detections of multiple bio-molecules in a single sensor using love wave biosensor," *Sensors*, vol. 14, no. 11, pp. 21 660–21 675, 2014.

[97] S. I. Zida, Y.-D. Lin, and Y. L. Khung, "Current trends on surface acoustic wave biosensors," *Advanced Materials Technologies*, vol. 6, no. 6, p. 2 001 018, 2021.

[98] P. Statistics, *Wireless sensor market*, `https://www.precedenceresearch.com/sensor-market` [Accessed: (25/01/2024)], 2023.

[99] P. Statistics, *Iot market*, `https://www.precedenceresearch.com/industrial-iot-market` [Accessed: (25/01/2024)], 2023.

[100] A. Pohl, "A review of wireless saw sensors," *IEEE transactions on ultrasonics, ferroelectrics, and frequency control*, vol. 47, no. 2, pp. 317–332, 2000.

[101] R. Kumar and N. Mandal, "Saw sensor basics on material, antenna and applications: A review," *IEEE Sensors Journal*, 2024.

[102] F. Lurz, T. Ostertag, B. Scheiner, R. Weigel, and A. Koelpin, "Reader architectures for wireless surface acoustic wave sensors," *Sensors*, vol. 18, no. 6, p. 1734, 2018.

[103] V. Kalinin, "Modelling of a wireless saw system for multiple parameter measurement," in *Proc. IEEE Ultrason. Symp.*, 2001, pp. 1790–1793.

[104] V. Kalinin, G. Bown, J. Beckley, and R. Lohr, "Pulsed interrogation of the saw torque sensor for electrical power assisted steering," in *IEEE Ultrasonics Symposium, 2004*, vol. 3, 2004, 1577–1580 Vol.3.

[105] B. Dixon, V. Kalinin, J. Beckley, and R. Lohr, "A second generation in-car tire pressure monitoring system based on wireless passive saw sensors," in *2006 IEEE International Frequency Control Symposium and Exposition*, 2006, pp. 374–380.

[106] M. Hamsch, R. Hoffmann, W. Buff, M. Binhack, and S. Klett, "An interrogation unit for passive wireless saw sensors based on fourier transform," *IEEE transactions on ultrasonics, ferroelectrics, and frequency control*, vol. 51, no. 11, pp. 1449–1456, 2004.

[107] M. P. Da Cunha, R. Lad, P. Davulis, *et al.*, "Wireless acoustic wave sensors and systems for harsh environment applications," in *2011 IEEE Topical Conference on Wireless Sensors and Sensor Networks*, IEEE, 2011, pp. 41–44.

[108] F. Schmidt, O. Sczesny, L. Reindl, and V. Magori, "Remote sensing of physical parameters by means of passive surface acoustic wave devices ("id-tag")," in *1994 Proceedings of IEEE Ultrasonics Symposium*, IEEE, vol. 1, 1994, pp. 589–592.

[109] A. Pohl and F. Seifert, "New applications of wirelessly interrogable passive saw sensors," *IEEE Transactions on Microwave Theory and Techniques*, vol. 46, no. 12, pp. 2208–2212, 1998.

[110] R. Hauser, R. Fachberger, G. Bruckner, *et al.*, *A wireless SAW-based temperature sensor for harsh environment*. IEEE, 2004.

[111] V. P. Plessky and L. M. Reindl, "Review on saw rfid tags," *IEEE transactions on ultrasonics, ferroelectrics, and frequency control*, vol. 57, no. 3, pp. 654–668, 2010.

[112] A. Pohl, F. Seifert, L. Reindl, G. Scholl, T. Ostertag, and W. Pietsch, "Radio signals for saw id tags and sensors in strong electromagnetic interference," in *1994 Proceedings of IEEE Ultrasonics Symposium*, IEEE, vol. 1, 1994, pp. 195–198.

[113] W.-E. Bulst, G. Fischerauer, and L. Reindl, "State of the art in wireless sensing with surface acoustic waves," *IEEE Transactions on Industrial Electronics*, vol. 48, no. 2, pp. 265–271, 2001.

[114] B. Bazuin, M. Atashbar, and S. Krishnamurthy, "A prototype burst transceiver for saw sensors interrogation," in *International Conference on Intelligent Sensing and Information Processing, 2004. Proceedings of*, IEEE, 2004, pp. 190–195.

[115] G. Goavec-Merou, N. Chretien, J.-M. Friedt, *et al.*, "Fast contactless vibrating structure characterization using real time field programmable gate array-based digital signal processing: Demonstrations with a passive wireless acoustic delay line probe and vision," *Review of Scientific Instruments*, vol. 85, no. 1, p. 015 109, 2014.

[116] B. O. Gombé, G. G. Mérou, K. Breschi, *et al.*, "A saw wireless sensor network platform for industrial predictive maintenance," *Journal of Intelligent Manufacturing*, vol. 30, no. 4, pp. 1617–1628, 2019.

[117] S. Schuster, S. Scheiblhofer, L. Reindl, and A. Stelzer, "Performance evaluation of algorithms for saw-based temperature measurement," *IEEE transactions on ultrasonics, ferroelectrics, and frequency control*, vol. 53, no. 6, pp. 1177–1185, 2006.

[118] C. Bernou, D. Rebière, and J. Pistre, "Microwave sensors: A new sensing principle. application to humidity detection," *Sensors and Actuators B: Chemical*, vol. 68, no. 1-3, pp. 88–93, 2000.

[119] M. Bariya, H. Y. Y. Nyein, and A. Javey, "Wearable sweat sensors," *Nature Electronics*, vol. 1, no. 3, pp. 160–171, 2018.

[120] N. C. Karmakar, E. M. Amin, and J. K. Saha, *Chipless RFID sensors*. John Wiley & Sons, 2016.

[121] S. Preradovic and N. C. Karmakar, "Rfid readers-a review," in *2006 International Conference on Electrical and Computer Engineering*, IEEE, 2006, pp. 100–103.

[122] S. Preradovic and N. C. Karmakar, "Design of short range chipless rfid reader prototype," in *2009 International Conference on Intelligent Sensors, Sensor Networks and Information Processing (ISSNIP)*, IEEE, 2009, pp. 307–312.

[123] L. Ukkonen, L. Sydänheimo, and M. Kivikoski, "Read range performance comparison of compact reader antennas for a handheld uhf rfid reader," in *2007 IEEE International Conference on RFID*, IEEE, 2007, pp. 63–70.

[124] C. S. Hartmann and L. T. Claiborne, "Fundamental limitations on reading range of passive ic-based rfid and saw-based rfid," in *2007 IEEE International Conference on RFID*, IEEE, 2007, pp. 41–48.

[125] U. Wolff, F. Schmidt, G. Scholl, and V. Magori, "Radio accessible saw sensors for non-contact measurement of torque and temperature," in *1996 IEEE Ultrasonics Symposium. Proceedings*, IEEE, vol. 1, 1996, pp. 359–362.

[126] H. Hallil, F. Chebila, P. Menini, and H. Aubert, "Feasibility of passive gas sensor based on whispering gallery modes and its radar interrogation: Theoretical and experimental investigations," 2010.

[127] A. Binder, R. Fachberger, and M. Lenzhofer, "Phase stability comparison of saw sensor evaluation with various cw type radars," *Procedia Engineering*, vol. 5, pp. 661–664, 2010.

[128] A. H. Rasolomboahanginjatovo, Y. Sanogo, F. Domingue, and A. O. Dahmane, "Custom pxie-567x-based saw rfid interrogation signal generator," *IEEE Sensors Journal*, vol. 16, no. 24, pp. 8798–8806, 2016.

[129] J. Humphries and D. Malocha, "Software defined radio for passive sensor interrogation," in *2013 Joint European Frequency and Time Forum & International Frequency Control Symposium (EFTF/IFC)*, IEEE, 2013, pp. 270–273.

[130] J. Humphries, M. Gallagher, D. Gallagher, A. Weeks, and D. Malocha, "Interrogation of orthogonal frequency coded saw sensors using the usrp," in *2015 Joint Conference of the IEEE International Frequency Control Symposium & the European Frequency and Time Forum*, IEEE, 2015, pp. 530–535.

[131] D. C. Malocha, J. Humphries, J. A. Figueroa, M. Lamothe, and A. Weeks, "915 mhz saw wireless passive sensor system performance," in *2016 IEEE International Ultrasonics Symposium (IUS)*, 2016, pp. 1–4.

[132] D. Rabus, J.-M. Friedt, L. Arapan, *et al.*, "Subsurface h2s detection by a surface acoustic wave passive wireless sensor interrogated with a ground penetrating radar," *ACS sensors*, vol. 5, no. 4, pp. 1075–1081, 2020.

[133] K. Shibata, E. Takahashi, H. Fujiwara, *et al.*, "Long range wireless saw passive tag system for vibration monitoring," in *2017 IEEE International Ultrasonics Symposium (IUS)*, IEEE, 2017, pp. 1–4.

[134] J. R. Humphries, D. R. Armstrong, A. R. Weeks, and D. C. Malocha, "Standalone saw sensor interrogator using an embedded computer and software defined radio," in *2015 IEEE International Conference on Wireless for Space and Extreme Environments (WiSEE)*, IEEE, 2015, pp. 1–5.

[135] H. Aubert, F. Chebila, M. Jatlaoui, *et al.*, "Wireless sensing and identification of passive electromagnetic sensors based on millimetre-wave fmcw radar," in *2012 Ieee International Conference on Rfid-Technologies and Applications (Rfid-Ta)*, IEEE, 2012, pp. 398–403.

[136] H. Aubert, F. Chebila, M. Jatlaoui, *et al.*, "Wireless sensing and identification based on radar cross section variability measurement of passive electromagnetic sensors," *annals of telecommunications-annales des télécommunications*, vol. 68, no. 7-8, pp. 425–435, 2013.

[137] A. Canabal, P. Davulis, E. Dudzik, and M. P. Da Cunha, "Cdma and fscw surface acoustic wave temperature sensors for wireless operation at high temperatures," in *2009 IEEE International Ultrasonics Symposium*, IEEE, 2009, pp. 807–810.

[138] J. Devkota, D. W. Greve, N. Diemler, R. Pingree, and R. Wright, "An impedance-loaded surface acoustic wave corrosion sensor for infrastructure monitoring," *Sensors*, vol. 24, no. 3, p. 789, 2024.

[139] D. Leff, A. Maskay, and M. P. da Cunha, "Wireless interrogation of high temperature surface acoustic wave dynamic strain sensor," in *2020 IEEE International Ultrasonics Symposium (IUS)*, IEEE, 2020, pp. 1–4.

[140] S. F. Jilani, D. Leff, A. Maskay, R. J. Lad, and M. P. Da Cunha, "Static strain modelling, calibration, and measurements for high-temperature wireless saw resonator operation," in *2020 IEEE International Ultrasonics Symposium (IUS)*, IEEE, 2020, pp. 1–4.

[141] Z. Tang, W. Wu, J. Gao, and P. Yang, "Saw delay line based iot smart sensing in water distribution system," in *2018 IEEE 20th International Conference on High Performance Computing and Communications; IEEE 16th International Conference on Smart City; IEEE*

4th International Conference on Data Science and Systems (HPCC/SmartCity/DSS), IEEE, 2018, pp. 1474–1478.

[142] P. Mengue, L. Meistersheim, S. Hage-Ali, *et al.*, "Magnetic saw rfid sensor based on love wave for detection of magnetic field and temperature," *IEEE Journal of Radio Frequency Identification*, 2023.

[143] P. Mengue, L. Meistersheim, S. Hage-Ali, *et al.*, "Multifunctional msaw sensor based on love wave with rfid tags functionalities," in *2023 IEEE 13th International Conference on RFID Technology and Applications (RFID-TA)*, IEEE, 2023, pp. 154–157.

[144] Y. Yin, W. Wang, Y. Jia, and Y. Liang, "Development of a novel wireless and passive love wave based ice sensor," in *2019 IEEE International Ultrasonics Symposium (IUS)*, IEEE, 2019, pp. 2553–2556.

[145] H. Jammoul, M. Rube, M. Sebeloue, *et al.*, "Investigating water contamination with lora-enabled surface acoustic wave sensors," in *2023 7th International Symposium on Instrumentation Systems, Circuits and Transducers (INSCIT)*, IEEE, 2023, pp. 1–5.

[146] W. Wang, X. Xue, Y. Huang, and X. Liu, "A novel wireless and temperature-compensated saw vibration sensor," *Sensors*, vol. 14, no. 11, pp. 20 702–20 712, 2014.

[147] X. Gao, L. Cheng, X. Xue, *et al.*, "Development of wireless and passive saw temperature sensor with very high accuracy," *Applied Sciences*, vol. 11, no. 16, p. 7422, 2021.

[148] W. Wang, H. Oh, K. Lee, and S. Yang, "Enhanced sensitivity of wireless chemical sensor based on love wave mode," *Japanese Journal of Applied Physics*, vol. 47, no. 9R, p. 7372, 2008.

[149] H. Oh, W. Wang, K. Lee, H. C. Yoon, and S. Yang, "Wirelessly driven and battery-free love wave biosensor based on dinitrophenyl immobilization," *Japanese Journal of Applied Physics*, vol. 48, no. 6S, 06FJ05, 2009.

[150] T. Song, M. Nam, S. Song, H. C. Yoon, and K. Lee, "A novel wireless love wave biosensor platform for multifunctional detection," in *Reliability, Packaging, Testing, and Characterization of MEMS/MOEMS and Nanodevices X*, SPIE, vol. 7928, 2011, pp. 199–209.

[151] W. Wang and S. He, "Passive and remote polymer-coated love wave chemical sensor," in *2008 IEEE Ultrasonics Symposium*, IEEE, 2008, pp. 1854–1857.

[152] L. Zou, C. McLeod, and M. R. Bahmanyar, "Wireless interrogation of implantable saw sensors," *IEEE Transactions on Biomedical Engineering*, vol. 67, no. 5, pp. 1409–1417, 2019.

[153] F. Li, D. Xiang, S. Chiang, B. R. Tittmann, and C. Searfass, "Wireless surface acoustic wave radio frequency identification (saw-rfid) sensor system for temperature and strain measurements," in *2011 IEEE International Ultrasonics Symposium*, IEEE, 2011, pp. 822–825.

[154] N. Saldanha and D. C. Malocha, "Pseudo-orthogonal frequency coded wireless saw rfid temperature sensor tags," *IEEE transactions on ultrasonics, ferroelectrics, and frequency control*, vol. 59, no. 8, pp. 1750–1758, 2012.

[155] T. T. Thai, J. M. Mehdi, F. Chebila, *et al.*, "Design and development of a novel passive wireless ultrasensitive rf temperature transducer for remote sensing," *IEEE Sensors Journal*, vol. 12, no. 9, pp. 2756–2766, 2012. DOI: 10.1109/JSEN.2012.2201463.

[156] "Hanna instruments." (), [Online]. Available: https://www.hannainstruments.fr/produits-hanna-instruments/conductimetres/. (accessed: 02.05.2024).

[157] X. Liang, L. Zhang, Q. Tan, *et al.*, "Temperature, pressure, and humidity saw sensor based on coplanar integrated lgs," *Microsystems & Nanoengineering*, vol. 9, no. 1, p. 110, 2023.

[158] A. Coon, "Saw filters and competitive technologies: A comparative review," in *IEEE 1991 Ultrasonics Symposium,*, IEEE, 1991, pp. 155–160. DOI: 10.1109/ULTSYM.1991.234146.

[159] C. Lam, C. Y. Wang, and S. Wang, "A review of the recent development of temperature stable cuts of quartz for saw applications," in *Proceedings of the Fourth International Symposium on Acoustic Wave Devices for Future Mobile Communication Systems, Chiba, Japan*, Citeseer, 2010, pp. 3–5.

[160] C. Campbell, *Surface Acoustic Wave Devices for Mobile and Wireless Communications, Four-Volume Set*. Academic press, 1998.

[161] L. Le Brizoual, F. Sarry, O. Elmazria, P. Alnot, S. Ballandras, and T. Pastureaud, "Ghz frequency zno/si saw device," *IEEE transactions on ultrasonics, ferroelectrics, and frequency control*, vol. 55, no. 2, pp. 442–450, 2008. DOI: 10.1109/TUFFC.2008.662.

[162] C. Zimmermann, "Conception, réalisation et étude de micro-capteurs à ondes de love pour applications en milieu gazeux: Cas de la détection de composés organophosphorés," Ph.D. dissertation, Bordeaux 1, 2002.

[163] C. Floer, "Capteurs à ondes élastiques confinées, sans fil et étirables: Application à l'électronique imperceptible sur peau," Ph.D. dissertation, Université de Lorraine, 2019.

[164] T. Aubert, O. Elmazria, B. Assouar, *et al.*, "Investigations on aln/sapphire piezoelectric bilayer structure for high-temperature saw applications," *IEEE transactions on ultrasonics, ferroelectrics, and frequency control*, vol. 59, no. 5, pp. 999–1005, 2012. DOI: 10.1109/TUFFC.2012.2285.

[165] M. Benetti, D. Cannata, F. Di Pictrantonio, and E. Verona, "Growth of aln piezoelectric film on diamond for high-frequency surface acoustic wave devices," *IEEE transactions on ultrasonics, ferroelectrics, and frequency control*, vol. 52, no. 10, pp. 1806–1811, 2005. DOI: 10.1109/TUFFC.2005.1561635.

[166] S. S. Hong, "Surface acoustic wave optical modulation," Ph.D. dissertation, Massachusetts Institute of Technology, 2001.

[167] G. S. Calabrese, H. Wohltjen, and M. K. Roy, "Surface acoustic wave devices as chemical sensors in liquids. evidence disputing the importance of rayleigh wave propagation," *Analytical Chemistry*, vol. 59, no. 6, pp. 833–837, 1987.

[168] T. Moriizumi, Y. Unno, and S. Shiokawa, "New sensor in liquid using leaky saw," in *IEEE 1987 Ultrasonics Symposium*, IEEE, 1987, pp. 579–582.

[169] R. L. Baer and C. A. Flory, "Some limitations on the use of leaky saw mode sensors in liquids," in *IEEE 1991 Ultrasonics Symposium,*, IEEE, 1991, pp. 279–284.

[170] C. Zimmermann, P. Mazein, D. Rebiere, C. Dejous, F. Josse, and J. Pistre, "A theoretical study of love wave sensors mass loading and viscoelastic sensitivity in gas and liquid environments," in *IEEE Ultrasonics Symposium, 2004*, IEEE, vol. 2, 2004, pp. 813–816.

[171] O. Tamarin, C. Déjous, D. Rebière, *et al.*, "Study of acoustic love wave devices for real time bacteriophage detection," *Sensors and Actuators B: Chemical*, vol. 91, no. 1-3, pp. 275–284, 2003.

[172] Y. Yang, C. Dejous, and H. Hallil, "Trends and applications of surface and bulk acoustic wave devices: A review," *Micromachines*, vol. 14, no. 1, p. 43, 2022.

[173] F. Caspers, "Rf engineering basic concepts: S-parameters," *arXiv preprint arXiv:1201.2346*, 2012.

[174] F. Fournel, E. Baco, M. Mamani-Matsuda, *et al.*, "Love wave biosensor for real-time detection of okadaic acid as dsp phycotoxin," *Sensors and Actuators B: Chemical*, vol. 170, pp. 122–128, 2012.

[175] A. Peyman, C. Gabriel, and E. Grant, "Complex permittivity of sodium chloride solutions at microwave frequencies," *Bioelectromagnetics: Journal of the Bioelectromagnetics Society, The Society for Physical Regulation in Biology and Medicine, The European Bioelectromagnetics Association*, vol. 28, no. 4, pp. 264–274, 2007.

[176] H. Ozbek, J. Fair, and S. Phillips, "Viscosity of aqueous sodium chloride solutions from 0-150o c," Lawrence Berkeley National Lab.(LBNL), Berkeley, CA (United States), Tech. Rep., 1977.

[177] Darren Rowland. "Density of nacl(aq)." (accessed: 02.05.2024). (2021), [Online]. Available: `https://advancedthermo.com/electrolytes/density_NaCl_Jun2021.html`.

[178] B. Archambeault, S. Connor, and J. Diepenbrock, "Time domain gating of frequency domain s-parameter data to remove connector end effects for pcb and cable applications," in *2006 IEEE International Symposium on Electromagnetic Compatibility, 2006. EMC 2006.*, IEEE, vol. 1, 2006, pp. 199–202.

[179] W. C. Wilson and G. M. Atkinson, "Rapid saw sensor development tools," in *CANEUS/NASA Workshop on Fly-by-Wireless for Aerospace Vehicles*, 2007.

[180] B. A. Auld, *Acoustic fields and waves in solids.* , 1973.

[181] B. Jakoby and M. J. Vellekoop, "Viscosity sensing using a love-wave device," *Sensors and Actuators A: Physical*, vol. 68, no. 1-3, pp. 275–281, 1998.

[182] F. Herrmann, D. Hahn, and S. Büttgenbach, "Separation of density and viscosity influence on liquid-loaded surface acoustic wave devices," *Applied physics letters*, vol. 74, no. 22, pp. 3410–3412, 1999.

[183] O. Tamarin, D. Rebiere, J. Pistre, *et al.*, "Simple analytical method to estimate the influence of liquids viscosity on love wave chemical sensors," in *2001 IEEE Ultrasonics Symposium. Proceedings. An International Symposium (Cat. No. 01CH37263)*, IEEE, vol. 1, 2001, pp. 343–346.

[184] G. Kovacs, M. Vellekoop, R. Haueis, G. Lubking, and A. Venema, "A love wave sensor for (bio) chemical sensing in liquids," *Sensors and Actuators A: Physical*, vol. 43, no. 1-3, pp. 38–43, 1994.

[185] M. Rube, O. Tamarin, S. Hemour, *et al.*, "A behavior-descriptive model of love wave sensor in liquid medium for circuit-design and analysis with qucsstudio," in *2021 IEEE Sensors*, IEEE, 2021, pp. 1–4.

[186] S. Martin, A. Ricco, T. Niemczyk, and G. Frye, "Characterization of sh acoustic plate mode liquid sensors," *Sensors and actuators*, vol. 20, no. 3, pp. 253–268, 1989.

[187] M. Margraf, "Qucsstudio—a free and powerful circuit simulator," *URl: http://qucsstudio.de/(visited on 09/09/2021)(cit. on p. 14)*, vol. 93, p. 94, 2020.

[188] A. Guerrero, J. Bisquert, and G. Garcia-Belmonte, "Impedance spectroscopy of metal halide perovskite solar cells from the perspective of equivalent circuits," *Chemical Reviews*, vol. 121, no. 23, pp. 14 430–14 484, 2021.

[189] K. Kadan-Jamal, M. Sophocleous, A. Jog, *et al.*, "Electrical impedance spectroscopy of plant cells in aqueous biological buffer solutions and their modelling using a unified electrical equivalent circuit over a wide frequency range: 4hz to 20 ghz," *Biosensors and Bioelectronics*, vol. 168, p. 112 485, 2020.

[190] Y. Liu, R. Zhao, M. Ghaffari, *et al.*, "Equivalent circuit modeling of ionomer and ionic polymer conductive network composite actuators containing ionic liquids," *Sensors and Actuators A: Physical*, vol. 181, pp. 70–76, 2012.

[191] G. Hernandez and A. Ramirez, "Dielectric response model for transformer insulation using frequency domain spectroscopy and vector fitting," *Energies*, vol. 15, no. 7, p. 2655, 2022.

[192] Y. Weng, S. Cheung, T. Yuk, and L. Liu, "Design of chipless uwb rfid system using a cpw multi-resonator," *IEEE Antennas and Propagation Magazine*, vol. 55, no. 1, pp. 13–31, 2013.

[193] D. Dominic, S. Krafft, N. Safdari, and S. Bhadra, "Multiresonator-based printable chipless rfid for relative humidity sensing," in *Proceedings*, MDPI, vol. 60, 2017, p. 367.

[194] E. M. Amin and N. Karmakar, "Development of a chipless rfid temperature sensor using cascaded spiral resonators," in *SENSORS, 2011 IEEE*, IEEE, 2011, pp. 554–557.

[195] E. M. Amin and N. C. Karmakar, "Development of a low cost printable humidity sensor for chipless rfid technology," in *2012 IEEE International Conference on RFID-Technologies and Applications (RFID-TA)*, IEEE, 2012, pp. 165–170.

[196] E. M. Amin, N. C. Karmakar, and B. W. Jensen, "Fully printable chipless rfid multi-parameter sensor," *Sensors and Actuators A: Physical*, vol. 248, pp. 223–232, 2016.

[197] R. Raju and G. E. Bridges, "Radar cross section-based chipless tag with built-in reference for relative humidity monitoring of packaged food commodities," *IEEE Sensors Journal*, vol. 21, no. 17, pp. 18 773–18 780, 2021.

[198] A. Vena, L. Sydänheimo, M. M. Tentzeris, and L. Ukkonen, "A fully inkjet-printed wireless and chipless sensor for co 2 and temperature detection," *IEEE Sensors Journal*, vol. 15, no. 1, pp. 89–99, 2014.

[199] H. Alemdar and C. Ersoy, "Wireless sensor networks for healthcare: A survey," *Computer networks*, vol. 54, no. 15, pp. 2688–2710, 2010.

[200] A. Alreshaid, J. Hester, W. Su, Y. Fang, and M. Tentzeris, "Ink-jet printed wireless liquid and gas sensors for iot, smartag and smart city applications," *Journal of The Electrochemical Society*, vol. 165, no. 10, B407, 2018.

[201] J. Zhang, A. I. Sunny, G. Zhang, and G. Tian, "Feature extraction for robust crack monitoring using passive wireless rfid antenna sensors," *IEEE Sensors Journal*, vol. 18, no. 15, pp. 6273–6280, 2018.

[202] "Bingfu antenna." (), [Online]. Available: `https://bingfushop.com/products/bingfu-police-radio-scanner-antenna-20-1300mhz-7-sections-telescopic-bnc-male-antenna-ham-radio-handheld-cb-radio-antenna-for-uniden-whistler-police-radio-scanner-two-way-radio-frequency-counter`. (accessed: 14.05.2024).

[203] "Fmuser." (), [Online]. Available: `http://www.fmuser.net/upLoad/down/month_1608/FMUSER%20Catalog-Antenna.pdf`. (accessed: 14.05.2024).

[204] J. Wang, J. Ge, Q. Zhang, *et al.*, "Radar cross-section measurements of ice particles using vector network analyzer," *Aip Advances*, vol. 6, no. 9, p. 095 310, 2016.

[205] M. I. Grace, "Measurement of radar cross section using the "vna master" handheld vna," *Anritsu, Appl. Note*, 2011.

[206] O. Rance, R. Siragusa, P. Lemaitre-Auger, and E. Perret, "Toward rcs magnitude level coding for chipless rfid," *IEEE Transactions on Microwave Theory and Techniques*, vol. 64, no. 7, pp. 2315–2325, 2016.

[207] R. C. Hansen, "Relationships between antennas as scatterers and as radiators," *Proceedings of the IEEE*, vol. 77, no. 5, pp. 659–662, 1989.

[208] S. Sefi, "Computational electromagnetics: Software development and high frequency modeling of surface currents on perfect conductors," Ph.D. dissertation, KTH, 2005.

[209] M.-Z. Xie, L.-F. Wang, L. Dong, W.-J. Deng, and Q.-A. Huang, "Low cost paper-based lc wireless humidity sensors and distance-insensitive readout system," *IEEE Sensors Journal*, vol. 19, no. 12, pp. 4717–4725, 2019.

[210] Q. Luo, S. Gao, M. Sobhy, J. Li, G. Wei, and J. Xu, "A broadband printed monofilar square spiral antenna: A circularly polarized low-profile antenna.," *IEEE Antennas and Propagation Magazine*, vol. 59, no. 2, pp. 79–87, 2017.

[211] D. R. Ribeiro, L. A. de Santana, M. C. Alves, J. F. Almeida, and C. L. da SS Sobrinho, "Spiral microstrip antenna," in *2007 SBMO/IEEE MTT-S International Microwave and Optoelectronics Conference*, IEEE, 2007, pp. 104–106.

[212] G. H. Huff and J. T. Bernhard, "Integration of packaged RF MEMS switches with radiation pattern reconfigurable square spiral microstrip antennas," *IEEE Transactions on Antennas and Propagation*, vol. 54, no. 2, pp. 464–469, 2006.

[213] G.-T. Jeong, W.-S. Kim, and K.-S. Kwak, "Design of a corner-truncated square-spiral microstrip patch antenna in the 5-GHz band," *Microwave and Optical Technology Letters*, vol. 48, no. 3, pp. 529–532, 2006.

[214] T. Rama Rao, "Design and performance analysis of a penta-band spiral antenna for vehicular communications," *Wireless Personal Communications*, vol. 96, pp. 3421–3434, 2017.

[215] S. K. Ghosh and R. K. Badhai, "Spiral shaped multi frequency printed antenna for mobile wireless and biomedical applications," *Wireless Personal Communications*, vol. 98, pp. 2461–2471, 2018.

[216] H. Khaleel, *Innovation in wearable and flexible antennas*. Wit Press, 2014.

[217] P. F. da Silva Júnior, A. J. R. Serres, R. C. S. Freire, *et al.*, "Bio-inspired wearable antennas," *Wearable Technologies*, vol. 219, 2018.

[218] A. Zulqarnain, R. Baber, S. Saeed, *et al.*, "Square spiral microstrip patch antenna," in *2019 International Conference on Electrical, Communication, and Computer Engineering (ICECCE)*, IEEE, 2019, pp. 1–5.

[219] J. Ely, C. Christodoulou, and D. Shively, "Square spiral microstrip antennas for wireless applications," in *IEEE NTC, Conference Proceedings Microwave Systems Conference*, IEEE, 1995, pp. 229–232.

[220] M. Andrade, R. C. Freire, P. Fernandes, *et al.*, "Compact monopole antenna for smart meter applications in ism band 900 mhz," in *Proceedings of the 23rd International Workshop on ADC and DAC Modelling and Testing IMEKO TC-4*, 2020.

[221] O. I. Sukharevsky, *Electromagnetic wave scattering by aerial and ground radar objects*. Taylor & Francis, 2014.

[222] W. Jiang, T. Hong, S. Gong, *et al.*, "Research on the scattering characteristics and the rcs reduction of circularly polarized microstrip antenna," *International Journal of Antennas and Propagation*, vol. 2013, 2013.

[223] A. Ballato, "Piezoelectricity: Old effect, new thrusts," *IEEE Transactions on Ultrasonics, Ferroelectrics, and Frequency Control*, vol. 42, no. 5, pp. 916–926, 1995. DOI: 10.1109/58.464826.

[224] J. Curie and P. Curie, "Développement par compression de l'électricité polaire dans les cristaux hémièdres à faces inclinées," *Bulletin de minéralogie*, vol. 3, no. 4, pp. 90–93, 1880. DOI: 10.3406/bulmi.1880.1564.

[225] G. Lippmann, "Principe de la conservation de l'électricité, ou second principe de la théorie des phénomènes électriques," *J. Phys. Theor. Appl.*, vol. 10, no. 1, pp. 381–394, 1881. DOI: 10.1051/jphystap:0188100100038100.

[226] W. P. Mason, "Piezoelectricity, its history and applications," *The journal of the Acoustical Society of America*, vol. 70, no. 6, pp. 1561–1566, 1981. DOI: 10.1121/1.387221.